J DOMINANCE
OF
SHORT CRACKS IN BENDING AND TENSION

BY

ABDUL M. ABBAS AL ANI

Submission for degree of

M.Sc

Department of Mechanical Engineering

University of Glasgow

Glasgow

Scotland

August -1988

ProQuest LLC.
789 East Eisenhower Parkway
P.O. Box 1346
Ann Arbor, MI 48106 – 1346

TO MY FATHER, MOTHER, BROTHERS, SISTERS and FIANCEE

WITH LOVE

CONTENTS

Chapter (5)- Short Crack-EPFM Calculations

Acknowledgements

I wish to express my indebtedness to my supervisor, Prof J. W. Hancock for his valuable guidance, advice and constant encouragement throughout the work. Many thanks are due to:
Hibbit Karlson and Sorenson Inc for access to ABAQUS, and the computer staff of the Mechanical Engineering Department, especially Mrs L. McCormick and Mrs C. Carmichael
my friends whose help will never be forgotten

My special thanks are due to my family particularly, my father and my brothers for their boundless patience and continual encouragement.

Finally, my great thanks are reserved for the Government of the Republic of Iraq for their continued financial support.

Synopsis

There are many structural situations involving shallow cracks, in which it is not possible to make direct measurements of the relevant fracture toughness using existing British (BSI) and American (ASTM) deep notch fracture mechanics tests. The objective of the present work to establish the size requirements for a one parameter characterisation the crack tip fields for short cracks in edge cracked bars subject to tension and bending.

Elastic and elastic-plastic plane strain finite element analyses were used. The stress and strain distribution ahead of short cracks was investigated, with small geometry change solutions with a sharp crack and for large geometry change solutions with a blunt crack with very small initial radius. For the small geometry change solution the calculated stress fields were compared with the HRR field. However for the large geometry change solution the fields were compared with the small scale yielding (SSY) solution given by McMeeking .

The comparison shows that the geometry with crack length (a) to width W ratios of (a/W) less than 0.3, J dominance is lost at crack lengths of order $200J/\sigma o$ for both tension and bending. However for geometries with ratios of $(a/W) \geq 0.3$ maintain J dominance up to criteria given by McMeeking and McMeeking and Parks.

Introduction

The failure of critical engineering structures has caused both injury and financial loss. Many of these failures can be attributed to pre-existing defects arising from material processing, or from cracks produced as a result of fatigue. It is thus important to be able to predict the ability of materials and structures to tolerate cracks and flaws. This is the prime purpose of fracture mechanics, which has led to the emergence of design concepts, which have been incorporated in standards and codes of practice.

The development of fracture mechanics has followed the development of welded structures. The first indication that the design and fabrication of welded structures needed to be substantially different to those of riveted structures was the failure of three welded truss bridges in Belgium between 1938 and 1940. In 1943, the first all welded tanker built by the Kaiser company of USA broke in half in cold but calm conditions in the fitting out dock. This was to be followed by a sequence of dramatic failures of American welded ships including Liberty ships, the tankers and victory ships, which have been reviewed by Anderson (1), Broek (2) and Biggs (3)

The conclusion arising from those failures is that classical engineering design criteria are inadequate to deal with the problems of structures containing defects, but fracture prevention criteria can be derived from fracture mechanics principles, and allow the integrity of costly structures to be maintained. Fracture mechanics is divided into two areas.

Firstly linear elastic fracture mechanics (henceforth LEFM)

which is concerned with fracture at stresses very much less than the yield stresses where when the body is largely elastic, and crack tip plasticity is still small enough to be viewed and treated as a small perturbation to the local stress field. Secondly yielding fracture mechanics, which is applicable as the plastic zone becomes significant in comparison to the dimensions of the body, and the LEFM treatment becomes inadequate. The critical dimensions of the body for valid LEFM as codified in British and American standards is given by:

$$B,W,W-a \geq 2.5\ (K/\sigma o)^2$$

Where σo is the yield stress measured in uniaxial tension, a is the crack length, (W-a) is the ligament and B is the thickness. Out with these requirements it is more appropriate to use elastic plastic-plastic fracture mechanics (EPFM), in which the deformation is characterised by the J-integral, and the field will be J dominated if the dimensions of the body satisfy certain size requirements. For deeply cracked geometries McMeeking and Parks (4) have shown that the J dominance occurs if :

$W-a \geq 25\ J/\sigma o$ for bending

$W-a \geq 200\ J/\sigma o$ for tension.

However many brittle fractures start at shallow surface cracks, in these instances the true fracture toughness may be dangerously overestimated by a standard test specimen having a relatively deep crack. From this view point it is clearly important to determine

the fracture toughness associated with short cracks.

In the work presented in this thesis, elastic-plastic finite element analysis has been used to study the stress and strain distribution ahead of short cracks in single edge cracked bend and tensile specimens using both small and large geometry change solutions. with the object of determining the conditions under which single parameter characterisation of the elastic plastic deformation ahead of the short cracks can be achieved by the J contour integral and the crack opening displacement.

Chapter (1)

STRESS and STRAIN

1.1 Stress

The state of stress at any point can be described by the stresses acting on three mutually perpendicular planes passing through the point of interest. The stresses acting on any other plane can then be determined by means of analytical or graphical methods. All the stresses shown in Fig (1.1) are positive according to the usual sign convention, in which tensile stresses are defined as being positive. The rationale behind the double-subscript notation, is that the first subscript designates the direction of the force while the second suffix indicates the direction to the normal of the plane on which it acts.

On this basis, the state of the stress can be conveniently written as a tensor, σ_{ij} and represented in matrix form

$$\sigma_{ij} = \begin{bmatrix} \sigma_{xx} & \sigma_{xy} & \sigma_{xz} \\ \sigma_{yx} & \sigma_{yy} & \sigma_{yz} \\ \sigma_{zx} & \sigma_{zy} & \sigma_{zz} \end{bmatrix} \quad ij = x, y, z \qquad (1)$$

Where σ_{yx}, σ_{xy}, σ_{yz} are the shear stresses. Although the tensor involves nine stress components, only six of these are independent as:

$$\sigma_{ij} = \sigma_{ji}$$

The stress system can always be referred as a set of orthogonal

axes 1,2,3 such that the shear terms become zero and the stress tensor takes the form

$$\sigma_{ij} = \begin{bmatrix} \sigma_{11} & 0 & 0 \\ 0 & \sigma_{22} & 0 \\ 0 & 0 & \sigma_{33} \end{bmatrix} , \qquad (2)$$

The axes 1,2,3 are referred to as principal axes, and $\sigma_{11}, \sigma_{22}, \sigma_{33}$ are the principal stresses. An important example of this occurs at a free surface, which is necessarily a principal plane.

The distribution of the stress throughout a body is limited by the need to satisfy equilibrium, which in the absence of body forces can be written as

$\sigma_{ij,j} = 0$

where the suffix ' , ' denotes differentiation

1.2 Strain

Forces acting on a body can produce both deformation and rigid body motion, both of which are described in terms of the displacements in the x, y and z directions denoted u,v,w respectively. The state of strain is a complete definition of the magnitude and directions of deformation excluding rigid body motion and is a second order tensor ε_{ij} analogous to the state of stress. For convenience, strains are always resolved into normal components and shear components, which can be written in terms of the displacements as:

$$\varepsilon_{ij} = 1/2\ [(\partial u_i/\partial x_j)+(\partial u_j/\partial x_i) \qquad (3)$$

This definition, defines the mathematical or tensor shear strains ε_{xy}, ε_{yz}, ε_{zx}, however it is also common to use the engineering shear strain.

$$\gamma_{ij} = [(\partial u_i/\partial x_j) + (\partial v_j/\partial x_i) \qquad (4)$$

Although the state of strain can vary through a body in response to the variation in the state of stress, the allowable distributions of stress are limited by the need to satisfy compatibility (Timoshenko (5))

$$\frac{\partial^2 e_{ij}}{\partial x_k \partial x_l} + \frac{\partial^2 e_{kl}}{\partial x_i \partial x_j} = \frac{\partial^2 e_{lk}}{\partial x_j \partial x_l} + \frac{\partial^2 e_{il}}{\partial x_i \partial x_k} \qquad (5)$$

Which ensures that the strain and displacement distributions are consistent.

1.3 Stress-strain relations for elastic solid

The relationships between stress and strain are fundamental to the analysis of deformation and fracture of engineering materials. Many materials can be considered to be isotropic, having identical physical properties in all directions. The present discussion is limited to isotropic materials.

The relationship between uniaxial stress and strain was first enunciated by Hooke (1635-1703) in connection with the application of a hair spring of a watch. Young(1773-1829) noted

that the constant of proportionality was a material property and in terms of Young's modulus E. Hooke's law can be written for uniaxial tension as :

$$\sigma_x = E\,\varepsilon_x \qquad \sigma_y = \sigma_z = 0 \tag{6}$$

Cauchy (1789-1857) generalized Hooke's law for general state three dimensional states stress, so that each of the six stress component σ_{ij}, is a linear function of all six strain components e_{kl} .

$$\sigma_{ij} = C_{ijkl}\, e_{kl} \tag{7}$$

Where C_{ijkl} is a fourth order tensor known as the stiffness. Symmetry of the tensor equation requires that:

$$C_{ijkl} = C_{jikl} = C_{ijlk} = C_{jilk} \tag{8}$$

This reduces the number of independent elastic constants to 21. Symmetry further reduces the number of constants to three for a cubic crystal; and for isotropic materials the constants can be further reduced two to, G and λ.

$$\begin{aligned}
\sigma_x &= (2G+\lambda)\,\varepsilon_x + \lambda\,(\varepsilon_y+\varepsilon_z) \\
\sigma_y &= (2G+\lambda)\,\varepsilon_y + \lambda\,(\varepsilon_z+\varepsilon_x) \\
\sigma_z &= (2G+\lambda)\,\varepsilon_z + \lambda\,(\varepsilon_x+\varepsilon_y) \\
\tau_{xy} &= G\gamma_{xy} \\
\tau_{yz} &= G\gamma_{yz} \\
\tau_{zx} &= G\gamma_{zx}
\end{aligned} \tag{9}$$

Here G is the shear modulus or modulus of rigidity, and λ is known as Lame's constant. Alternatively these equations can be written using Young's modulus E, and Poisson's ratio υ

$$\begin{aligned}
\varepsilon_x &= 1/E[\ \sigma_x - \upsilon\ (\ \sigma_y + \sigma_z\ )] \\
\varepsilon_y &= 1/E[\ \sigma_y - \upsilon\ (\ \sigma_z + \sigma_x\ )] \\
\varepsilon_z &= 1/E[\ \sigma_z - \upsilon\ (\ \sigma_x + \sigma_y\ )]
\end{aligned} \qquad (10)$$

$$\begin{aligned}
\gamma_{xy} &= \tau_{xy}/G = 2(1+\upsilon)\ \tau_{xy}/E \\
\gamma_{yz} &= \tau_{yz}/G = 2(1+\upsilon)\ \tau_{yz}/E \\
\gamma_{zx} &= \tau_{zx}/G = 2(1+\upsilon)\ \tau_{zx}/E
\end{aligned}$$

For the special case in which the x, y, z axes are coincident with the principal axes 1, 2 and 3 equation (7) reduces to

$$\begin{aligned}
\varepsilon_1 &= 1/E\ [\ \sigma_2 - \upsilon\ (\ \sigma_2 + \sigma_3\ )] \\
\varepsilon_2 &= 1/E\ [\ \sigma_3 - \upsilon\ (\ \sigma_3 + \sigma_1\ )] \\
\varepsilon_3 &= 1/E\ [\ \sigma_3 - \upsilon\ (\ \sigma_1 + \sigma_2\ )]
\end{aligned} \qquad (11)$$

For an isotropic material the stress strain relations can also be written in terms of the stress deviators s_{ij}

$$s_{ij} = \sigma_{ij} - \delta_{ij}\ \sigma_{kk}/3 \qquad (12)$$

The corresponding strain deviators $\mathbf{e}_{ij}$ can be defined in a similar way

$$\mathbf{e}_{ij} = e_{ij} - \delta_{ij}\, e_{kk}/3 \qquad (13)$$

The isotropic elastic stress strain relations can then be written in terms of the deviatoric and volumetric strain $\mathbf{e}_{ij}$ and e_{kk}

$$\mathbf{e}_{ij} = s_{ij}/2G$$
$$e_{kk} = s_{kk}/3B \qquad (14)$$

Or in terms of total strains e_{ij}

$e_{ij} = s_{ij}/2G + s_{kk}/3B$

Where B is the bulk modulus $B= E/3(1-2\upsilon)$

1.4 Yield Criteria

Linear elastic deformation is limited to stress states which do not satisfy the conditions for the onset of yielding or plastic flow as defined by the Tresca or von Mises yield criteria. The von Mises yield criterion is often written in terms of the stress deviators or the equivalent stress σ_e

$$\sigma_e^{\,2} = 3/2\ Sij\, Sij \qquad (15)$$

In uniaxial tension ($\sigma_1 = \sigma_o$, $\sigma_2 = \sigma_3 = 0$)

$$\sigma_e = \sigma_1 = \sigma_o$$

where σ_o is the initial yield stress. The Tresca yield criterion is sometimes used as an alternative to that proposed by von Mises. This criterion is written in terms of the maximum and minimum principal stresses σ_{max} and σ_{min}

$$\sigma_{max} - \sigma_{min} = 2k = \sigma_o \qquad (16)$$

where k is the yield stress as measured in shear. $de_{ij}^{plastic}$, Reuss assumed the plastic component of the strain increments to be proportional to the deviatoric stresses

$$de_{ij}^{plastic} = S_{ij}\, d\lambda \qquad (17)$$

$d\lambda$ is a factor of proportionality, which is not necessarily constant. If the total plastic strain is required it must be integrated along the strain path taken. The total strain increment for an elastic-plastic material is written as the sum of elastic and plastic components

$$de_{ij} = de_{ij}^{plastic} + de_{ij}^{elastic} \qquad (18)$$

Then

$$de_{ij} = S_{ij}d\lambda + dS_{ij}/2G + (1-2\upsilon)\, d\sigma_{kk}/E \qquad (19)$$

$$d\lambda = de_e/\sigma_e$$

1.5 Plane Stress and Plane Strain

Full three dimensional problems are in general very difficult to solve without introducing simplifications such as those allowed by symmetry. It is thus very desirable to simplify three dimensional problems by reducing them to two dimensions and thus diminish the number of variables in the problem. In this context it is appropriate to introduce the concepts of plane stress and plane strain as applied to fracture mechanics. The mathematical definition of plane strain, requires that the out of plane

displacement shall be zero, or constant for generalized plane strain. Thus the displacements are only dependent on the x,y, coordinates.

$$U = u(x,y)$$
$$V = v(x,y) \qquad (20)$$
$$W = 0 \quad \text{(or constant)}$$

Alternatively the definition can be given in terms of strains:

$$\varepsilon_z = \partial w/\partial z = 0$$
$$\varepsilon_{zx} = \partial w/\partial x + \partial u/\partial z = 0$$
$$\varepsilon_{xz} = \partial w/\partial y + \partial v/\partial z = 0 \qquad (21)$$

Using Hooke's Law for an isotropic elastic material the corresponding stresses are.

$$\sigma_z = \upsilon\,(\sigma_x + \sigma_y)$$
$$\tau_{zx} = \tau_{xy} = 0 \qquad (22)$$

In contrast, in plane stress the out of plane components of stress are zero and :

$$\sigma_z = \tau_{xz} = \tau_{yz} = 0 \qquad (23)$$

Hooke's law gives the out of plane strains as:

$$e_z = \upsilon\,(\sigma_x + \sigma_y) \qquad (24)$$
$$\gamma_{zx} = \gamma_{yz} = 0$$

1.6 Slip Line Field and Cracks

An important class of solution used for plasticity problems is rigid-plastic slip line field analysis (Hill (6)). The solution based on slip line field theory assumes that the plastic strains are very much greater than the elastic strains, and the material has a sufficiently low hardening rate to enable the stress-strain equations to be idealised as rigid elastic non-hardening plastic. It is also generally assumed that the plastically deforming material moves in plane strain condition by sliding along the lines of maximum shear stress

The slip line field consists of a set of curvilinear (α and β) axes which are orthogonal and represent the curvilinear axes of the planes of maximum shear stress and strain rate. As the stress of system changes, the orientation of these new axes can also change and the α and β lines also curve but must always lie at $\pm \pi/4$ to the direction of the principal stresses σ_1 and σ_2. The equilibrium equations referred to the α and β slip lines is

$$\sigma_m - 2K\phi = C\alpha = \text{constant on } \alpha \text{ line} \qquad (25)$$
$$\sigma_m + 2K\phi = C\beta = \text{constant on } \beta \text{ line}$$

These equations which are attributed to Hencky, restate the equilibrium equations for a material which is deforming plastically. The α and β axes can be identified correctly , by recalling that the largest principal stress must lie between the $+\alpha$ and $+\beta$ axes.

The stress at any point can be described completely if only $\sigma 1$, $\sigma 2$ and $\sigma 12$ are known. In the slip line field solution these three

variables can be reduced to two, the mean stress ($\sigma m = \sigma kk/3$) and the orientation of the plane of maximum shear stress, and the stresses at any point can be determined by identifying α and β lines. For an incompressible material under plane strain conditions:

$$\sigma_m = \sigma_{kk}/3 = \sigma_3 = 1/2\ (\sigma_1+\sigma_2) \qquad (26)$$

Therefore the principal stress in plastic deformation can be found if the mean stress is known. However the non principal stresses σ_{xx}, σ_{yy} and τ_{xy} can only be found if the orientation of the stress system is known.

The slip line field for three plane strain configurations are shown in Figs (1.2,1.4,1.5). The near tip stress field of the central crack panel (CCP) Fig (1.2) can be determined by identifing the α and β lines. The analysis starts at the free surface where the stresses are known to be

$$\sigma_z = \sigma_m = k$$
$$\sigma_y = 2\ k \qquad (27)$$
$$\sigma_x = 0$$

Because the slip lines are straight intense shear deformation is confined to slip planes eminating at 45 degree from the tensile direction, and the Hencky equation indicate that the stresses are constant at any point on the slip planes. The stress at the crack tip, is small, $\sigma_y = 2K$ and constant every where on the slip planes as represented by the broken line in Fig (1.3). The stress in this

geometry is independent of the distance from the tip and depends only on the angular coordinate ø, which is consistent with limiting HRR singularity for the sharp crack.

For the double edge deeply crack specimen the slip line field is shown in Fig (1.4), where the stress can be determined by following Hencky equations, starting at the free surface (3) where the stresses are 2K, K, and zero.

Following the α line the rotation of the slip line field through region (2) gives the stresses to be

$$\sigma_z = \sigma_m = k\,(1+ 3/2\ \pi\ -ø)$$
$$\sigma_ø = \sigma_r = \sigma_\alpha = \sigma_m \qquad (28)$$

where ø is measured from an axis straight ahead of the crack tip. Following the same slip line into the region a head of the crack the stress in region (1) can be given as

$$\sigma_z = \sigma_m = k\,(1+\pi)$$
$$\sigma_y = k\,(2+\pi) \qquad (29)$$
$$\sigma_x = k\pi$$

Although the stress at the crack tip is limited by yielding the strain becomes infinite at the crack tip and the strain singularity causes the crack tip to open and blunt to a radius δ. Within 2δ from the crack tip the stresses depend on the distance X of the point ahead of the crack, and the crack opening δ. For this geometry the stresses can obtained in terms of the crack tip opening δ and the slip line field are shown in Fig (1.5)

The smallest value of the stress at the crack tip,which is a free

surface is σ_y =2K, and the largest value at the end of the log spiral at 2δ as shown by the solid line in Fig (1.3). Following the α line the stress can be calculated to be

$$\sigma_m = \sigma_z = 2/3\ \sigma_o\ (1+2\ \ln(1+2x/\delta))$$
$$\sigma_y = 2/3\ \sigma_o\ (1+\ \ln(1+2x/\delta)) \qquad (30)$$
$$\sigma_x = 2/3\ \sigma_o\ (\ln(1+2x/\delta))$$

The slip line field solution of deeply notched bar under pure bending or by a combination of bending and shear force, was given by Green (7), and Green and Hill (8). They assumed that the strain in the direction parallel to the length of the notched is zero and the initial deformation develops through the ligament and does not extend to the surface of the bar on either side of notch Fig (1.6). They concluded that the shape of slip line field depends only on the shape of the root of the notch and the loading condition and is independent of the ratio of the notch to the thickness of the bar at the minimum section.

Green (9) emphasised that the above condition can only be true if the notch is sufficiently deep. In his modification of the slip line field for shallow cracks he assumed that the deformation extended to the back face of the bar on one or both sides of the notch as supported by the experimental work of Green and Hundy (10).

Following Green (9), an analysis of the slip line field of the shallow crack was performed by Ewing (11) who defined the critical width of the notch as a minimum width for which the depth-notch slip lines field solution applies Fig (1.6). For pure

bending the critical ratio (a/W) is close to 0.3 for plasiticity to be limited to the uncracked ligamen.

1.7 References

1. Anderson, W.E., An Engineer Views Brittle Fracture History, Boeing Report,(1969)

2. David Broek., Elementary Engineering Fracture Mechanics, Noordhoff International Publishing Co, Leyden, The Netherlands, (1974)

3. Biggs,W. D., The Brittle Fracture of Steel, McGraw-Hill, New York,(1969).

4. McMeeking, R.M., and Parks, D. M., "Elastic-Plastic Fracture Mechanics" , ASTM. STP 668, pp 175-191, (1971).

5. Timoshenko, S, and Goodier J.N "Theory of Elasticity" McGraw-Hill, New York (1951).

6. Hill R., "The Mathematical Theory of Plasticity" Oxford Univ, Press, (1950)

7. Green, A. P., J. Mech. Phys. Slds,. Vol 2, pp 254-268, (1953).

8. Green, A. P. and Hill R., J. Mech. Phys. Slds,. Vol 4, pp 256-268 (1956).

9. Green, A.P, J. Mech. Phys. Slds,. Vol 4, pp 254-268, (1956).

10. Green, A. P. and Hundy, B. B. , J. Mech. Phys. Slds,. Vol 4, pp 128-144, (1956).

11. Ewing, D. J. F., J. Mech. Phys. Slds,. Vol 16., pp 205-213 (1956).

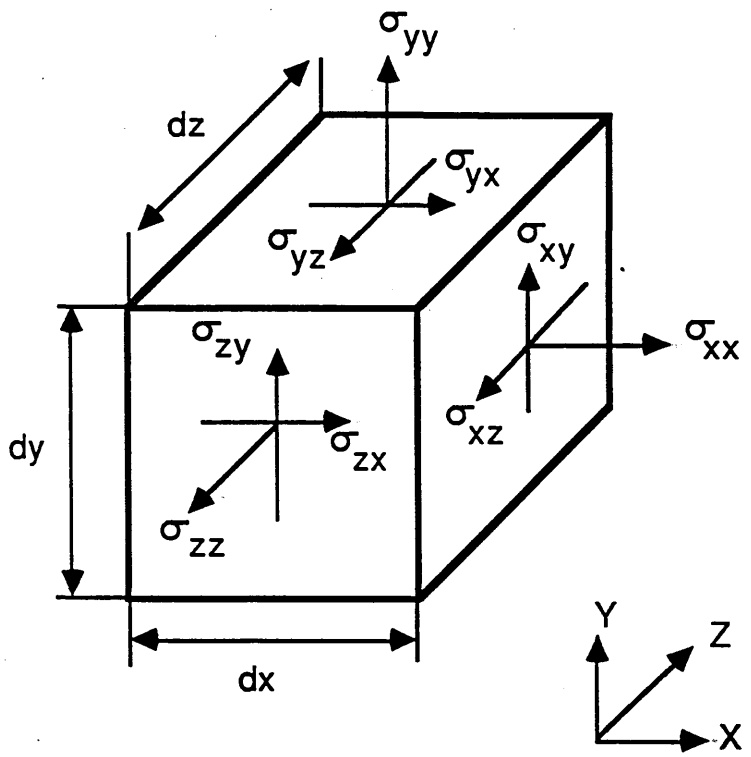

Fig (1.1)

State of stress in a small element.

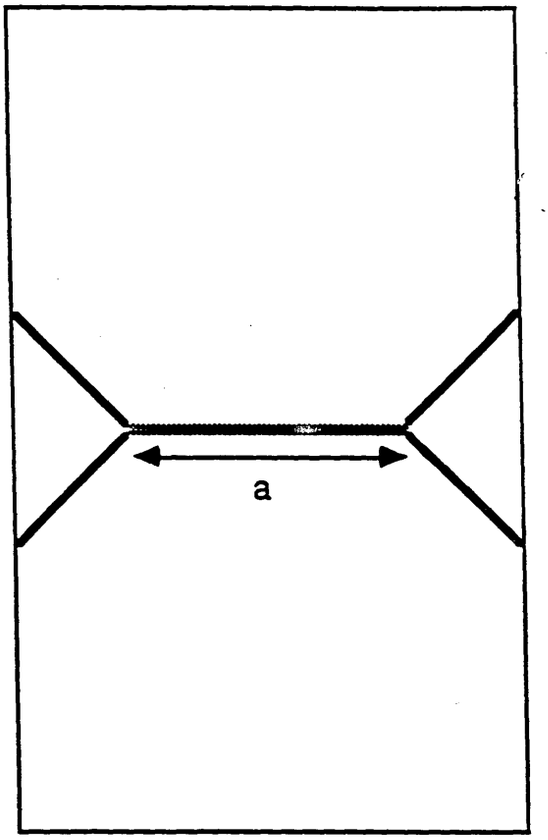

Fig (1.2)

The slip line field of the CCP

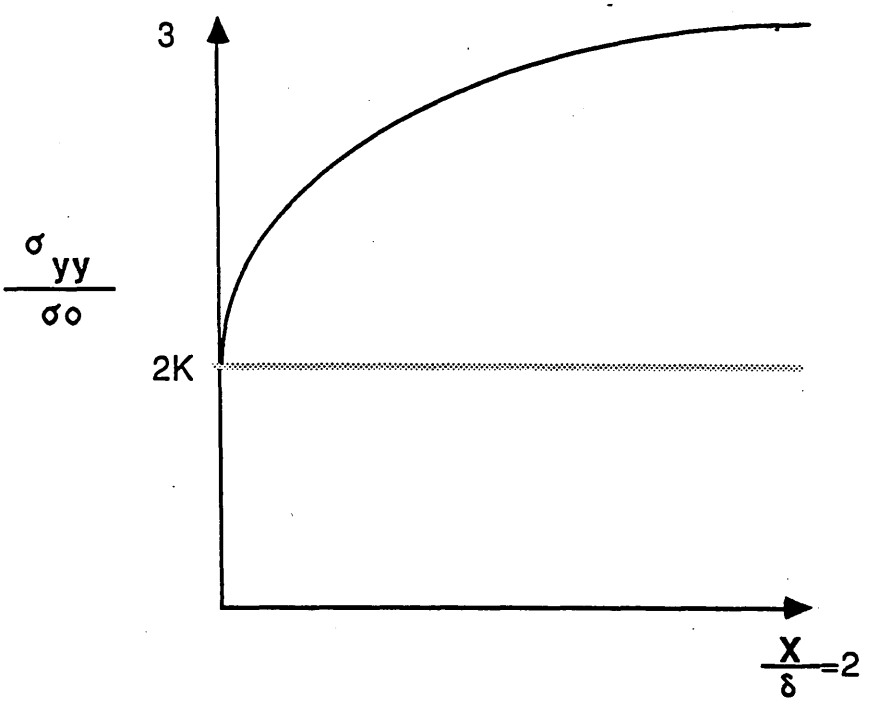

Fig (1.3)

The stress value of the CCP and blunted Crack

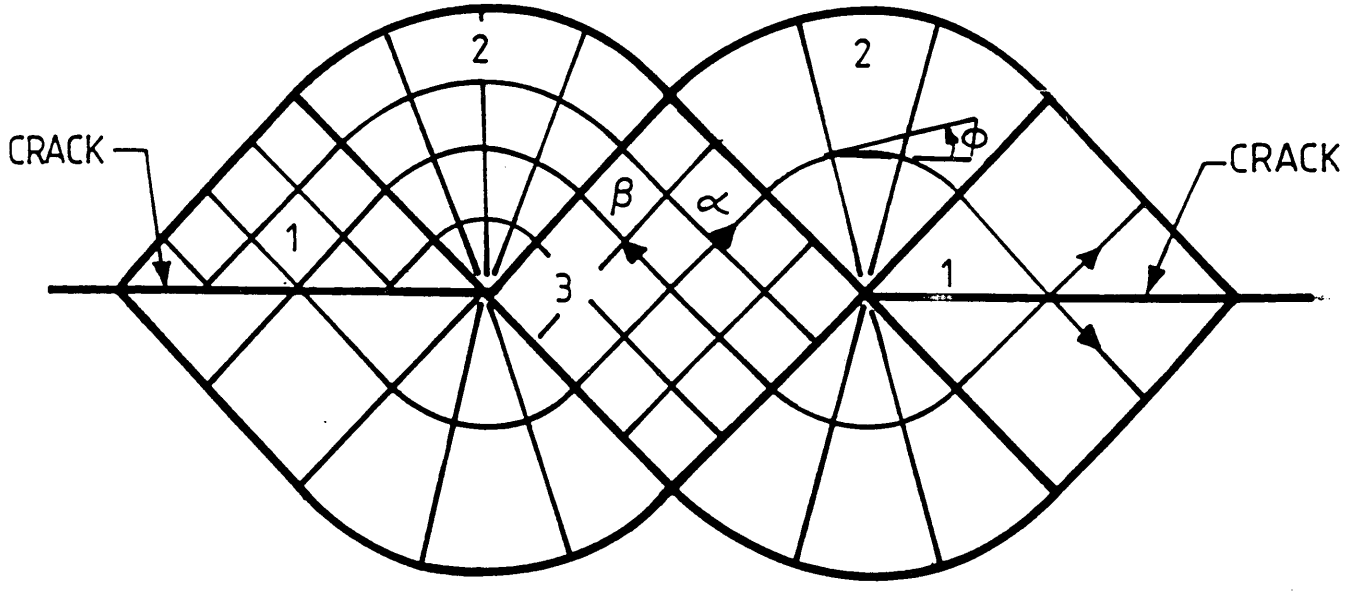

Fig (1.4)

The slip line field for the double edge deeplycrackedspecimen.

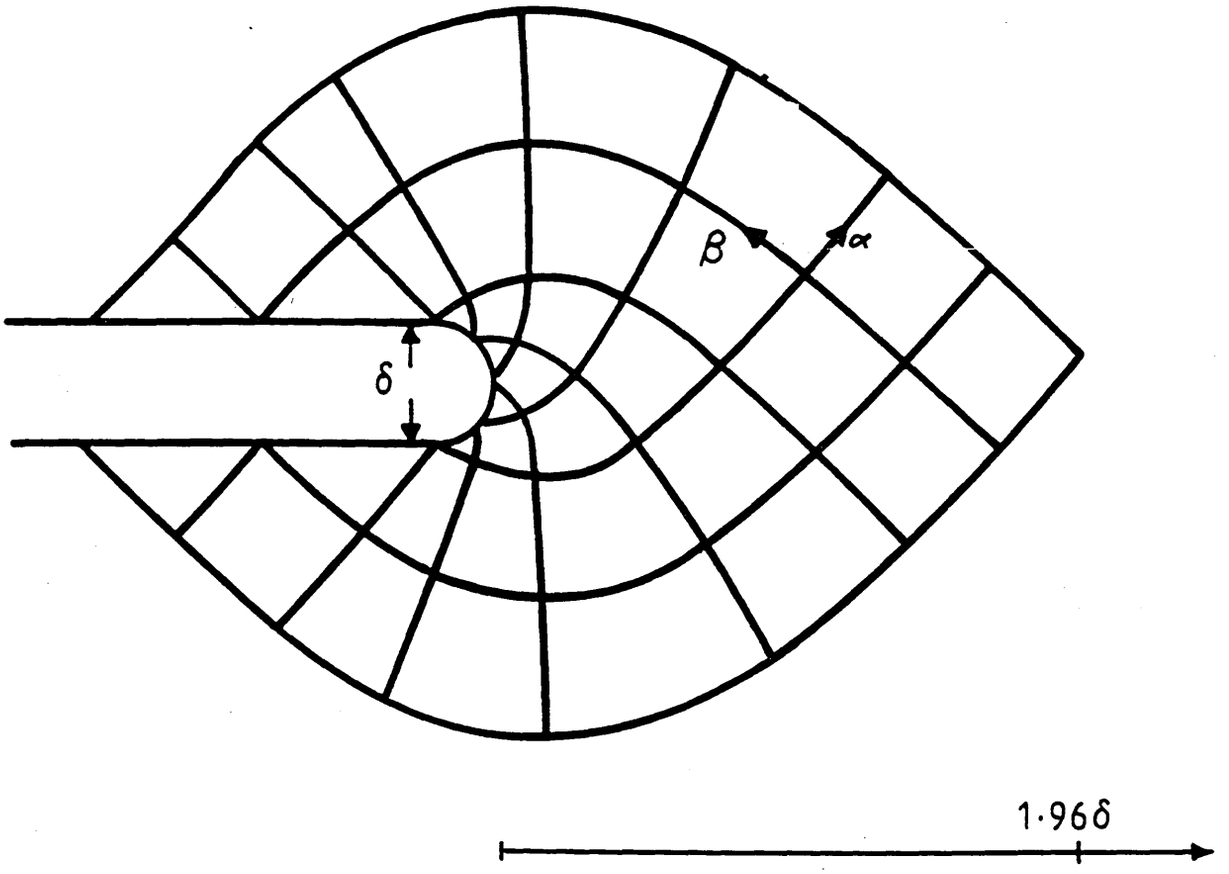

Fig (1.5)

The slip line field of the blunted crack

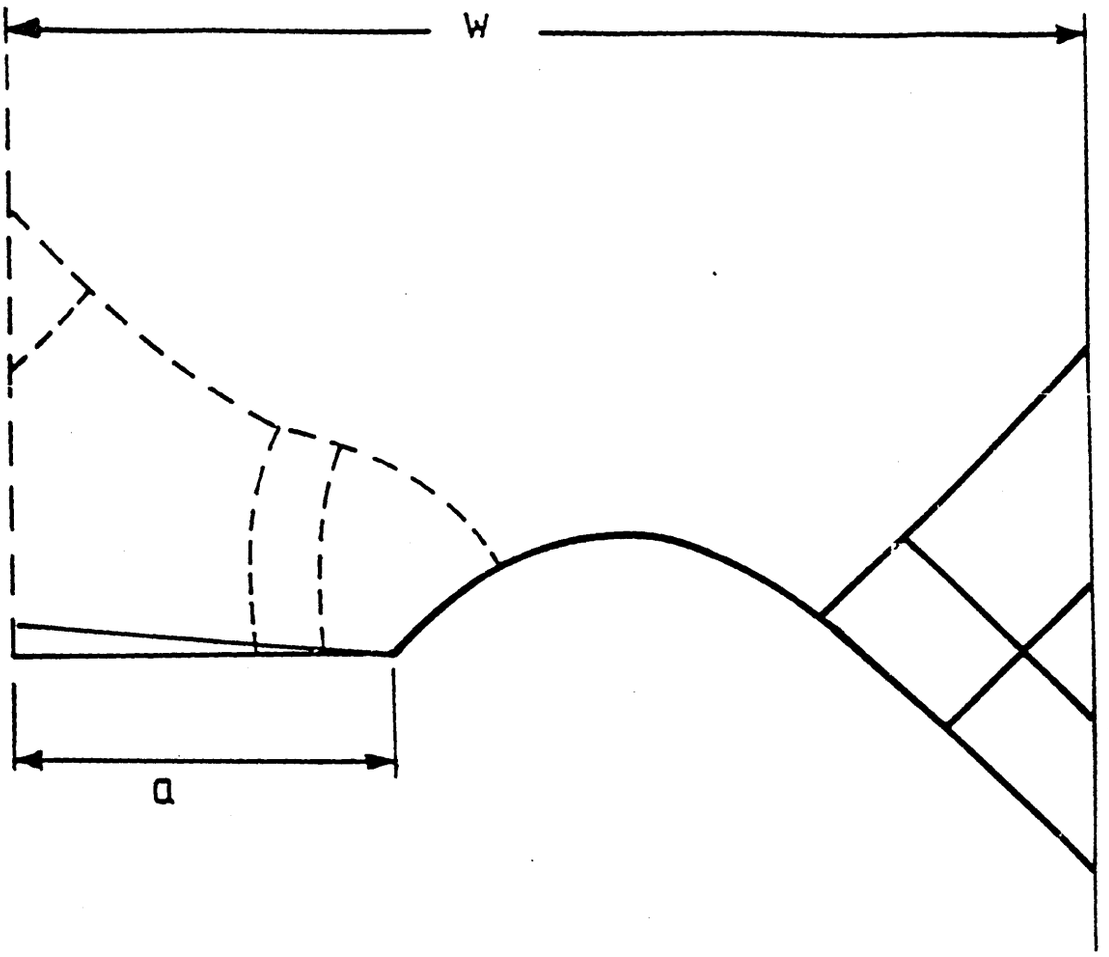

Fig (1.6)

The slip line field of deep and shallow cracks under bending follow Green (39)

Chapter (2)

LINEAR

ELASTIC FRACTURE MECHANICS

2.1 Introduction

For structures which contain cracks or flaws it is necessary to predict both the conditions under which the cracks will grow, and the residual strength of the structure. These predictions are the object of fracture mechanics. The main aim is to predict the critical crack size at which failure occurs and how long it takes for the crack to grow from an initial size, to the critical condition at which failure occurs. As a starting point for a discussion of fracture mechanics it is essential to realise that cracks and flaws produce severe stress concentrations.

2.2 Stress Concentration Factors

Stress concentrations assume major importance in engineering design because virtually all failures occur at stress concentrations The maximum stress at any section is customarily expressed in terms of the nominal stress multiplied by a stress concentration factor, which is the ratio of the maximum stress in the body to the applied stress

Stress concentration factors can be obtained from fatigue tests by comparing the fatigue life of corresponding notched and unotched specimens, and experimental methods for determining stress concentration factors have been used extensively since 1930. The first mathematical analysis of stress concentration

factors appeared in the literature shortly after 1900. As an example consider the problem of an elliptical hole, with semi axes a and b, in a large plate subject to tension, as illustrated in Fig (2.1). The plate is sufficiently large, in comparison with the hole that the reduction of cross-sectional due to the hole can be neglected. The plate may be considered to be infinite Fig (2.1), and the stress- concentration factor pertaining to the peak stresses has been given by Robert (1) as:

$$k=1 + 2(a/b) \qquad (25)$$

Three limiting cases can be distinguished:

(a). For a circular hole a/b=1 and k=3

(b). For a crack parallel to direction of loading (a –> 0), k=1

(c). For a crack perpendicular to the direction of loading b->o and $k = \infty$

The infinite stress concentration factor associated with the final load case is particularly important. Cracks under loading modes which produce stress singularties are fundamental to the study of fracture.

2.3 Cracks in Linear Elastic Materials

A crack in a solid can be subject to three different modes of loading, namely the opening mode, or mode I, in which the displacements of the crack surfaces are perpendicular to the plane of the crack. The sliding mode or, mode II, in which the displacements of the crack surface are in the plane of the crack and perpendicular to the leading edge, and mode III, the tearing or

antiplane mode surface in which the displacements are parallel to the leading edge of crack. The superposition of these three modes describes the perfectly general case, although in practice mode I is usually the most important Fig (2.2).

Westergaard (2) has studied the stress field of an infinite plate of linear elastic material containing a crack of length 2a subject to a remote tensile loading, Fig (2.3). With respect to the crack plane the stresses at the crack tip can be expressed as a series in which the leading term has the form.

$$\sigma_{xx} = \sigma \sqrt{(a/2r)}\ fij(\text{ø}) + \text{"other terms"}$$
$$\sigma_{yy} = \sigma \sqrt{(a/2r)}\ fij(\text{ø}) + \text{"other terms"} \qquad (26)$$
$$\tau xy = \sigma \sqrt{(a/2r)}\ fij(\text{ø}) + \text{"other terms"}$$

Here, a is the crack length and the other terms on the series are bounded at the crack tip. Fig (2.3) shows the cylindrical co-ordinate system (r, ø) centered at the leading edge of the crack and the stress components on an element ahead of the crack. As r approaches zero, the stresses approach infinity and there is a singularity at the crack tip r=0. In fact whatever the geometry and loading, the stresses at a crack tip have a singularity of the order $r^{-1/2}$ and the asymptotic linear elastic solution for the stress ahead of the crack can be written in the generalised form.

$$\sigma_{ij}\ (r,\text{ø}) = \frac{\sigma\sqrt{(\pi a)}}{\sqrt{2\pi r}}\ f_{ij}\ (\text{ø}) \qquad (27)$$

Rearranging equation (26) the stress intensity factor K_I can be defined as:

$$K_I = \lim_{r \to 0} \sqrt{(2\pi r)}\ \sigma_{22} \qquad (28)$$

The parameter K_I is the stress intensity factor which is a function of loading and geometry, and has the dimension of ($Nm^{-3/2}$), and for the other modes the stress intensity factors can be formally defined as:

$$K_{II} = \lim_{r \to 0} \sqrt{(2\pi r)}\ \sigma_{21}$$

$$K_{III} = \lim_{r \to 0} \sqrt{(2\pi r)}\ \sigma_{23} \qquad (29)$$

Shih (3) has pointed out that there is a mistake in Westergaard's work (27), but this mistake does not affect the solution of the strength of the stress singularity. Generally the stress intensity factor can be expressed in the form.

$$K_I = F(a/w)\ \sigma\sqrt{(\pi a)} \qquad (30)$$

Here F(a/w) is a dimensionless function of the geometry which has been tabulated for many practical cases by Tada et al (4).

The strains ahead of the crack can also be expressed in terms of the stress intensity factor.

$$\varepsilon_{ij} = \frac{K_I}{\sqrt{(2\pi r)}\ E}\ f_{ij}(\text{ø}) \qquad (31)$$

As the strain is the derivative of the displacement with respect to length, the displacement is the integral of strain and the displacements approach the crack tip as $r^{1/2}$

$$u = \left\{K_I\ [r/2\pi]^{1/2}\ h_x(\text{ø})\right\} / E \qquad (32)$$

$$v = \left\{K_I\ [r/2\pi]^{1/2}\ h_y(\text{ø})\right\} / E \qquad (33)$$

Here hx(ø), hy(ø) express the angular variation of displacement. Along the crack surface ø = π, and u is directly proportional to $r^{1/2}$ and v=0, and the crack opens into a parabola near the tip.

2.4 Small Scale Yielding and Limits of Applicability of L.E.F.M.

In the elastic field a stress singularity exists at the crack tip and the components of stress σ_x and σ_y approach infinity as the crack tip is approached. In real materials, however there is always a region around the crack tip where plastic deformation occurs because the yield criteria are violated by the elastic stress system. The condition in which there is only local yielding at the

crack tip and the surrounding elastic field controls the crack tip region is called small scale yielding. It is to this problem that linear elastic fracture mechanics or LEFM is applicable. When the plastic zone is small compared with the other dimensions of the body, plasticity can be viewed as a minor perturbation to the elastic field which can be described by equation (27), and characterized by the stress intensity factor K.

The radius of the plastic zone r_p can be derived from the von Mises yield criterion

$$(\sigma_1-\sigma_2)^2 + (\sigma_2-\sigma_3)^2 + (\sigma_3-\sigma_1)^2 = 2\,\sigma_o^2 \qquad (34)$$

The asymptotic elastic stress field can be written in terms of the principal stresses $\sigma_1, \sigma_2, \sigma_3$ as

$$\sigma_1 = \frac{K_I}{\sqrt{(2\pi r)}} \left[\cos\frac{\phi}{2}\left(1+\sin\frac{\phi}{2}\right)\right]$$

$$\sigma_2 = \frac{K_I}{\sqrt{(2\pi r)}} \left[\cos\frac{\phi}{2}\left(1-\sin\frac{\phi}{2}\right)\right] \qquad (35)$$

For plane strain

$$\sigma_3 = \upsilon(\sigma_1+\sigma_2) = \frac{K_I}{\sqrt{(2\pi r)}} \left[\cos\frac{\phi}{2}\right]$$

for plane stress

$\sigma_3 = 0$

The boundary of the plastic zone as a function of ø can be derived to a first approximation by substituting equation (35) into equation (34)

For plane strain

$$K^2/(2\pi r)\ [3/2\ \sin^2\text{ø}\ (1-2\upsilon)^2(1+\cos\ \text{ø}\ )] = 2\ \sigma_o{}^2 \qquad (36)$$

while for for plane stress:

$$K^2/(2\pi r)\ [1+3/2\ \sin^2\text{ø} + \cos\ \text{ø}\ ] = 2\ \sigma_o{}^2 \qquad (37)$$

Therefore the plastic zone as a function of ø can be written for plane stress as

$$r_p(\text{ø})\ = (1/4\pi)\ (K/\sigma_o)^2\ [1+3/2\ \sin^2\text{ø} + (\cos\ \text{ø}\ )] \qquad (38)$$

For plane strain

$$r_p(\text{ø})\ = (1/4\pi)\ (K/\sigma_o)^2\ [3/2\ \sin^2\text{ø}\ (1-2\upsilon)^2(1+\cos\ \text{ø}\ )] \qquad (39)$$

It is clear that the plastic zone in plane stress is larger than that in plane strain, particularly ahead of the crack tip ø=0 as illustrated in Fig (2.4). This is because a higher hydrostatic stress occurs in plane strain which does not promote yielding.

Due to the high stress-strain gradient near the crack tip, the zone of plasticity at the tip is constrained against contraction along the crack front by the elastic material, thus creating plane strain conditions in thick plates

The ratio of the plastic zone radius r_p to the thickness of the

specimen B, determines whether plane stress or plane strain exists. If (r_p/B) is very much less than unity, plane strain exists. The critical stress intensity factor for thick bodies in which perfect plane strain conditions apply is a material constant known as the plane strain fracture toughness, denoted K_{Ic}. The British Standard (5), requirement for small scale yielding and valid LEFM is:

$$B,a,(w-a) \geq 2.5\ (K_{Ic}/\sigma_0)^2 \qquad (40)$$

where B is the thickness of the specimen, a is the crack length, and w is the width of the specimen as shown in Fig (2.5).

A different approach to determine the extent of the plane stress plastic zone was developed by Dugdale (6). In his analysis plastic deformation is assumed to occur in a strip in front of the crack In these calculations the plastic zone radius is:

$$r_p = 0.393\ (K_I/\sigma_o)^2 \qquad (41)$$

Dugdale (6) argued with Irwin (7) that the effective crack length is longer than the physical crack length as shown in Fig (2.6). The Dugdale plastic zone is larger than that calculated by Irwin, the latter analysis gives a plastic zone diameter as:

$$r_p = 0.318\ (K_I/\sigma_o)^2 \qquad (42)$$

As pointed out by Hahn et al (8) the plastic zone is effected by

both the plane state and slightly by strain hardening. Many experimental investigations have measured the plastic zone size and shape, however experimental methods are difficult particularly in plane strain conditions. Hahn et al (8), used specimens of silicon-iron and pointed out that the shape of the plastic zone was reasonably approximated by the Dugdale strip yield models in plane stress. Davidson and Lankford (9) used other experimental techniques including the use of electron microscopy.

2.5 Potential Energy Release Rate (G)

The energetics of crack advance were first-considered by Griffiths (10) who considered crack advance in an infinite plate of unit thickness with a central crack of length 2a, loaded with a remote tensile stress σ. The basic argument is that as the crack extends, elastic strain energy in the material is released to create the new area which absorbs the energy. When the energy release rate, is greater than or equal to the energy consumption rate crack propagation is energetically favourable. If Ue is the elastic energy of an uncracked plate, Us is the change in surface energy caused by creating the crack surface, Uc is the change in elastic strain energy caused by introducing a crack in the plate and W, is the work performed by the external forces. Then the total potential energy of the system U_t can be written as:

$$U_t = Ue + Uc + Us - W \qquad (43)$$

The change in strain energy produced by introducing a crack of length 2a can be calculated by the work done by a stress σ acting

between +a and -a on the uncracked body, to produce a traction free surface which deforms into an ellipse:

$$Uc = \int_{-a}^{a} \sigma\, u\, dx = 2\int_{o}^{a} \sigma * 2\,\sigma \sqrt{(a^2-x^2)/E^-}\, dx \qquad (44)$$

Giving

$$Uc = \pi\, \sigma^2\, a^2/E^- \qquad (45)$$

Where $E^- = E$ for plane stress and $E^- = E/(1-\vartheta^2)$ for plane strain. The surface energy of the crack can be written in terms of the surface energy per unit area of the material γ_e:.

$$Us = 2\,(2a\,\gamma_e) \qquad (46)$$

The condition for crack extension is obtained by setting

$$(\partial U_t/\partial a) = 0$$

$$\partial(\pi\,\sigma^2\,a^2/E^- + 4\,a\,\gamma_e)\,/\partial a = 0 \qquad (47)$$

Then

$$\pi\,\sigma^2\,a/E^- = 2\,\gamma_e \qquad (48)$$

$(\pi\,\sigma^2\,a^2/E^-)$ is called potential energy release rate G, and it is defined to be the energy release per unit area of crack advance.

$$G = (\partial U_t/\partial a)\,(1/B) \qquad (49)$$

While the right hand side of equation (48) is called the crack

resistance.

As pointed out by Irwin (11) the Griffith theory strictly applies to a material in which there is no plasticity at the crack tip. However Irwin proposed equation (49) could be modified for materials which exhibit plastic deformation by replacing the surface energy by the sum of the surface energy and plastic strain work γ_p:

$$\pi \sigma^2 a/E^- = 2 (\gamma_e + \gamma_p) \qquad (50)$$

For most materials ($\gamma_e << \gamma_p$), and the surface energy can be neglected

Within the context of the linear theory of elasticity, there is an important connection between the stress intensity factor and the rate of change of the potential energy of a cracked body. Fracture occurs when the stress intensity factor reaches it's critical value (K_C), and identically when the strain energy release rate reaches a critical value (G_C). The energy approach is thus equivalent to the stress field approach. The relationship between the stress intensity factor and the energy release rate can be generalised to cover the three basic loading modes I, II , III

$$G_I = K_I^2/E^-$$
$$G_{II} = K_{II}^2/E^-$$
$$G_{III} = (1-\upsilon)\, K_{III}^2/E^-$$
$$G = G_I+G_{II}+G_{III}$$
$$G = [(1-\vartheta)\, K_I^{\,2}/2G]+[(1-\vartheta)\, K_{II}^{\,2}/2G]+[K_{III}/2G] \qquad (51)$$

Where $E=2(1-\vartheta)G$ and $E^{-}= E$ for plane stress and. $E^{-}=E/(1-\vartheta^2)$ for plane strain.

2.6 Methods of determining Stress Intensity Factors

Many methods of determining stress intensity factors have been developed, and a wide range of solutions, for two-dimensional configurations are now available in the literature (Isida (12))

The common methods are set out in Fig (2.7). These methods are divided into three groups, in which the choice of the method depends on the time available, the required accuracy, the cost,the frequency of use and how simply the structure can be modelled. Some of the methods are described briefly and emphasis is placed on those methods which are most suitable for planar geometries in tension and bending.

2.6.1 Finite Element Methods

Finite element analysis is a numerical method which can be used to determine the stress intensity factor, when the structure cannot be modelled analytically. The application of the finite element method to determine stress intensity factor has undergone rapid development, as the method has great versatility, and allows the analysis of complicated engineering geometries (13,14). It also enables the treatment of three dimensional problems and permits the analysis of crack tip plasticity. Finite element methods fall into three categories. Firstly those which allow stress intensity factors to be determined directly, secondly those which require stress intensity factor to be determined indirectly

by considering the change in the energy due to the presence of the crack, and thirdly, those involving special crack tip elements.

2.6.1.1 Direct Finite Element Methods

Chan et al (15) have discussed the methods which can be used to estimate the stress intensity factor directly, once the numerical solution has been obtained from a particular finite element representation. Two specific methods were considered .

(i)- Stress method

(ii)- Displacement method.

2.6.1.1.1 The Stress Method:

The stress intensity factor can be determined directly from the stress numerically calculated ahead of the crack. The asymptotic elastic stresses take the form :

$$\sigma_{ij}=(K_I/\sqrt{2\pi r})\ f_{ij}(\text{ø}) \qquad (52)$$

where fij are the following universal functions of angle (ø).

$$f\text{xx}(\text{ø})= \cos(\text{ø}/2)\ [1-\sin\ (\text{ø}/2)\ \sin\ (3\text{ø}/2)]$$
$$f\text{yy}(\text{ø})= \cos(\text{ø}/2)\ [1+\sin\ (\text{ø}/2)\ \sin\ (3\text{ø}/2)] \qquad (53)$$
$$f\text{xy}\ (\text{ø})= \sin(\text{ø}/2)\ \cos(\text{ø}/2)\ \cos(3\text{ø}/2).$$

The stress σ_{ij} in the vicinity of the crack tip can be substituted into eqs (27) and the value of K_I can be calculated as the limit of

$$\sigma_{ij}\ (\sqrt{2\pi r})\ /\ f_{ij}(\ \text{ø}) \quad \text{as } r \to 0 \qquad (54)$$

This is most conveniently evaluated straight ahead of the crack with ø=0 when

$f_{ij}(ø) = 1$

and

$$K_I = \lim_{r \to 0} \sigma_{ij}\sqrt{(2\pi r)} \qquad (55)$$

2.6.1.1.2 The Displacement Method:

Major emphasis has been placed on the displacement method due to it's simplicity and the easy with which displacements can be extrapolated to the crack tip. In particular Kobayashi et al (16) conclude that the results obtained from the displacement method are more accurate than those obtained from the stresses. The displacement method involves a correlation of the finite element nodal point displacements with the asymptotic crack tip displacement. The plane strain displacements are:

$$u = K_I\,[r/2\pi]^{1/2}\, f_{ij}(ø) / G \qquad (56)$$

By substituting the displacement u at some point near the crack tip K can be calculated from a parameter which is here defined as K_I^*

$$K_I^* = ui\, G\, \sqrt{(2\pi/r)}\, /f_{ij}(ø) \qquad (57)$$

The stress intensity K_I is given by the limit of K_I^* as $r \to 0$,

$$K_I = \lim_{r \to 0} K_I^*$$

From a plot of K_I^* as a function of r at a fixed angle and a particular displacement component, the stress intensity factor K_I can be obtaind. K_I may also be determined from the crack surface displacement at some small distance r from the crack tip. The most accurate estimates are obtained from the v displacement on the crack surface.

2.6.1.2 Indirect Finite Element Methods

Indirect techniques involve the determination of the stress intensity factor from the potential energy decrease per unit crack advance G for plane strain and unit thickness, or from the change of compliance with crack length. If C is the compliance, of the plate and the displacement V = CP, where P is the load. The elastic energy contained in a cracked plate is written as

$$U_t = 1/2\ CP^2 \qquad (58)$$

$$G = -(\partial U_t/\partial a)/B = P^2/2B\ (\partial C/\partial a) \qquad (59)$$

From the relation between G and K .

$$K_I^2 = E^- G = E^-\ P^2/2B\ (\partial C/\partial a) \qquad (60)$$

The stress intensity factor is here related to the rate of change of compliance with crack length. Mowbray (17) analysed the same specimen geometry for several cracks of slightly different lengths

and was able to obtain the compliance as a function of the crack length, numerical differentiation of this relationship with respect to crack length enabled the determination of G and hence K.

2.6.2 The Virtual Crack Extension Method

The compliance method is limited by the need to compute complete solutions for incrementally different crack lengths. This problem is over come by the virtual crack extension method, which is an finite element technique based on the relation between the crack stress intensity factor and the potential energy release rate. The potential energy U_t can be expressed in terms of the stiffness matrix [M], the nodal force {F} and the nodal displacement {u} Zienkiewicz (18)

$$U=1/2\ \{u\}^t\ [M]\ \{u\}\ -\{u\}^t\{F\} \qquad (61)$$

where the superscript (t) indicates a matrix transpose. By differentiating equation (49), with respect to the crack length, the energy release rate G can be found as:

$$G=\left[\partial U_t/\partial a\right]_{load}=-\partial\{u\}^t\left[[M]\{u\}/\partial a-\{F\}\right]1/2\{u\}^t\partial[M]\{u\}/\partial a+\{u\}^t\partial\{F\}/\partial a \qquad (62)$$

The factor in square brackets on the right hand side of the above equation is zero, because [M] is symmetric.

$$G=\left[\partial U_t/\partial a\right]_{\text{load}} = (1-\upsilon^2)K^2/E = -1/2\{u\}^t\partial[M]\{u\}/\partial a+\{u\}^t\partial\{F\}/\partial a \qquad (63)$$

The matrix $\partial\{F\}/\partial a$, represents the change in the master stiffness per unit crack advance. Let the nodes surrounding the crack tip be arranged in two contours r_1 and r_2, and the crack direction be in the X direction as shown in Fig (2.8a). Virtual crack extension can be effected by moving the nodes within in the first contours r_1 in X direction, a small distance ∂a and while the other nodes remain their initial position as shown in Fig (2.8b). The master stiffness [M], which depends only only individual element geometries, displacement function and elastic properties, remains unchanged in regions interior to r_1 and exterior to r_2, except in the band of element between the contours.

The master stiffness matrix [M], can be written as the sum over all the element stiffness matrices [M], therefore:

$$-1/2\ \{u\}t\ \partial[M]\ \{u\}/\partial a = 1/2\ \{u\}t\ \sum_{i=1}^{Nc}\partial[mi]\ /\partial a\ \{u\} \qquad (64)$$

[mi] represents the element stiffness matrix. Therefore the stress intensity factor can be determined by:

$$G = (1-\upsilon^2)\ K_I^2/E = G\ = -1/2\ \{u\}^t\ \partial[M]\ \{u\}/\partial a \qquad (65)$$

The virtual crack extension method has the advantage that no special elements are required and it avoids determining the potential energy before and after crack extension. A solution for

only a single crack is required, and the crack is advanced by moving nodal points rather than by moving nodal tractions at the crack tip and performing a second analysis. The virtual crack extension method can be applied to three dimensional problems, and has been extended for the use in non-linear`elastic and elastic-plastic materials by Parks (19) .

2.6.3 Special Crack Tip Elements

Many types of special elements have been developed for calculating stress intensity factors. Blackburn (20), Barsoum (21) and Henshell and Shaw (22) have pointed out that second order elements with the mid side nodes of the crack tip element moved to the 1/4 -point position are particulary useful. The idea is to use 8 noded isoparametric element as a focused mesh concentric with the crack tip. In these elements the mid-side nodes are located at the quarter point position. This procedure allows the element to adopt the correct form of displacement function in which the displacements approach the crack tip as $r^{1/2}$ as given by eqs (32) and (33). These techniques provide the capability to model, the singularity which dominates the solution close to the crack front. This method enables stress intensity factors to be determined directly or in conjunction with virtual crack extension and, in general, requires fewer elements than the methods previously described.

2.6.4 Experimental Methods

Experimental methods are sometimes useful for obtaining approximate values of the stress intensity factor. They either use a known relationship between a measurable quantity such as the fatigue crack growth rate and the stress intensity factor, or attempt to measure the stress intensity factor by direct stress measurement on a model. Most methods are applicable only in laboratory conditions, but a few have a limited use under service conditions provided the load on a structure can also be measured (1). Photoelastic techniques have several advantages as, photoelasticity is a well known method for which experimental equipment and materials are widely available. By using the frozen stress technique photoelastic analysis can be extend to three dimensional configurations. Considerable use has been made of photoelasticity in determining stress concentration factors and this technique has been used for determine the stress intensity factor.

The growth rate of cracks extending under fatigue has been used to determine the stress intensity factor (Kobayshi (23)) .

$$da/dn = f(\Delta K) \qquad (66)$$

Here the rate of fatigue crack propagation is related to the range of the stress intensity factor ΔK. Where $f(\Delta K)$ can be determined from fatigue crack propagation in a specimen with known K_I solution to determine the stress intensity factor for a new configuration. This method generally gives reliable results, it is simple and can be applied to any three dimensional crack

problem in which crack growth experiments are possible.

The most widely applied experimental procedure is the compliance measurement. If the displacement measurements are made close to the crack tip, the effect of the crack size on the displacement decreases rapidly. The most accurate measurement of compliance can be expected if the point of the load application is as close to the crack as possible, which makes crack line loaded cases particularly suitable for this technique.

2.7 References

1. Robert, C. J., Stress, Strain and Strength, McGraw-Hill, New York,(1967).

2. Westergaard, H. M. : J. Appl. Mech., Vol 61, pp 49, (1939).

3. Sih, G. C., Int J. of Fracture. Mech., Vol 2 ,pp 475, (1966).

4. Tada, H., Paris, P.C. and Irwin, G.R., " The Stress Analysis of Crack Handbook",Del Research Corp Hellertown, Pennsylvania, (1973).

5. A.S.T.M, Standard E394-78 A. Standard Test method Plane Strain Fracture Toughness of Metalic Materials., Annual book of ASTM, Standard, part 10, pp 540-561., (1979)

6. Dugdale, D.S., J. Mech. Phys. Sol., Vol 8, pp 100-108, (1960)

7. Irwin,G.R: Fracture Hand Book VI pp 551-590 ,(1958).

8. Hahn, G.T, and Rosenfield, A.R., Acta Metallurgica, Vol 13, pp 293-306 (1966).

9. Davidson, D.L and Lankford., J. Fatigue Eng Material and Structure pp 439-446,(1979).

10. Griffith, A.A., Phil Trans Roy Soc, A221, pp 163., (1920).

11. Irwin, G.R., Appl Mater Res., Vol 3, pp 65, (1964)

12. Isida, M., Eng Fract Mech., Vol 2 , pp 61., (1970).

13. Parks, D. M., Int J of Fracture Mech.Vol 10., pp 487., (1974)

14. Hayes ,E., Int J of Fracture Mech., Vol 8.,P157., (1972)

15. Chan , S.K., Tuba, and, Wilson, W.K., Eng Fract Mech., Vol 2., pp 1, (1970).

16. Kobayshi, A.S.,Maiden, D.E, Simon, J.B., American Society of Mechanical Engineering, 69-wA/pvp-12, (1969).

17. Mowbray, P.M.,Eng Fract Mech., Vol 2 , pp 173, (1970)

18. Zienkiewicz, O. C., "Finite Element Methods in Engineering Science" McGraw-Hill , (1971).

19. Parks, D.M., Comp Meth Applied Mech and Eng., vol 12, pp 353, (1977)

20. Blackburn, W.S., "Calculation of the Stress Intensity Factor at Crack Tip".,(1972).

21. Barsoum, N. O., Int J Num Method Engineering., Vol, 10, pp,25-37. (1976)

22. Henshell, N.B and Shaw, K.G.,Int J Num Method Engineering. Vol, 9, pp249-509, (1975)

23. Kobayshi, A.S., Experimental Techniques for Fracture Mechanics SESA Monograph (1973).

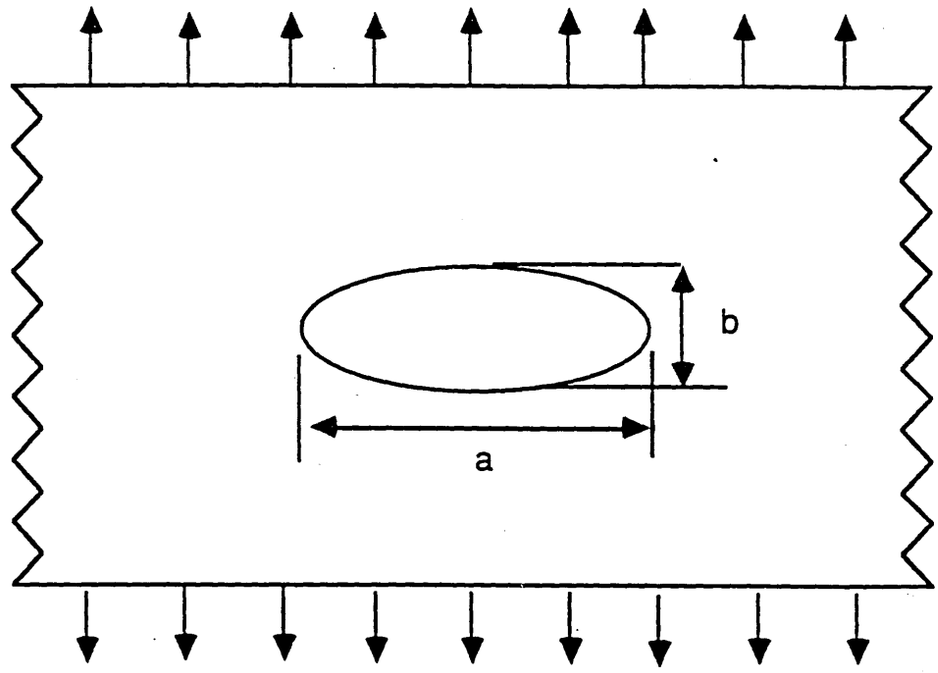

Fig (2.1)

An infinite plate with an elliptical hole under remote tensile loading.

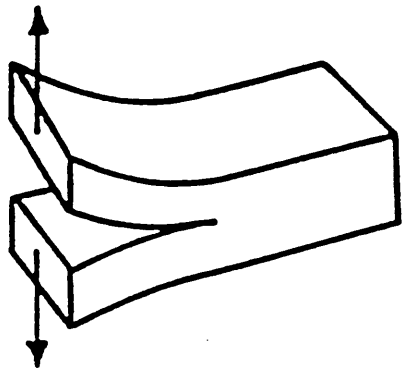

Mode 1

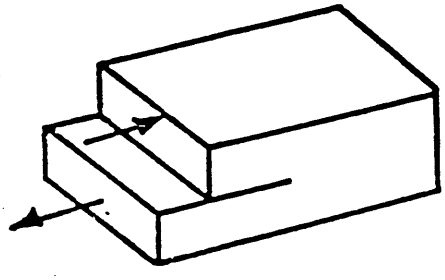

Mode II

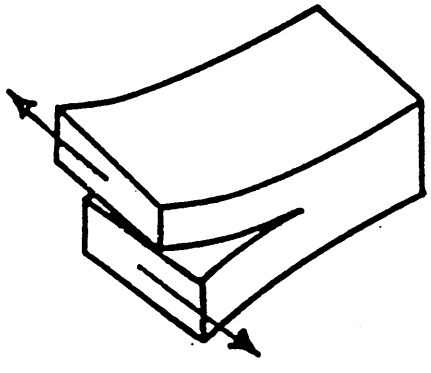

Mode III

Fig (2.2)

The three basic mode of cracking.

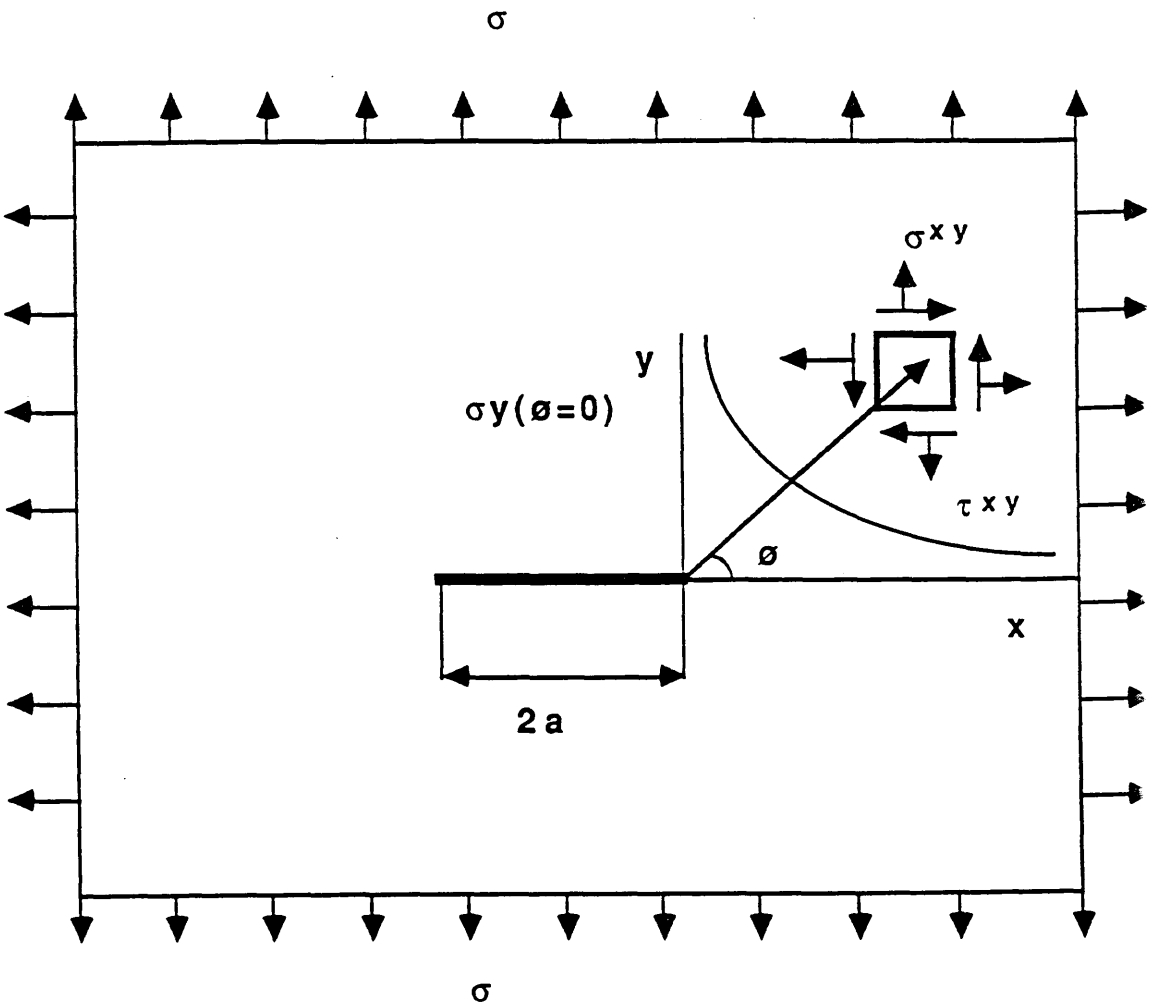

Fig (2.3)

An infinite plate containing a central crack under remote tensile loading.

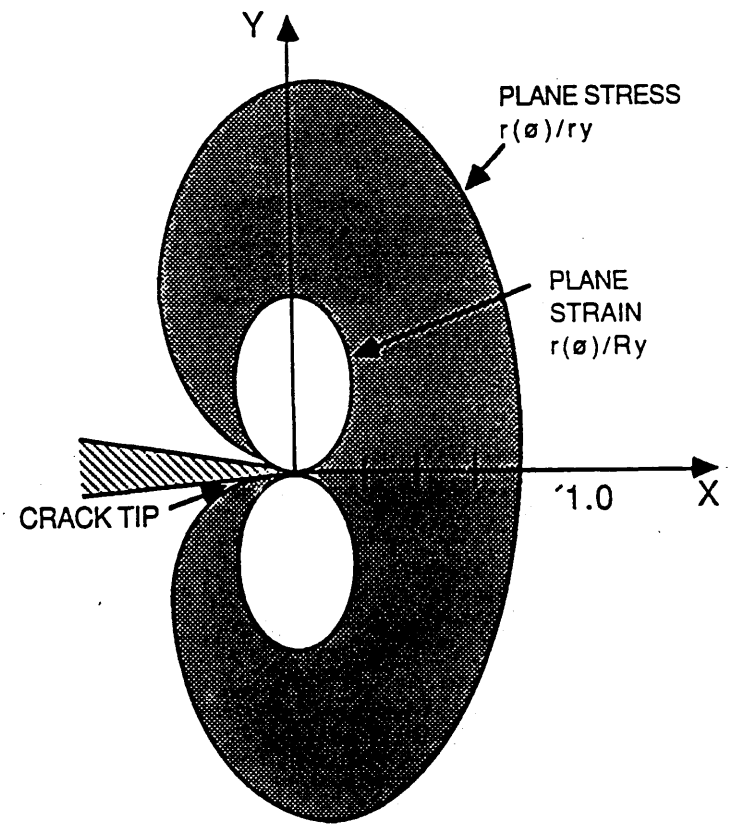

Fig (2.4)

Dimensionless plane stress and plane strain plastic zone.

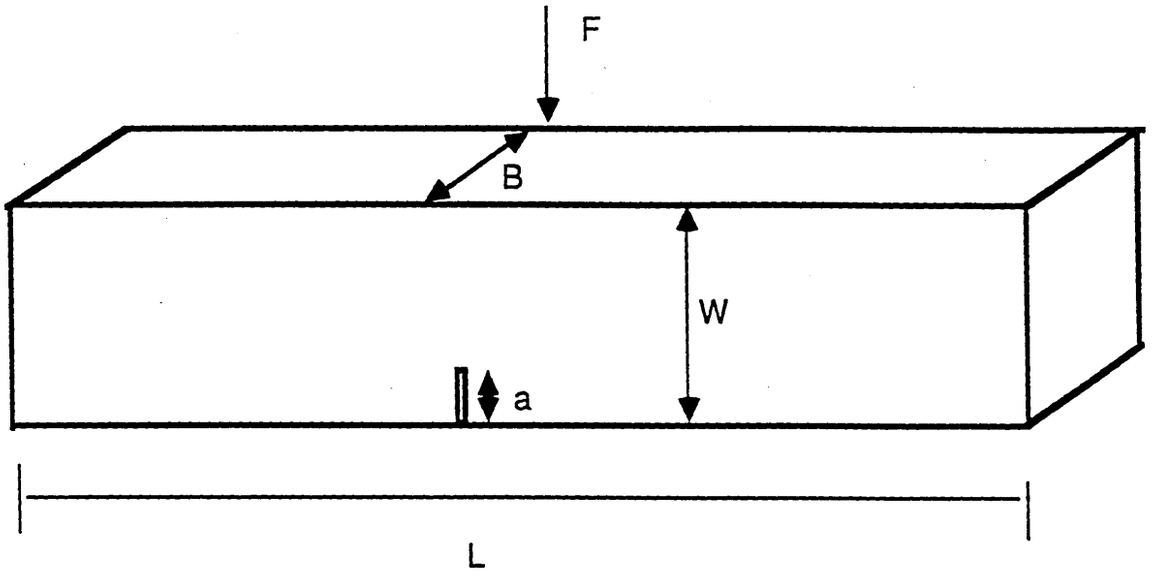

Fig (2.5)

Fracture mechanics standard three point bend specimen.

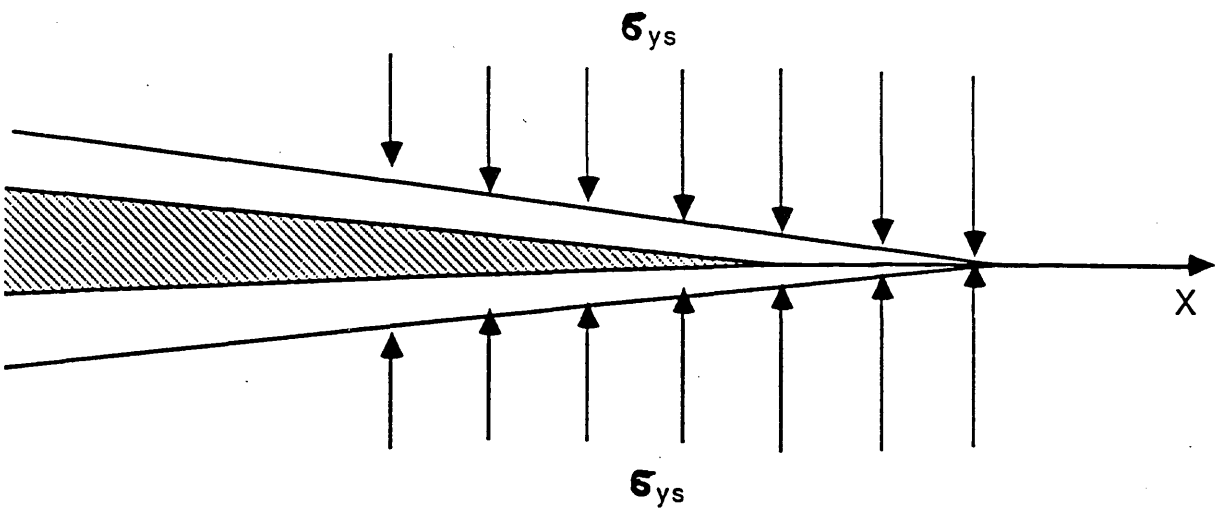

Fig (2.6)

Schematic of Dugdales analysis.

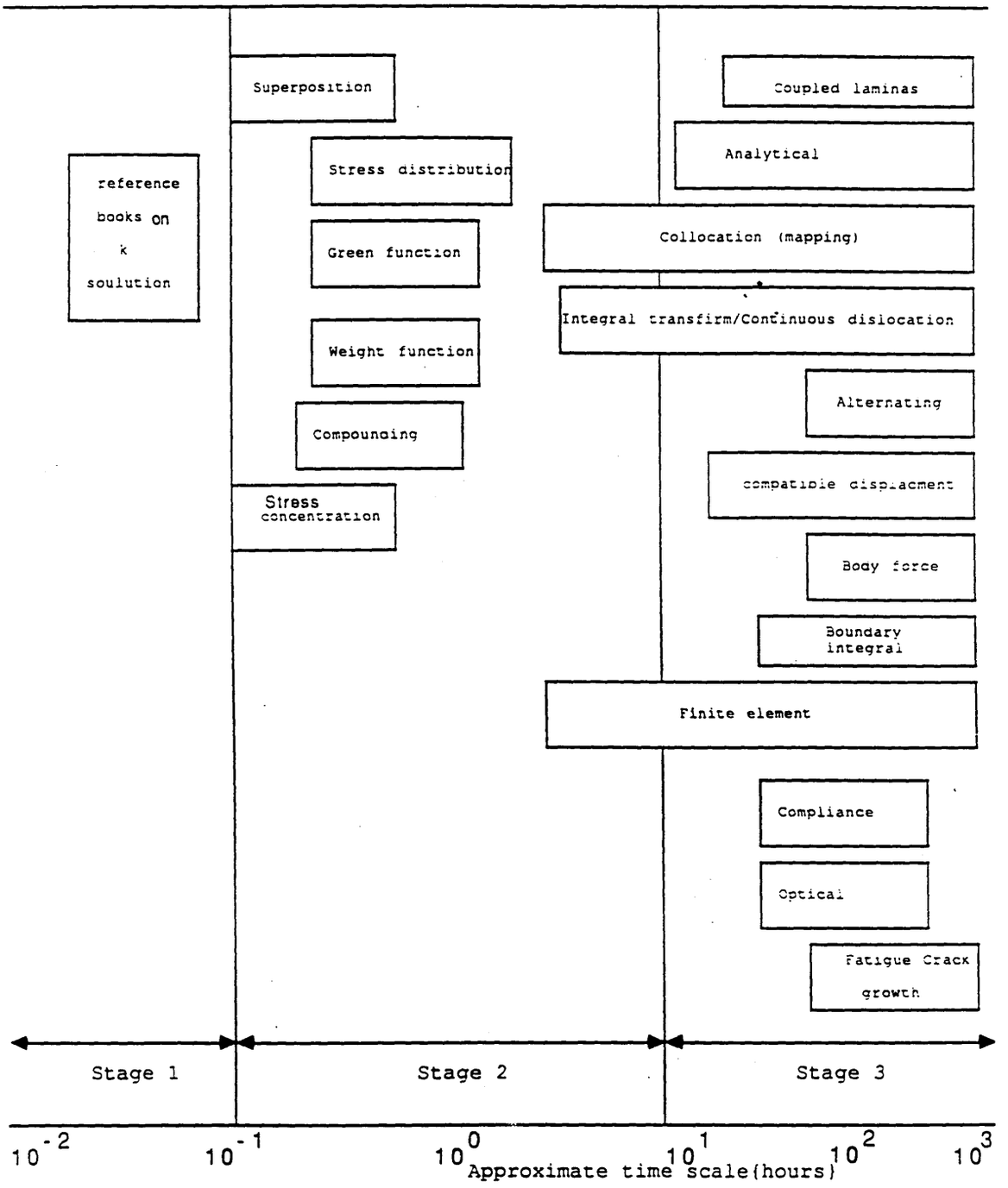

Fig (2.7)

Methods for determining stress intensity factors.

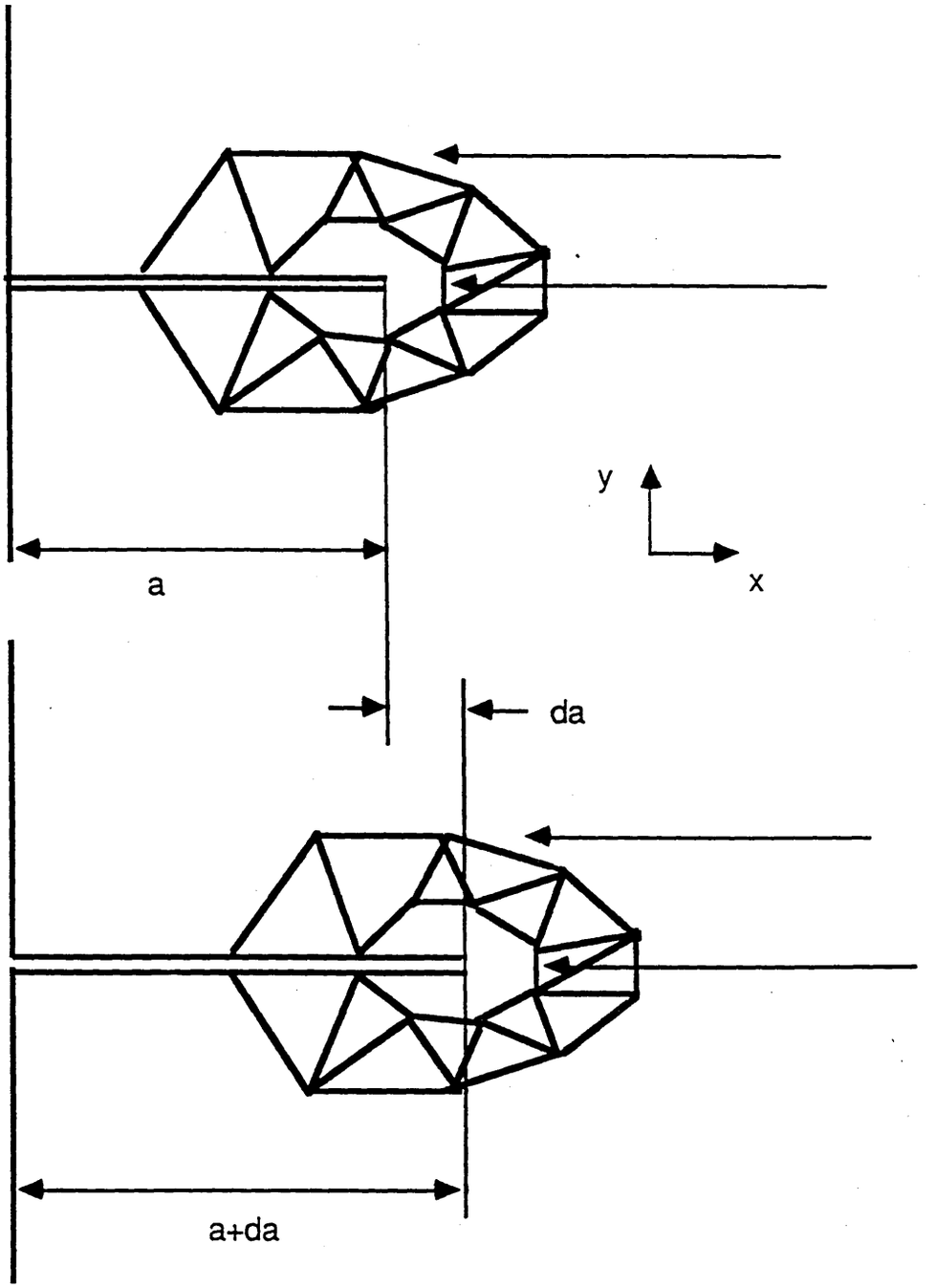

Fig (2.8)

The arrangement of nodes in the crack tip area for virtual crack extension method

Chapter (3)

RESULTS OF LEFM CALCULATIONS

3.1 Introduction

It has been noted that the stress intensity factor can be estimated by comparing numerical solutions with the asymptotic crack tip field. In this section finite element calculations of the stress intensity factor are given as a precursor to elastic-plastic calculation on short cracks.

3.2 Finite Element Models

The mesh used 8 noded quadratic isoparametric elements with a focused mesh concentric with crack tip. To allow these elements to adopt the correct form of the displacement function, in which the displacements approach crack tip as $r^{1/2}$, as given by equations 32 and 33, the mid side nodes were located at the quarter point positions Fig (3.1).

The configurations considered were single edge cracked bars (SEC) with non-dimensionalised crack depths a/W=0.1 and a/w=0.5 subject to pure bending as shown in Fig (3.2.a and 3.2. b)

The finite element models were generated with aid of a commercial program called FEMGEN. Fig (3.3) shows the idealisation of a plate of width W containing a crack of length a with a/w=0.1. The model consisted of 70, eight noded plane strain isoparametric elements consisting of, 393 nodes with 786 degree of freedom. Fig (3.4) represents the mesh of the deep crack a/w=0.5 in it's undeformed configuration. It contained 112, eight noded plane strain isoparametric element comprising, 613 nodes

and 1226 degrees of freedom. Poisson's ratio υ was set at 0.3 and the modulus of elasticity E was 2.E11. The models were forced loaded on the remote boundary either by a uniform tensile stress or by pure bending

3.3 Elastic Stress Field at the Crack Tip

The distribution of the elastic stress straight ahead of the crack at ø=0 is shown in Fig (3.5) and Fig (3.6), for a/w=0.1 and a/w=0.5 respectively, for both specimens subject to bending using force boundary conditions. The variation of the stress (σ_{yy}/σ_o) with respect to the distance along the ligament is shown in Fig (3.5,3.6).

3.4 Methods of Calculating the Stress Intensity Factor

3.4.1 The Stress Method.

The stress ahead of the crack is of the form:

$$\sigma_{ij} = K_I/\sqrt{(2\pi r)}\ f_{ij}(ø) \qquad (1)$$

Here $f_{ij}(ø)$ =1 for ø=0 . At this point it is convenient to introduce a parameter K_I^* defined by

$$K_I^* = \sigma_{yy}\sqrt{(2\pi r)} \qquad (2)$$

This can be evaluated at point ahead of the crack using the stress extrapolated to the nodes. The stress intensity K_I factor the defined as the limit of K_I^* as r goes to zero.

$$K_I = Lim\ K_I^* \qquad (3)$$
$$r \to 0$$

From plots of K_I^* as a function of r, at ø=0 , K_I is obtained as the limiting value at r=0 shown in Fig (3.7) and (3.8). This is given in non-dimensionalised form in Table (1) for the short and deep cracks.

3.4.2 The Displacement Method

According to the Westergaard equations, the plane strain displacements are of the form :

$$Ui = (K_I/G)\ \sqrt{(r/2\pi)}\ f_{ij}(ø) \qquad (4)$$

$$f_{xx}(ø) = \text{Cos}\ (ø/2)[1-2\upsilon + \text{Sin}^2(ø/2)]$$
$$f_{yy}(ø) = \text{Sin}\ (ø/2)[2-2\upsilon - \text{Cos}^2(ø/2)]$$

By substituting a nodal point displacement Ui* at some (r,ø) near the crack tip in equation (4) a quantity K_I^* was calculated:

$$K_I^* = \sqrt{(2\pi/r)}\ (G\ Ui^*)\ /f_{ij}(ø) \qquad (5)$$

The stress intensity K_I was then given the limit of K_I^* as $r \to 0$. By plotting K_I^* as a function of r for ø=0 as shown in Fig (3.9) and (3.10), the value of non-dimensionalised K_I is given Table (1), for the short and deep cracks.

3.4.3 Virtual Crack Extension Method

The value of K_I can also calculated from J .

$$K_I = \sqrt{[J\ E/(1-\upsilon^2)]} \qquad (6)$$

Where J-integral was determined by the virtual crack extension method of Parks (1) as implemented in ABAQUS (2). Five contours were used, although the contours were largely path independent the values have been always been taken from the second contour which generally exhibts the best results, for reasons that are considered to be more fortuitous than fundamental.

The stress intensity factors obtained using this method are given in table (1)

3.5 Brown and Srawley's Results

The present calculations have been compared with those presented by Brown and Srawley (3), who used the boundary collocation technique, for pure bending and obtained

$$K_I/K_o = 1.12 - 1.39(a/w) + 7.32(a/w)^2 - 13.1(a/w)^3 + 14.(a/w)^4 \qquad (7)$$

Where at a bending moment per unit thickness M. K_o takes the following form

$$K_o = 6\ M\ (\sqrt{(\pi a)}\ /w^2 \qquad (8)$$

The value of (K_I/K_o) estimated from equation (3) for a/W=0.1 is found to be (1.05). For a/w=0.5, under the same conditions (K_I/K_O)

is found to be (1.459).

3.6 Discussion of the Results

The values of the stress intensity factor obtained by using direct finite element methods, displacement, stress and virtual crack extension methods are given in Table (1). The results obtained by using the displacement method are shown to be more accurate results than those of the stress method when compared with the method of Brown and Srawley (3) which have an an accuracy of 1%.

In the present work the displacement method and the virtual crack extension method agree with those given by Brown and Srawley with a maximum error of 2%. In comparison the stress method which gives an error of 13%. From these results, one can conclude that the displacement and virtual cracks extension methods give better results than those given by the stress method, and both are consistent with published data (3)

3.7 References:

1. Parks, D. M.,Int J of Fracture Mech.Vol 10., pp 487., (1974)

2. Hibbitt, Karlsson and Sorensen , ABAQUS Users Manual, (1984.). Providence R. I.

3. Brown , W. F., and Srawley , J. E., STP ASTM 410, pp 51 (1966)

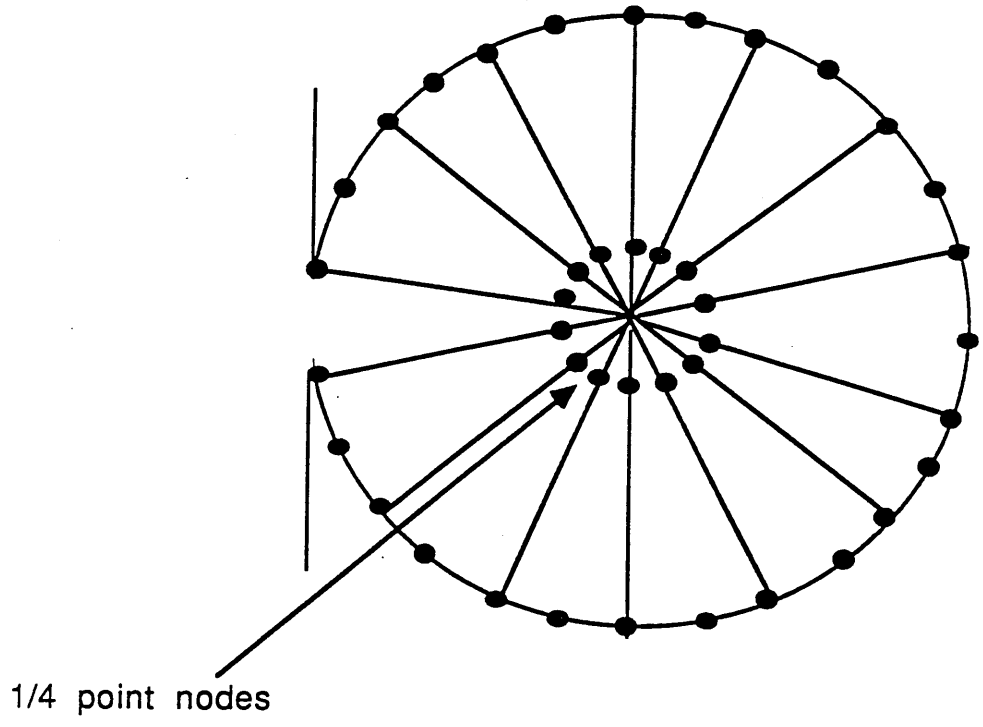

Fig (3.1)

Second order element with mid side nodes of the crack tip element moved to 1/4 point position

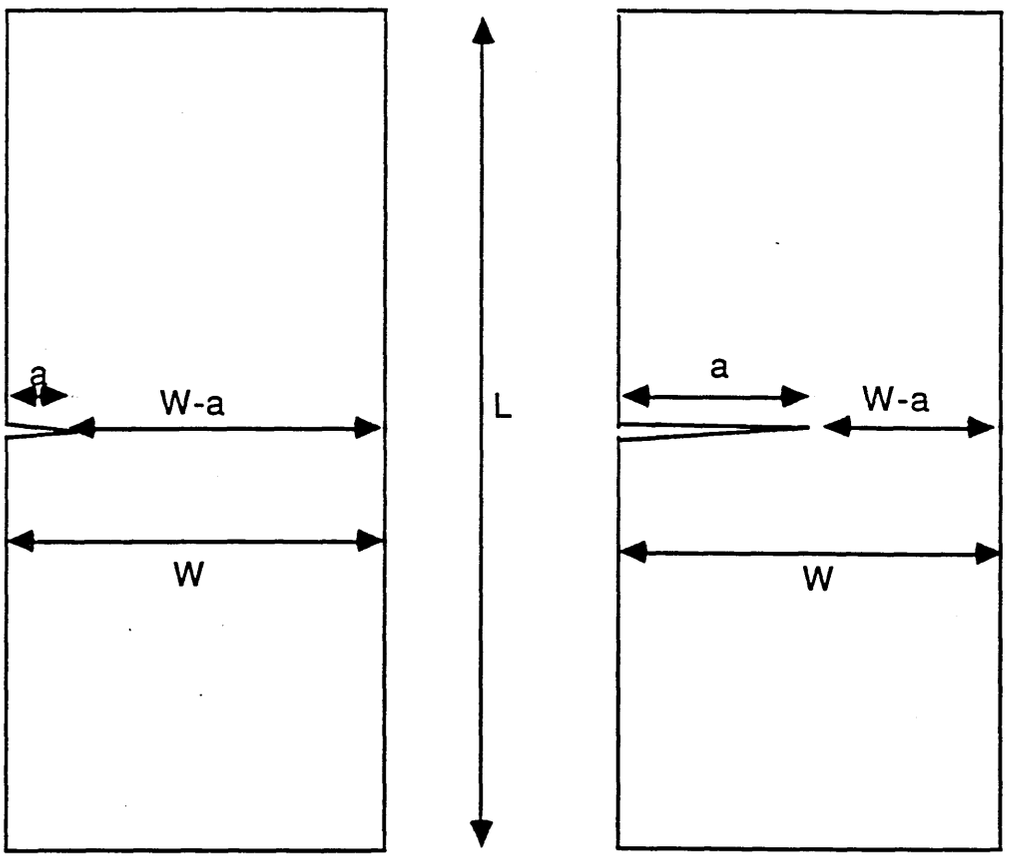

Fig (3.2)

Single edge cracked (SEC) configuration (a) for a/w=0.1 and (b) for a/w=0.5

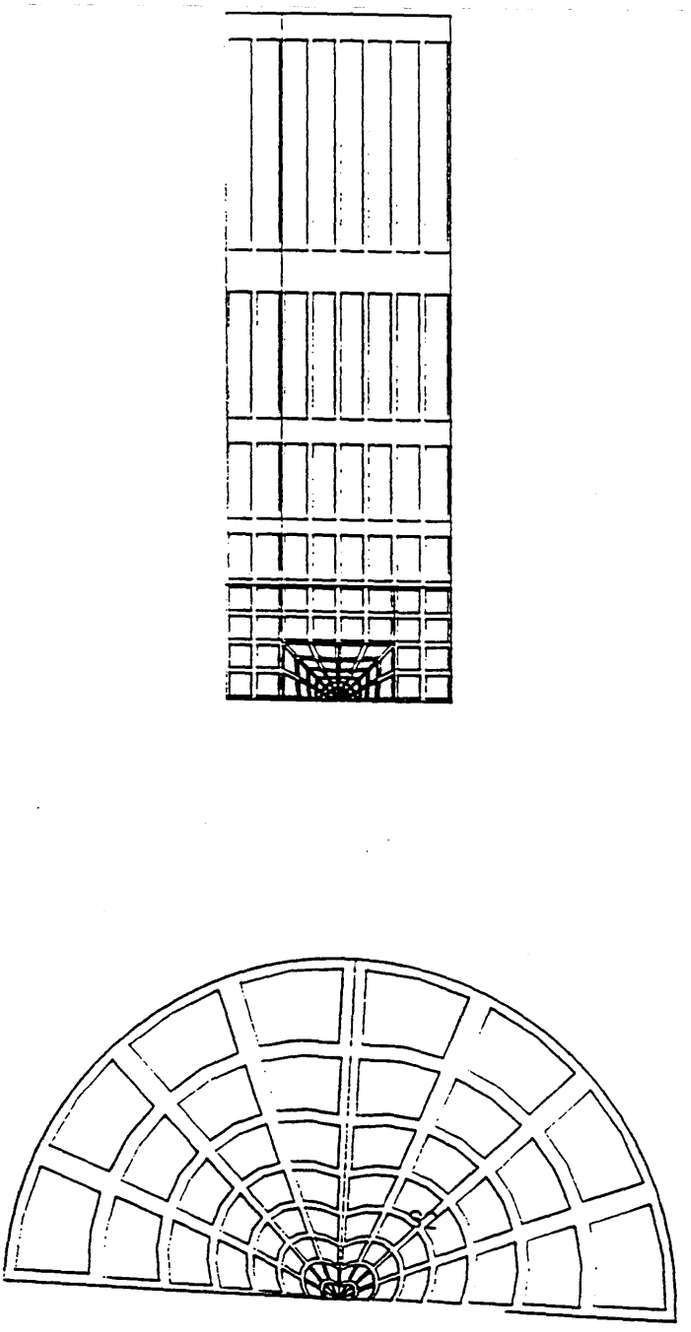

Fig (3.3)

Finite element mesh for deep crack specimen.

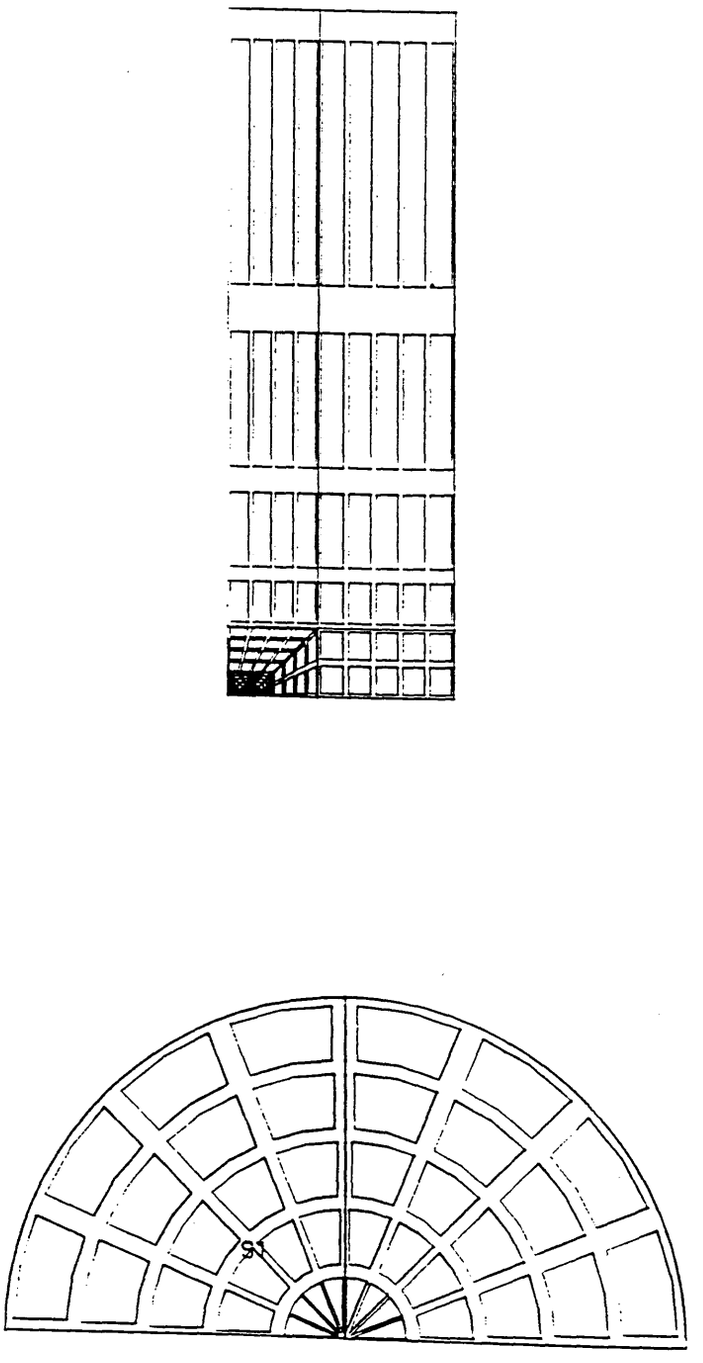

Fig (3.4)

Finite element mesh for short crack specimen.

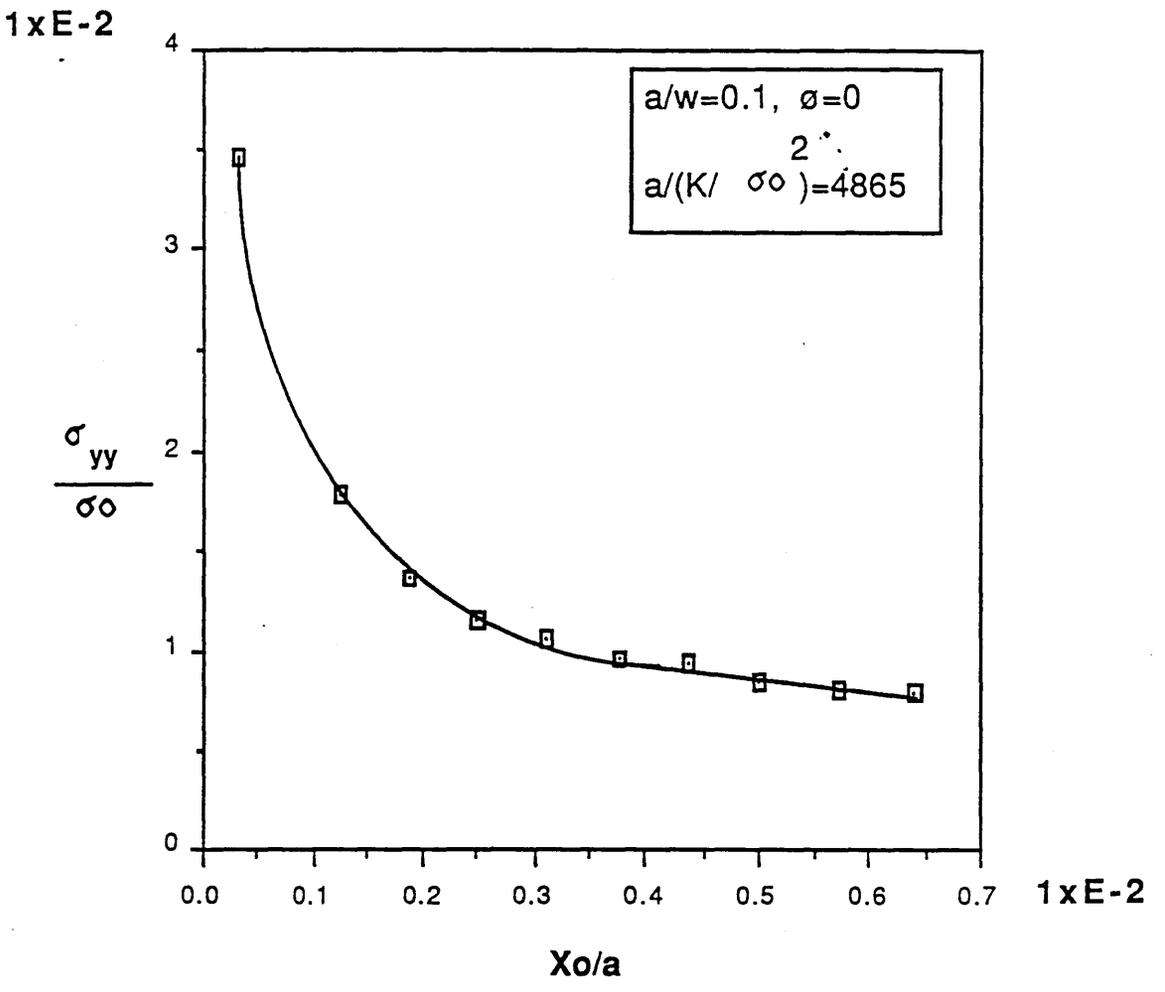

Fig (3.5)

The elastic distribution ahead of the short crack tip.

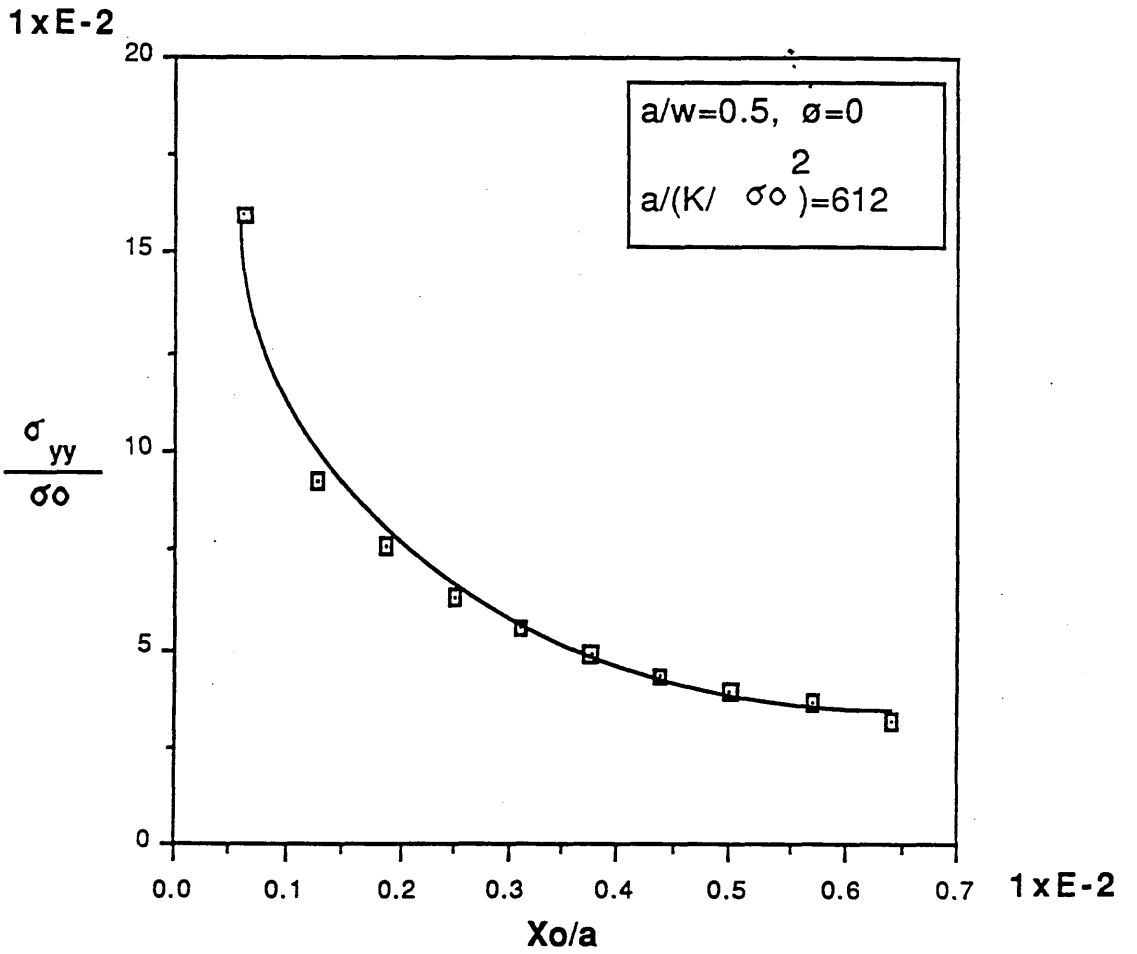

Fig (3.6)

The elastic distribution ahead of the deep crack tip.

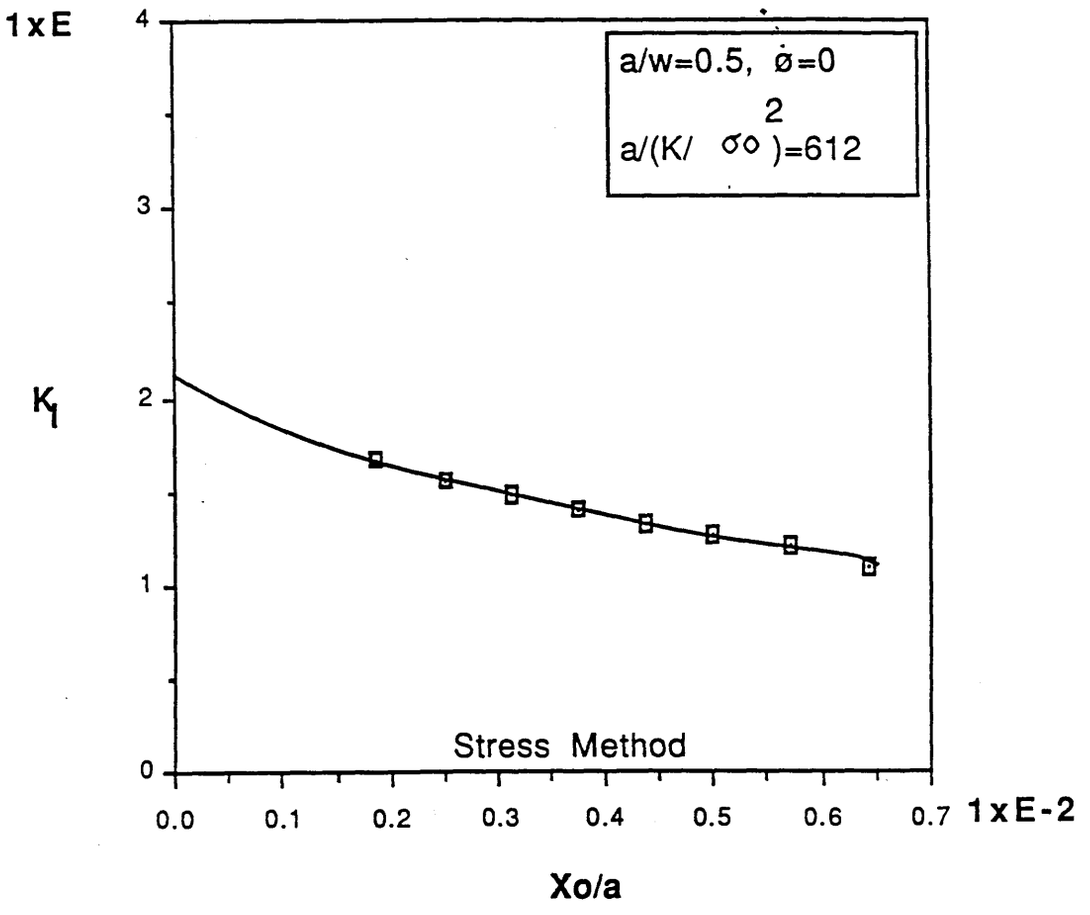

Fig (3.7)

The stress intensity factor for the deep crack obtained by using the stress method.

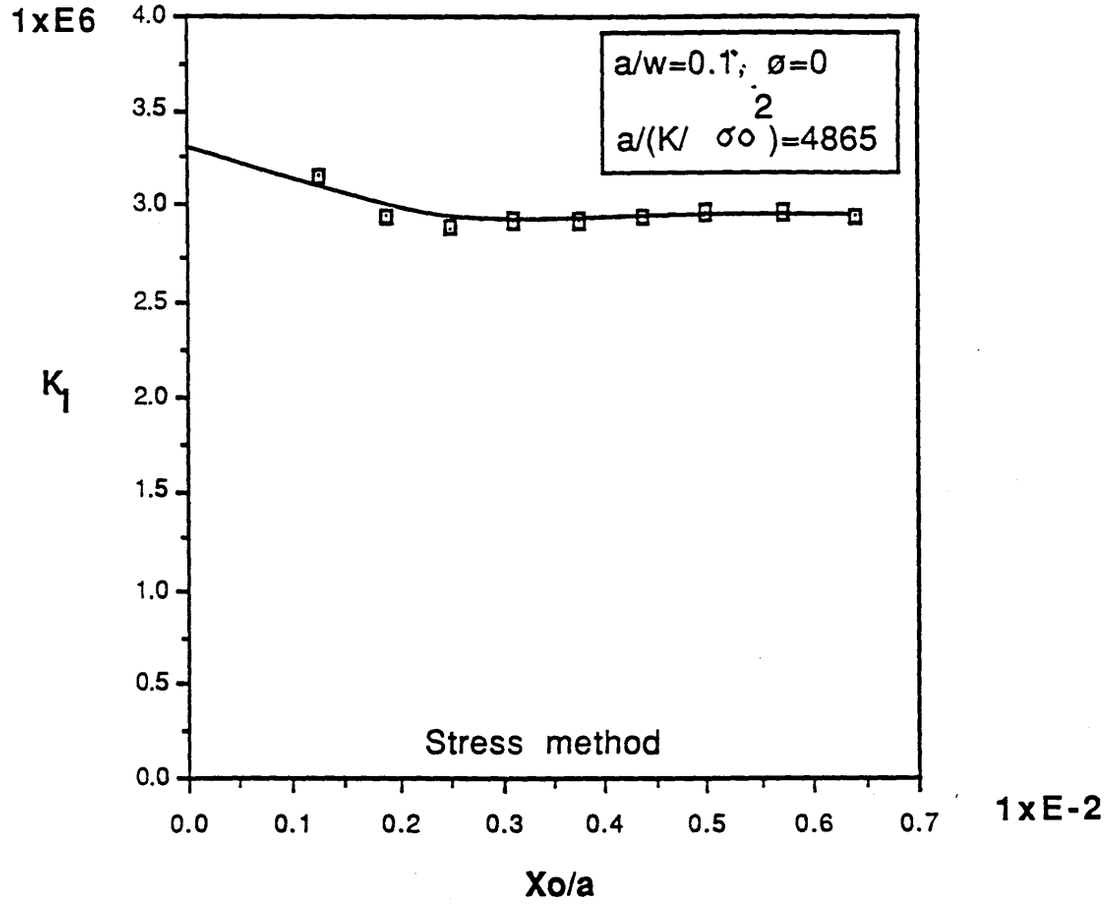

Fig (3.8)

The stress intensity factor for the short crack obtained by using the stress method

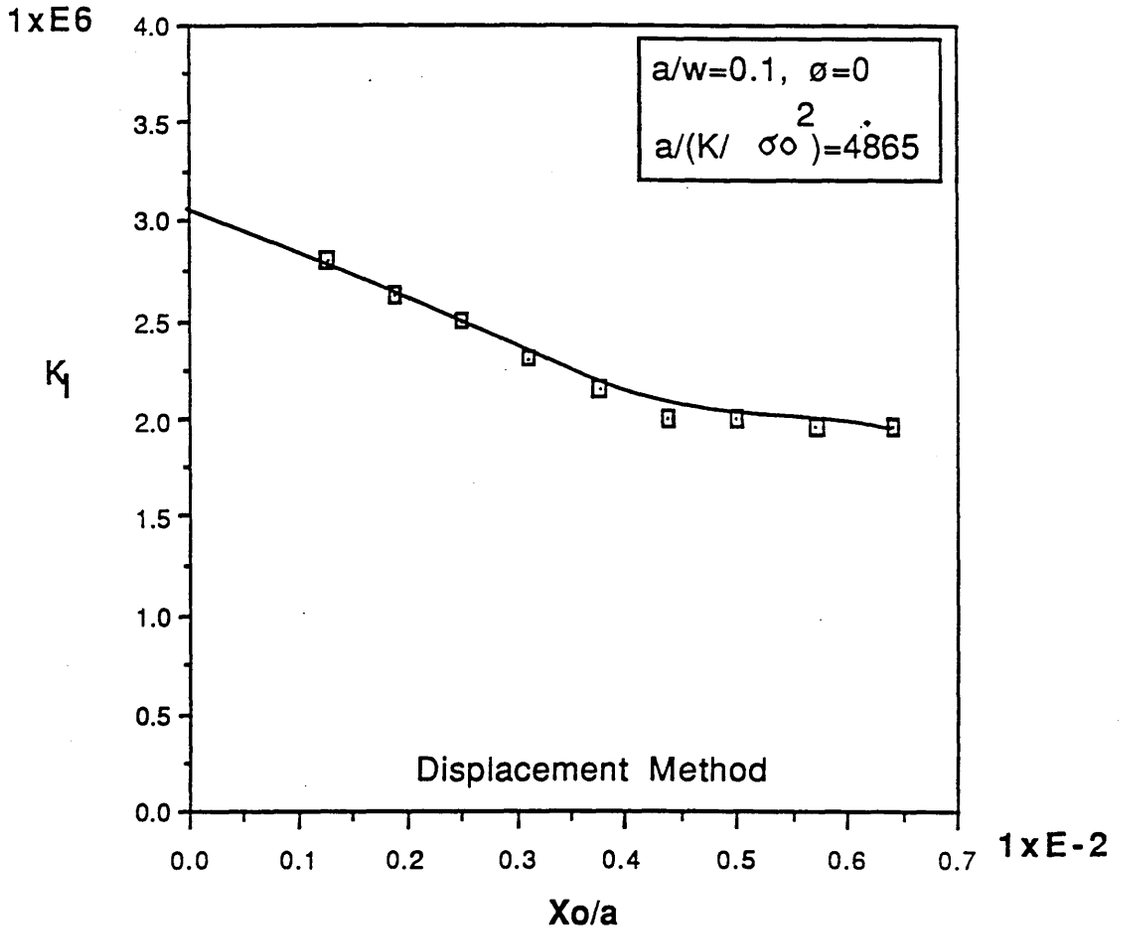

Fig (3.9)

The stress intensity factor for the short crack obtained by using the displacement method.

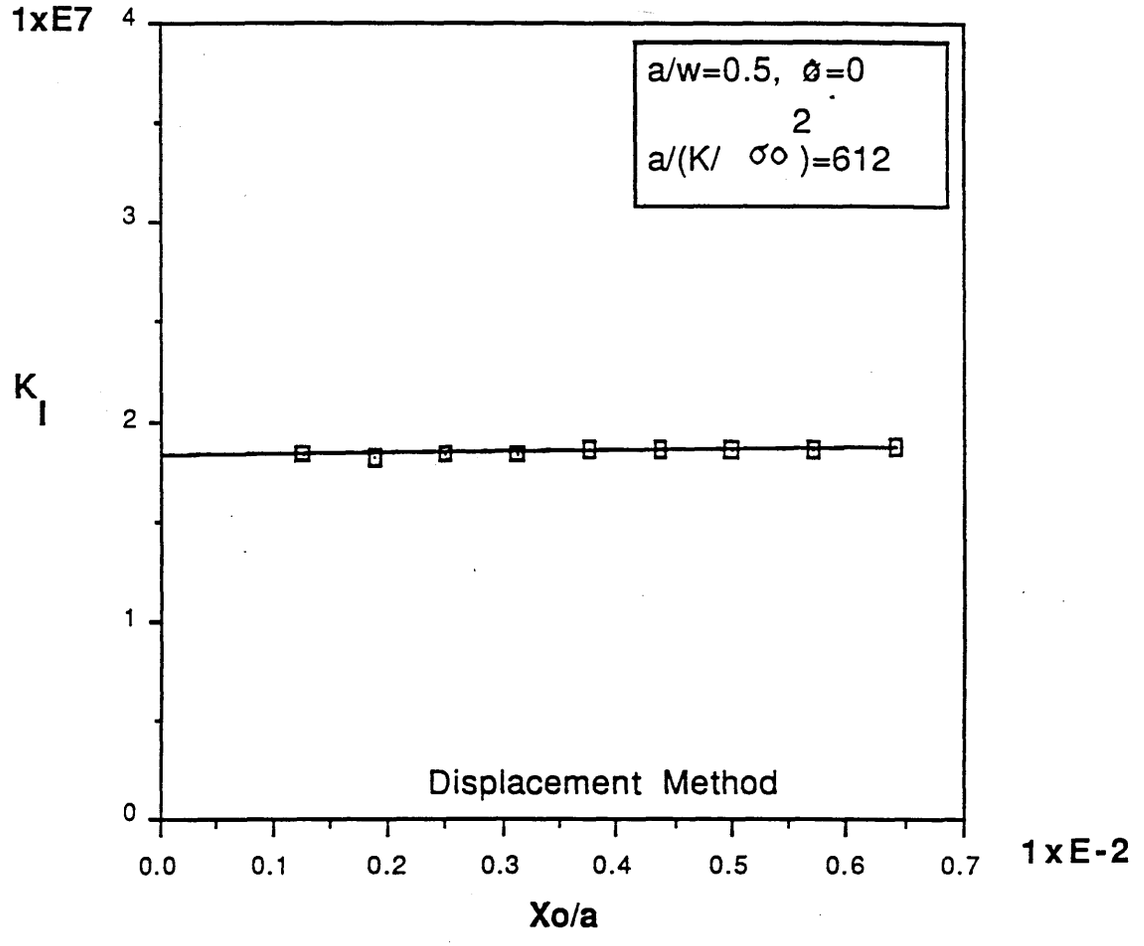

Fig (3.10)

The stress intensity factor for the deep crack obtained by using the displacement method.

	a/w = 0.1 (K_I/Ko)	a/w = 0.5 (K_I/Ko)
Brown and Srawley [Boundary Collocation] Method [2]	1.045	1.459
[Displacement Method] [Finite Element Method] Present work	1.02	1.45
[Stress Method] [Finite Element Method] Present work	1.19	1.78
[Virtual Crack Extension] [Method]	1.06	1.46

TABLE (1)

Chapter (4)

ELASTIC-PLASTIC FRACTURE MECHANICS

4.1 Introduction

For monotonic loading problems, linear elastic fracture mechanics has found extensive application to high strength, relatively brittle materials which fail when small scale plasticity is exhibited at the crack tip. LEFM essentially applies only when the material behaviour is dominantly elastic and the fracture response, brittle. However above the ductile-brittle transition temperature fracture takes place with sufficient plasticity to invalidate LEFM. This is the territory of elastic-plastic fracture mechanics as shown schematically in Fig (4.1)

Realistic measures of fracture behaviour and design criteria can be obtained through the use of elastic-plastic analysis which has identified two parameters to characterise elastic -plastic crack tip deformation.

1. The J-integral introduced by Cherepanov (1) Eshelby (2) and Rice (3).
2. The crack tip opening displacement (CTOD) introduced by Wells (4).

4.2 The J Integral

The unifying theoretical idea underlying non-linear elastic fracture mechanics is the J-Integral, which was introduced independently by Cherepanov (1), Eshelby (2), and Rice (3), but whose application to fracture mechanics is primarily attributable

to Rice (3). Rice considered a homogeneous body of non-linear elastic material, free of body forces subject to a two dimensional deformation field, such that the stresses σ_{ij} depend only on the coordinates x and y. The body contains a notch of the type shown in Fig (4.2), having a flat surface parallel to the x-axis and with this geometry the J-integral was.defined by Rice (3) as

$$J = \int_{\Gamma} [W\, dy - F_i \cdot (\partial u_i / \partial x_i) ds] \qquad (1)$$

Γ is an anticlockwise curve surrounding the notch tip fig (4.3), F_i is the traction vector defined according to the outward normal along r, u is the displacement vector and ds is an element of arc length along Γ. The strain energy density w is defined by

$$W = \int \sigma_{ij}\, d\varepsilon_{ij} \qquad (2)$$

Which for a linear elastic fracture material is simply $1/2\ \sigma_{ij}\ \varepsilon_{ij}$ The traction factor F_i, is the force vector acting on an infinitesimal area, with an outward normal n_j, the area is regarded as a scalar so that F_i is a first order tensor with units of force per unit area, in contrast to the stress tensor σ_{ij} which is of second order, but also has the units of force per unit area. The two tensors are related by

$$F_i = \sigma_{ij}\ n_j$$

Rather than reproduce the formal derivation of J given by Rice (3), it is perhaps more useful to illustrate the form of J by a non - rigorous derivation attributable to Finnie.

Fig (4.3) shows an arbitrary contour from the lower crack face to the upper face around the crack tip. On each small element ds, of this surface there is a force F which is a vector. If the crack advances, by a small amount Δa the surface also moves, and the element ds moves by a small displacement Δu. As the crack advances, the stress field only changes by a negligibly small amount and because both the force F and the displacement Δu are vectors the work done on the element is $F.\Delta u$ where the dot or scalar produce takes care of the fact that Δu and F may not be in the same direction. The total work done the material inside the contours is obtained by integrating around the circuit

$$\int_{\Gamma} (F \bullet \Delta u)\, ds \qquad (3)$$

The displacement Δu can be written in terms of crack advance in the x direction

$$\Delta u = (du/dx)\, \Delta a \qquad (4)$$

Thus the work done by external forces

$$\Delta a \int [F \bullet (du/dx)] ds \qquad (5)$$

As the crack advances and the contour moves the material inside

the contour "loses" and "gains" strain energy from the shaded regions. If W is the strain energy per unit volume change of strain in small strip indicated in Fig(4.3)

$$W \Delta a \, dy \tag{6}$$

The net loss in strain energy of the material inside the contour is obtained by integration around the path

$$\Delta a \int_{\Gamma} W \, dy \tag{7}$$

The material inside the contour losses strain and external forces do work on it so the net loss in energy is

$$\Delta U = a \int_{\Gamma} W \, dy - \Delta a \int [F \bullet (du/dx)] ds \tag{8}$$

The energy released per unit area of crack advance defines J

$$J = \Delta U / \Delta a = \int_{\Gamma} W \, dy - [F \bullet (du/dx)] ds \tag{9}$$

An important feature of the integral demonstrated by Rice is its path independence for both linear and non linear elasticity. Non linear elastic stress strain relations are identical to the plastic relation as long as the material is not unloaded. The stress-strain

relations of plasticity take account of history of the material and are written in terms of increments, whereas in elasticity the stresses and strains only depend on the current values and are history independent. However at the moment this difference does not appear cause problems in practice.

Path independence may be shown by considering the difference between J values evaluated over two contours Γ_1 and Γ_2 Both terms of the integral vanish on the crack surface, and on transforming from a line to an area integral. Rice (3) has shown that the difference is zero assuming that the region between Γ_1 and Γ_2 is simply connected and free of singularities.

J thus characterises the crack tip singularity, and can be evaluated remote from the tip. As an illustration it is useful to consider the example given by Rice (3). Consider an infinitely long cracked strip with clamped boundaries subject to a constant displacement $v_1=v$, $v_2=0$ as shown in Fig (4.4)

Evaluating J on the outer boundary, dy and (du_i/dx) are zero on the clamped boundaries, and σ_{ij} and F_i disappear at $X = \pm\infty$. The only term arises from the contribution at $X=\pm\infty$ but as (du_i/dx) is zero at $x=\infty$,

$$J = 1/2\ \sigma_2\ \varepsilon_2\, h = Eh/2(1-\upsilon^2)\ \varepsilon_{22}^{\ 2} \qquad (x=\infty) \qquad (10)$$

This allows J to be evaluated purely from the remote field. In the case of L.E.F.M

$$J = G = (K^2/E^-) \qquad (11)$$

The line integral as a parameter derived from non-linear elastic behaviour has the same function as G does in linear elastic theory. It is an expression of the rate of change of potential energy with respect to an incremental extension of crack length, Rice (3).

$$J = - (\partial U / \partial a) (1/B) \qquad (12)$$

For a linear elastic material J is thus identical to the potential energy release rate G and establishes contact with the stress intensity factor K

Unfortunately as demonstrated by Turner (5) when applied to elastic-plastic material, the physical meaning of J as a energy release rate is lost, since in incremental plasticity the energy term, is no longer available for crack propagation.

4.3 HRR Field

It has been noted that the J-integral can be used as an energy based fracture criterion, however Rice and Rosengren (6) and Hutchinson (6) have also shown that J has a role in characterising the deformation field ahead of stationary cracks. The material behaviour is taken to be described by a plastic power law. For such materials the plastic strain ε is simply proportional to the tensile stress σ raised to some power

$$\varepsilon_p/\varepsilon_o = \alpha (\sigma/\sigma_o)^n \qquad (13)$$

Using J_2 deformation theory with $\sigma_e^2 = 3/2\ s_{ij}\ s_{ij}$

$$\varepsilon_{ij}/\varepsilon_o = [3/2\ \alpha\ (\sigma_e/\sigma_o)^{n-1}\ (s_{ij}/\sigma_o)] \qquad (14)$$

The method of solution employed by Hutchinson (8) used the minimum complementary energy theorem, under which of all the stress distributions which satisfy equilibrium and the stress boundary conditions, the correct distribution is the one which minimizes the complementary energy Uc over the volume v.

$$U_c = \int_v \int \varepsilon_{ij}\, d\sigma_{ij}\, dv \qquad (15)$$

In plane stress or plane strain the complementary energy can be written in terms of the stress as

$$Uc = \int_A (1/3(\ 1+\upsilon)\ \sigma_e)^2 + (\ 1+2\upsilon/\sigma)\ \sigma_{kk}{}^2 + (\alpha/N+1)\ \sigma_e{}^{n+1} \qquad (16)$$

Equilibrium is satisfied by a non-dimensional stress distribution Σ, which in cylindrical co-ordinates satisfies the following relations.

$$\sigma_r = 1/r\ (\partial\Sigma/\partial r) + 1/r^2\ (\partial^2\Sigma/\partial\varnothing^2) \qquad (17)$$

$$\sigma_\varnothing = (\partial^2\Sigma/\partial r^2) \qquad (18)$$

$$\sigma_{r\varnothing} = -\ \partial\ (1/r\ (\partial\Sigma/\partial\varnothing))\ /\partial r \qquad (19)$$

On this basis a solution is sought in the vicinity of the crack which satisfies the equilibrium equations, and the local boundary

conditions.

$$\Sigma = \partial\Sigma/\partial\phi = 0 \qquad (\phi = -\pi , +\pi) \qquad (20)$$

The solution is assumed to take the form of an asymptotic expansion whose dominant term is

$$\Sigma = Kr^{s}\, \Sigma(\phi) \qquad (21)$$

With this form of solution the complementary energy can be evaluated and minimised by using the amplitude K and the exponent s. The solution is given by

$$s = (2n+1)/(n+1) \qquad (22)$$

Hence the crack tip stress and strain field could be obtained in terms of J as

$$\sigma_{ij} = \sigma_o \left[J / \alpha \varepsilon_o \sigma_o I_n r \right]^{1/n+1} f_{ij}(\phi) \qquad (23)$$

$$\varepsilon_{ij} = (\sigma_o \alpha/E) \left[J / \alpha \varepsilon_o \sigma_o I_n r \right]^{n/n+1} f_{ij}(\phi) \qquad (24)$$

Where $f_{ij}(\phi)$ is a function of ϕ and, I_n is a tabulated function of n (6,7). The J-integral thus characterises the crack tip stress and strain field and is not only a energy parameter but also a stress field parameter.

4.3.1 Measurement of the J-Integral

4.3.1.1 Form of Solution

Before introducing techniques for determining J, experimentally or numerically, it is appropriate to consider the non-dimensional form that the solution must adopt in a power law problem. If P is a load parameter, the solution to any power law problem necessarily has the property that the stress and strain are everywhere proportional to P and P^n respectively.

$\sigma_{ij} \alpha P$

$\varepsilon_{ij} \alpha P^n$

Using the energetic definition of J , it can then seen that J has the units of the product of stress and strain per unit thickness and is thus proportional to P^{n+1}.It can thus always be written in the non dimensional form

$$J / a \sigma_o \varepsilon_o \alpha = (P/P_o)^{n+1} h(n) \qquad (25)$$

Where h is a function of the strain hardening exponent n and a dimensionless group of geometry parameters. Contact with limit analysis can be made using the limit load (P_o) of the perfectly plastic cracked body as a reference load.

It is appropriate to write J as the sum of an elastic and plastic terms

$$J = Je + Jp \qquad (26)$$

For example for the centre cracked infinite panel Hutchinson (7) gives:

$$J = (1-\upsilon^2)\,\pi a\,\sigma^2/E + \alpha\,\sigma_o\,\varepsilon_o\sqrt{(n\pi)}\,(\sqrt{3}\,\sigma/2\,\sigma_o)^{n+1} \qquad (27)$$

which is asymptotically correct for large and small stresses.

4.3.1.2 Energy Approach

The most straight forward experimental and numerical method for the evaluation of J derives from it's definition as the rate of change potential energy with crack length. For example, consider specimens containing cracks of incrementally different length a and a+Δa. The J-integral value for both nonlinear elastic and elastic-plastic conditions is given by

$$J = -1/B\int_{0}^{\Delta} (\partial U / \partial a)\, d\Delta \qquad (28)$$

This can be interpreted graphically as the area between the load displacement curves and converted to absorbed energy per unit thickness as shown schematically in Fig (4.5)

$$J = (U_1 - U_2) / (a_1 - a_2)\, B \qquad (29)$$

Although this method is conceptually easy, it is very inconvenient, as it requires the use or analysis of two specimens. The use of J as a practical fracture -mechanics criterion required

the ability to measure J from one specimen.

The first development in this process was made by Rice et al (9) for deeply cracked specimens in which the uncracked ligament is the only relevant length dimension.

If the load point rotation for an uncracked specimen is denoted by ϕ_{nc} and that of the cracked specimen is ϕ_{cr}, the total rotation is given by:

$$\phi = \phi_{nc} + \phi_{cr} \qquad (30)$$

By taking the length L to be large compared to the width W, ϕ_{cr} takes the form.

$$\phi_{cr} = f\,[(M/\sigma_o\,(w-a)^2),\ (w-a)/a,\ \sigma_o/E,\ n] \qquad (31)$$

Here f is dimensionless function which independent of (W-a)/W. For a sufficiently deep crack (w-a)/w<<1. For linear elastic deformation the rotation under a moment M per unit thickness is given by:

$$\phi_{cr} = 16M/E(w-a)^2 \qquad (32)$$

For full plasticity, deformation is confined to the uncracked ligament (w-a). and the general expression for J is

$$J = \int_0^M \partial\phi_{cr}/\partial a\ (M,a)\ dM \qquad (33)$$

$$[\partial \phi_{cr}/\partial a]_M = -[\partial \phi_{cr}/\partial (w-a)]_M = 2\, f_1,\, [M/\sigma_o (w-a)^3] - f_2,\, 1/w \quad (34)$$

Where the commas denote the partial-derivatives and

$$\partial \phi/\partial a = \partial \phi_{cr}/\partial a$$

$$[\partial \phi_{cr}/\partial M]_a = f_1,\, (1/\sigma_o (w-a)^2) \quad (35)$$

So that equation (34) can be rewritten as

$$[\partial \phi_{cr}/\partial a]_M = -[\partial \phi_{cr}/\partial M]_a\, 2\, M/(w-a)] - f_2, 1/w \quad (36)$$

Substitution of equ (36) into equ (33) and noting that $(\partial \phi_{cr}/\partial M)\, dM = d\phi_{cr}$

$$J = 2/(w-a) \int_0^M M \partial \phi_{cr} - 1/(w-a) \int_0^M f_2,\, dM \quad (37)$$

For the deeply cracked specimens J takes the following form

$$J = 2/(w-a) \int_0^M M \partial \phi_{cr} \quad (38)$$

This has the geometric interpretation of 2/(w-a) time the area under a plot of M vs ϕ_{cr}

$$J = 2U_m/B(w-a) \quad (39)$$

By using the area under the load vs displacement relation equ (39) can be written as

$$J = 2U/B(w-a) \qquad (40)$$

Where U is the total area under the load-displacement curve, B is the specimen thickness and (w-a) is the ligament. As pointed out by Rice (9), the J-integral for center cracked panel takes the form

$$J = G + [(2\ U_p - p\ \delta_p)][(w-2a)\ B]^{-1} \qquad (41)$$

where P is the load and δ_p is the displacement due to plastic deformation for all (2a/w).

Sumpter and Turner (10) pointed out that the above equation can be applied to any test piece geometry for which elastic stress intensity and plastic limit load solution are available. By splitting the total energy (U_G) into elastic components U_e and plastic components U_P, J can be expressed in the form

$$J = J^e + J^P$$
$$J^e = \eta_e\ U_e / (w-a)\ B \qquad (42)$$
$$J^p = \eta_p\ U_p / (w-a)\ B$$
$$J = \eta_e\ U_e / (w-a)\ B + \eta_p\ U_p / (w-a)\ B$$

Where η_e, η_p are geometry dependent dimensionless constants given by Turner (11). Sumpter (12) has recommended the use of a

similar formula based on clip guage displacement for J-determination in three point bending specimens for all (a/w).

$$J = \{[K_I^2 / E^-] + [\eta_p \, Uv_p / (w-a) \, B] \, [0.25 \, S/a + r(w-a)]\} \qquad (43)$$

Where K is the the stress intensity factor calculated from the load.

S is the specimen loading span S = 4w .

Uv_p is the plastic component of the area under the load versus clip gauge displacement .

r is a constant

r=0.4 for $a/w \geq 0.3$

r= 0.3 +0.5 a/w for $a/w \leq 0.3$

η_p is constant

$\eta_p = 2$ for $a/w \geq 0.283$

$\eta_p = 0.32 - 11.2(a/w) - 49(a/w)^2 + 99.8(a/w)^3$ for $a/w < 0.283$

4.3.1.3 E.P.R.I. Method

The approach developed by E.P.R.I. is designed to permit fracture fracture evaluations of flawed structures to be carried out by personal who are not specialists in fracture mechanics or inelastic analysis. The evaluation does not require any further finite element analysis, rather only desk top calculation and simple graphical procedures using the Ramberg-Osgood power hardening relation in equation (5). Elastic-plastic solutions are obtained by combining elastic and fully plastic terms, with a plastically adjusted crack length (a_e).

$$J = J^{e}(a_e) + J^{p}(a_e, N) \quad (44)$$

$$a_e = a + \phi r_y \quad (45)$$

Where

$$r_y = (1/\beta\pi)\ [N-1/N+1]\ [K_I/\ \sigma_o) \quad (46)$$

$$\phi = 1/[\ p+(\ p/p_o)^2\ ] \quad (47)$$

For plane stress β =2 and for plane strain β =6. LEFM provides a solution for the stress intensity factor, which can be converted to the J-integral through the relation

$$J^{e} = [K^2 / E^{-}] \quad (48)$$

To provide a smooth interpolation between elastic and elastic plastic terms using the crack length (a_e) suggested by Irwin (13).

J^{e} solutions are available from elastic hand books, in which the data are generally tabulated in the following form Kumar et al (14)

$$J^{e} = [\ f(a_e)\ p^2 / E^{-}\ ] \quad (49)$$

For the case of a single edge cracked bar of length L under three point bending

$$f(a_e) = 9\ \pi\ a_e\ (L/2)^2\ F^2 / w^4 \quad (50)$$

where F is a tabulated dimensionless function (14). J^{p}, which is the full plastic contribution, is written as:

$$J^p = \alpha \sigma_o \varepsilon_o a [p/p_o]^{n+1} f(a/b, n) \qquad (51)$$

Here P_o is a reference load per unit thickness defined as :

$$P_o = f (w-a) \sigma_o/(L/2) \qquad (52)$$

f is a dimensionless function, whose value depend on whether plane stress or plane strain applies. Substituting in equation (44) and (49) and the estimation formula equation (53), one gets the following expression.

$$J = [f(ae) p^2/ E-] + [\alpha \sigma_o \varepsilon_o a [p/p_o]^{N+1} f(a/b, N)] \qquad (53)$$

where the function for a range of standard geometries are available in the EPRI hand book (14).

4.4. Crack Opening Displacement

Wells (4) noticed that the tip of a slot crack subject to plastic deformation opened giving a definite tip opening called the crack tip opening displacement (C.T.O.D). Wells (4) proposed that the C.T.O.D characterized crack tip deformation and fracture would occur at a critical value of this parameter. This proposal was pursued experimentally and theoretically by Burdekin and Stone (15). who provided the basis for the practical application of the C.T.O.D concept, using Dugdales' strip yield model (16). The crack tip opening displacement is related to the stress intensity factor for LEFM, and plane strain conditions by:

$$\delta = m K^2 / E \sigma_o \qquad (54)$$

Alternatively in terms of the potential energy release rate G

$$\delta = m G / \sigma_o \qquad (55)$$

Where m is a constant. In elastic-plastic conditions the Dugdale strip yield model gives the crack opening as:

$$\delta = (8 \sigma_o a/\pi a) \ln \sec (\pi \sigma/2 \sigma_o) \qquad (56)$$

Where σ is the remotely applied tensile stress. In LEFM ($\sigma/\sigma_o << 1$) recovers the LEFM identify

$$J = G = K^2 / E^- \qquad (57)$$

The relation between J and CTOD can be written in the form

$$\delta = m J/\sigma_o \qquad (58)$$

Here m depends both on the hardening rate, the extent of plasticity, and for fully plastic situations the nature of loading. The range of m values reported in the literature is summarised in Table (1)

Using the Hutchinson-Rice-Rosengren (HRR) singularity the relation between J and δ can be derived for the elastic-plastic conditions. The separation between the opened cracked faces

according to the HRR field will be denoted by (δ).

$$\delta = \alpha \varepsilon_o [J / \alpha \varepsilon_o \sigma_o I_n]^{n/n+1} r^{1/n+1} 2\bar{v}_y(n) \qquad (59)$$

The relative displacement of the faces of the crack tip in the x direction u_x is given as:

$$u_x = \alpha \varepsilon_o [J / \alpha \varepsilon_o \sigma_o I_n]^{n/n+1} r^{1/n+1} \bar{u}_x(n) \qquad (60)$$

$\bar{v}_{y(n)}$, $\bar{u}_x(n)$ are a function of the displacement in y and x direction respectively given by Hutchinson (25). As shown in Fig (4.6) δ_t is the opening at the intercepts of the two 45^o lines drawn back from the tip of the deformation profile where

$$r - u_x = \delta/2 \qquad (61)$$

Rice(20) and Tracey (24) used this definition of δ_t which can be used for both hardening and non-hardening materials In general the crack tip opening can be expressed in terms of J by an expression of the form (Dawes (23))

$$\delta_t = dn \ (J/\sigma_o) \qquad (62)$$

Values of dn, which are dependent on n and σ_o/E, are given in tabulated form by Hutchinson (25) and Shih (26)

4.5 Elastic Plastic Fracture Mechanics Size Requirement

McClintock (27) has observed that the fully plastic slip-line field solution for a cracked bar subjected to bending, and the center-cracked panel subjected to tensile loading are radically different in the limit of a non hardening material. In the fully plastic state there is no unique stress and strain in the crack tip region. Rice (28) pointed out in his solution of the anti-plane shear problem that the elastic-plastic size requirement will be a function of the extent of plastic deformation, and the strain hardening rate.

From these observations it is clear that valid elastic-plastic fracture mechanics must be subject to a size requirement in the same manner as LEFM. This means that a one parameter singularity characterisation of the crack tip field by J or δ is dependent on a geometric criterion. As a minimum requirement the dimensions must be large enough to fully encompass the fracture process zone, which exceeds some multiple of δ. According to these considerations the elastic-plastic size requirement may be expressed in the form:

$$.(w-a) \geq M_1 (\varepsilon_o, n) \; J_{Ic}/\sigma_o \qquad (63)$$

or equivalently

$$(w-a) \geq M_2 (\varepsilon_o, n) \; \delta_c \qquad (64)$$

To ensure plane strain condition in the process zone, Paris (29) has suggested a value of M ranging from 25 to 50. Using large deformation plane strain finite element methods McMeeking and Parks (30) have studied the deeply cracked center-crack panel

(CCP) and single edge cracked bend bar (CBB), using a power law hardening constitutive law. They compared the full plastic field with that of small scale yielding obtained in earlier finite element analyses by McMeeking (31), For the CBB specimen they found that the stress and strain distribution ahead of the crack at J values as large as $\sigma_o(W-a)/25$, were virtually identical to the standard field within a region of 2 to 5 blunted openings. In conclusion they suggest the minimum size requirement to be

$$(W-a) \geq (25 \text{ to } 50)\ J_C/\sigma_o \qquad (65)$$

For the CCP geometry, even with a moderate amount of strain hardening their results shown that a more stringent size requirement is necessary for elastic-plastic toughness test to ensure a sensible J characterization of the crack tip region. They suggest a value of M equal to 200 in equation (2) so that in tension the size requirement becomes

$$(W-a) \geq 200\ J_C/\sigma_o \qquad (66)$$

This means that for the CCP geometries, the size requirement for valid elastic-plastic fracture toughness parameter, is almost as severe restriction as those of LEFM

Shih and German (32) carried out a plane strain finite element study of CBB, SECP and CCP specimens, in order to compare their results with the HRR field, employing a small strain formulation, with the assumption that the finite deformation at the crack tip

region does not invalidate the small strain theory. McMeeking's analysis (31) suggests that the effect of finite deformation is important over distances of order 2 to 3 times the crack opening displacement ahead of the crack tip. Shih and Germans' results (32) show that under well-contained plasticity or small scale yielding, the HRR field is achieved over distances ranging from 2 to 6 δ for different geometries. These results are consistent with the size requirement, which is independent of specimen type for small scale yielding. Under large scale yielding the dominance of the HRR singularity is shown to be quite dependent on the hardening rate and the specimen type. For the case of a single edge cracked bar subject to remote bending, their results show that the stresses and strains fields remain essentially similar to the HRR singularity at all levels of plastic deformation. In conclusion Shih and German suggest that the current size requirement (that the ligament must exceed 25 to 50 J/σ_o) (27) will be sufficient to ensure J dominance in the crack tip region for CBB or similar specimens subject to bending, for law strain hardening and perfect plastic materials. For the CCP they draw a similar conclusion, that $((W-a)\ \sigma_o/J)$ has to be $\geq$ 200 to ensure J dominance of the crack tip region.

Shih (33) has also carried out solutions for a semi-infinite crack aligned perpendicular to free edge of a semi-infinite half space, where the ligament is subject to arbitrary combinations of tension and bending. The finite element solution was compared with HRR singularity fields. These comparisons show that the size requirement for J dominance is strongly dependent on the relative amount of bending to tension. For the case of pure bending the zone

of J-dominance was shown to be a significant function of the ligament and does not depend on the hardening behaviour, whereas for pure tension the zone of J dominance is substantially smaller and depends strongly on the hardening characteristics

Finally Shih drew the conclusion that the zone of J-dominance depends very strongly on the type of loading and less strongly on the hardening behaviour. The results show that the moment about the ligament greatly elevates stress triaxiality in the crack tip regions, therefore increasing the zone of J-dominance. In his solution Shih suggests that the centre-crack tensile configuration studied by McMeeking (30,31) and the configuration of the pure tensile load should be considered as a special cases, because these particular configuration do not permit any rotation about the ligament.

For the edge cracked tensile configuration with crack of sufficient depth, in which a positive moment about the ligament is induced and accompanied by a rotation, the results show that the J-dominance size is substantially larger than that suggested by McMeeking (30,31).

Three dimensional non linear finite element analyses have also been carried by Parks and Wang (34). They analysed a wide plate which was contained a semi-elliptical surface crack under remote uniaxial tension. In order to measure the effect of parameters such as the load level, amount of strain hardening and the aspect ratio, on the size requirements for J-dominance, they compared their result with the asymptotic singular field (HRR). By considering the stress component σ_{yy} ahead of the crack where ø =0

their results show that for the lower load the local stress profile is slightly beneath the smale scale yielding result, which in turn falls below the HRR field, and for the higher load the local stresses diverged rapidly from the HRR field. The result for the lower load for angles ø=0,30,45, showed nearly identical degree of one parameter (J) characterisation of their local stresses field, although the trend of decreasing of dominance with decreasing ø still existed.

In conclusion Parks and Wang (35) pointed out that the semi-circular crack geometry is more resistant to abrupt loss of HRR dominance in the fully plastic region than the semi-elliptical crack configuration, and at the highest applied stress the divergence from the J dominance is accelerated in a low hardening material.

4.6 References:

1. Cherepanov, G. P.,J Appl Math Mech., Vol 31, pp 503, (1967)

2. Eshelby, J. D., "Stress Analysis of Cracks , ISI publication, Vol (121), pp13-48, (1968)

3. Rice, J. R., J Appl Mech, Vol 35 pp 379-386, (1968).

4. Wells, A. A., In Proceedings Crack Propagation Symposium, Cranfield, England, Vol 1 paper B4 , (1961).

5. Turner,C.E.,and Sumpter., J.D.G, Int J Fracture, Vol 12, pp 816-871 (1976).

6. Rice,J. R., and Rosengren, G. F., J Mech Phys Slds, Vol 16, pp 1, (1968).

7. Hutchinson, J.W., J Mech Phys Slds, Vol 16, P13-31, (1968).

8. Hutchinson, J. W., J of Appl Mech, pp 1042-1051, (1983)

9. Rice, J. R., Paris, D. C. and J. G. Merkle., ASTM STP 559, pp 139-158, (1974)

10. Sumpter, J. D. G. and Turner C. E., " Method for Laboratory Determination of Jc" ASTM Special Technical Publication STP 601, pp. 3-18, (1976)

11. Turner C. E., "Post yield fracture mechanics" ed. D.G.H Latzko , Applied Science Publishers, London, (1979).

12. Sumpter, J. D. G. "Jc Determination for Shallow Notch Bend Specimens, Admiralty Research Establishment. (I987).

13. Irwin, G. R., Plastic zone near a crack and fracture toughness Proc 7th Sagamore conf., pp IV-63, (1969)

14. Kumar, V. German, M. D., and Shih, C. F. , An Engineering approach to Elastic-Plastic Fracture Analysis, Report No .EPRI Np-1931, July, (1981), General Electric Co, Schenectady

15. Burdekin, F.M and Stone, D.W , J of Strain analysis, Vol 1,

pp144, (1966) .

16. Dugdale, D.S., Yielding of Steel Sheet Containing Slits, J Mech Phys Slds., Vol 8 (1960)

17. Rice, J. R., J Appl Mech Trans ASME, Vol. 35, pp 191. (1968).

18. Rice, J. R. and Johnson, M. A., In Inelastic Behaviour of Solids, ed. Kanninen et al, McGraw Hill, New York, pp 641, (1970).

19. Shih, C. F., General Electric Company, Technical Information Series Report, TIS No. 79CRD075, (1979).

20. Rice J R Proc 3rd Int Conf Fracture, Mech, p I441, (1973).

21. Tracey, D. M., Trans. ASME, J Eng Material and Technol., Vol. 98, p 146, (1976).

22. Robinson J. N. and Tetelman, A. S., ASTM STP 599, pp. 139-158, (1974).

23. Dawes M.G , ASTM STP 668 , pp 307-331, (1971)

24. Tracey, D. M. J Eng Mat and Tech, Vol 98, PP 146, (1976)

25. Hutchinson, J. w., J. Mech Phys Slds Vol 26, pp 163, (1978).

26. Shih C. F..' The Relationship Between Initation and Growth Parameters Based on the J-integral and Crack Opening Displacement, Oct ,(1978)

27. McClintock, F.A., An Advanced Treatise, H. Leibowitz. Ed Vol 3, Acedemic Press, New York, pp71-225 (1975)

28. Rice, J. R., J of Appl Mech, Vol 34, pp 287-298, (1967) ASME Vol 19, pp23-53 (1976)

29. Paris, P.C., ASTM STP 514 , pp 210-220 (1972)

30.McMeeking, R. M. and Parks, D. M. " Elastic-Plastic Fracture Mechanics" ASTM STP 668, pp 175-191, (1979).

31. McMeeking, R. M., J Mech Phys Slds,. Vol 25, pp 375-381, (1977).

32. Shih, C. F. and German, M. D., Int J of Fracture, Vol 29, pp 73-83, (1981)

33. Shih, C. F.,Int J Fracture, Vol 12, (1985).

34. Parks, D. M. and Wang Y.Y. "Elastic-Plastic Analysis of Part Through Surface Crack " To appear in ASME Symp (1988)

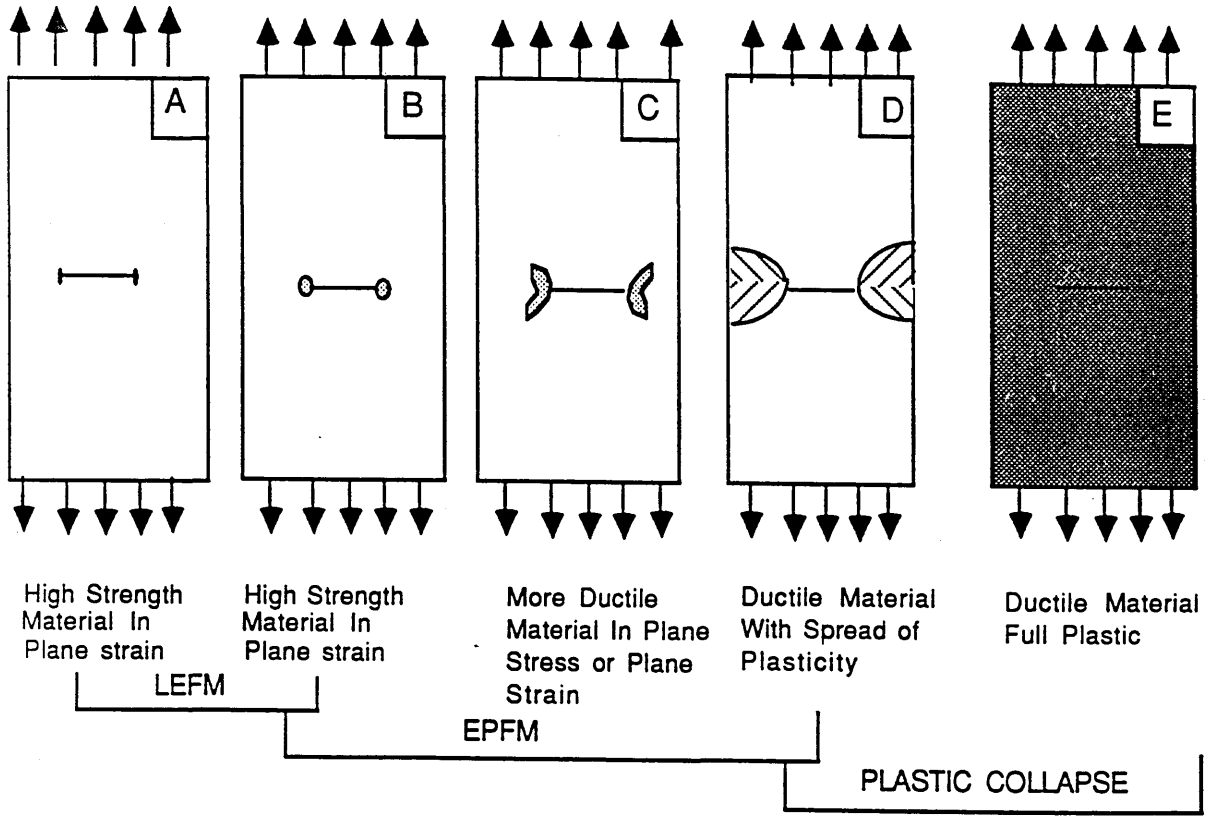

Fig (4.1)

Ranges of applicability of LEFM and EPFM

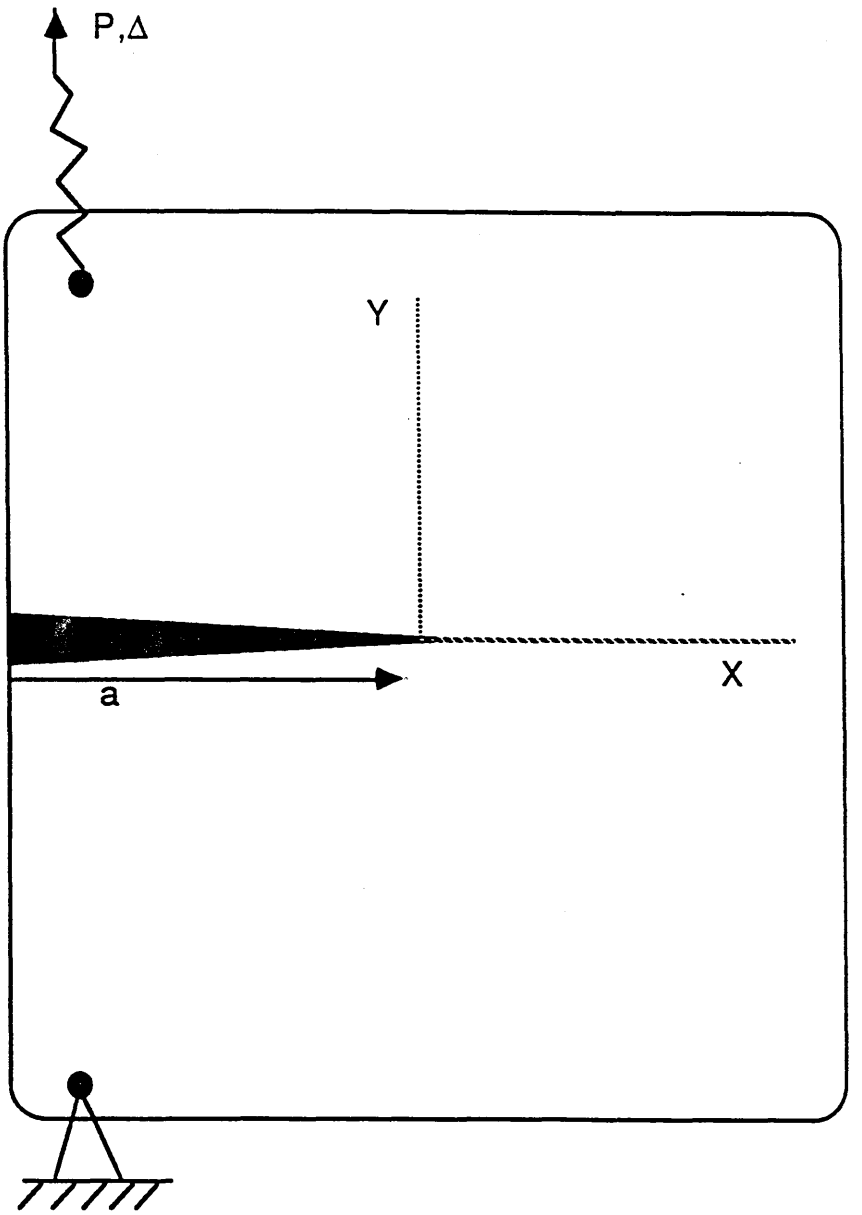

Fig (4.2)

Convention for a cracked body in mode I

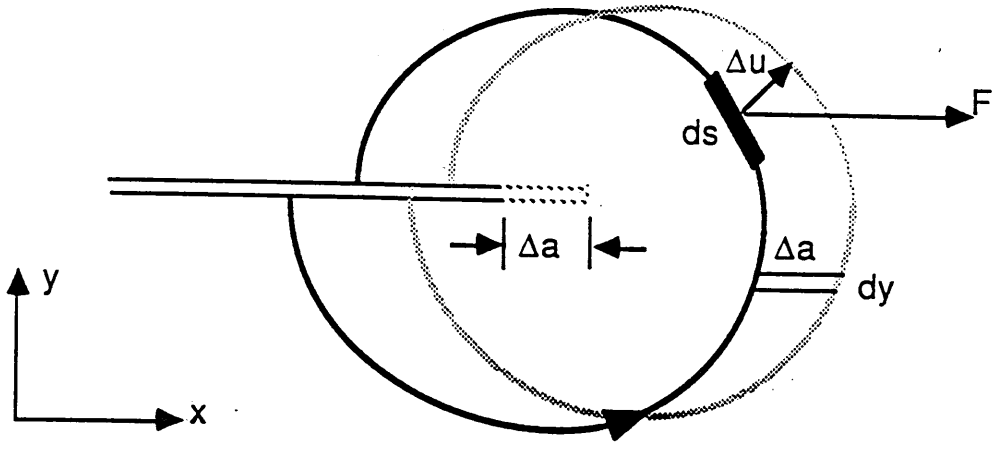

$$J = \int_{r} (W dy - (F - \frac{du}{dx}) ds)$$

Fig (4.3)

Crack tip coordinate system and arbitrary line integral.

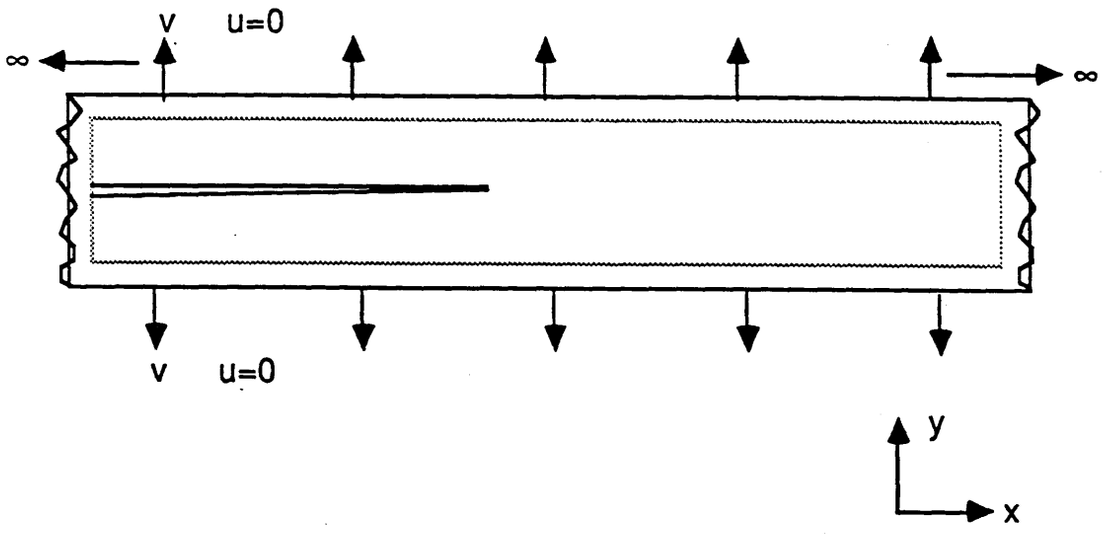

Fig (4.4)

Infinitely long cracked strip with clamped boundaries subject to constant vertical displacement.

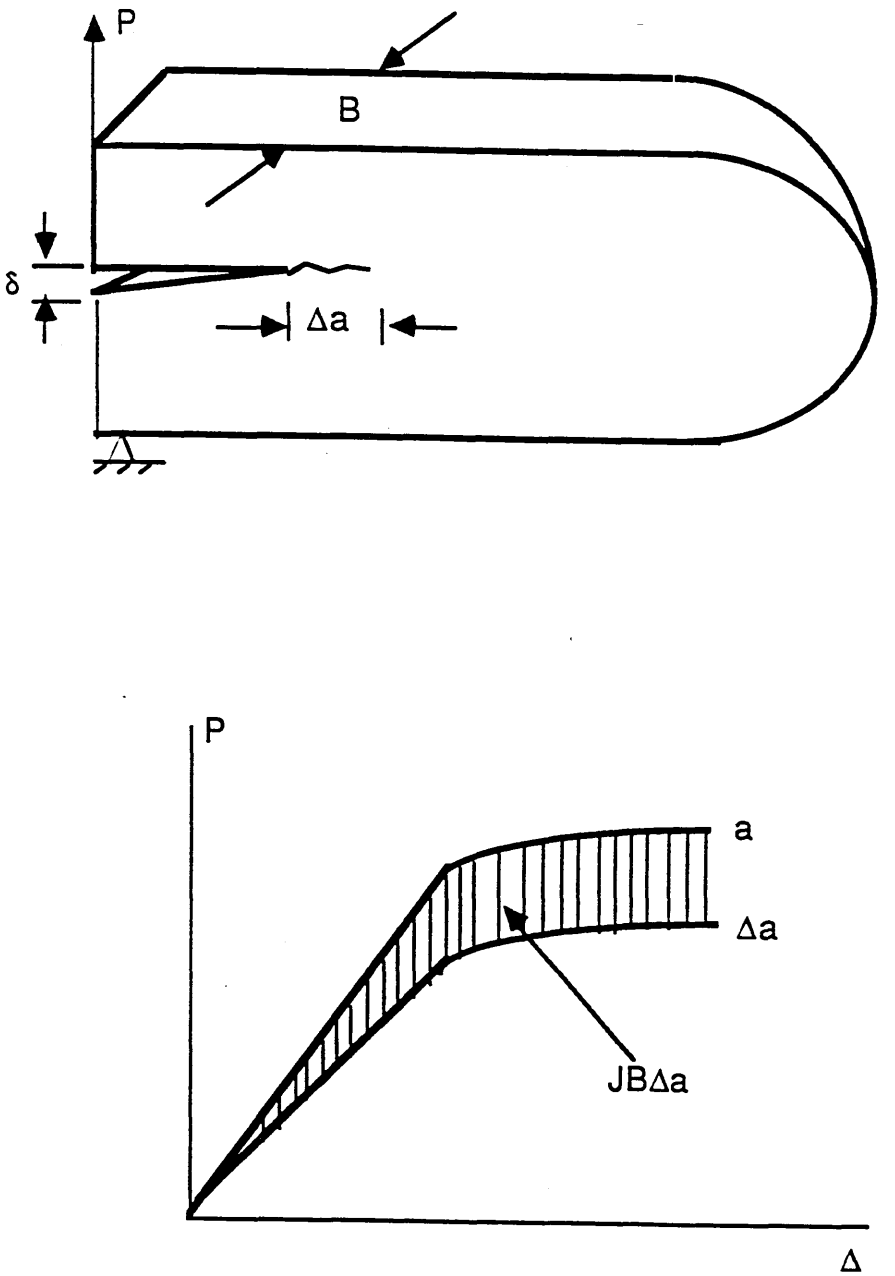

Fig (4.5)

Interpretation of the J-Integral

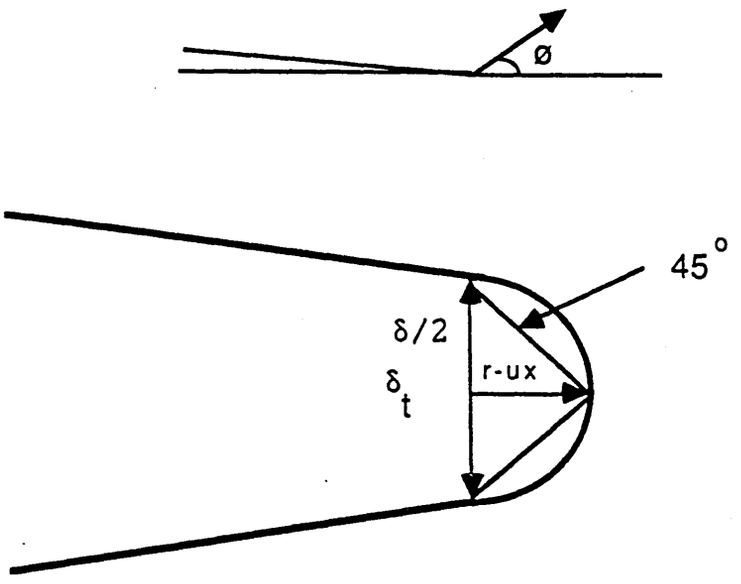

Fig (4.6)

The crack opening displacement defined as the opening at the intercept of two 45° lines from the crack tip

		$m = \delta / (J/\sigma_o)$
Rice (17)	Non-hardening material based on estimates for velocities on slip lines near crack tip	0.67
Rice and Johnson (18)	Non-hardening limit of HRR singularity	0.79
Shih (19)	Finite element analysis using HRR singularity	0.63
Rice (20)	Using hardening material	0.55
Tracey (21)	Finit element analysis for small scale yielding	0.54(1+n)
Robinson and Tetelman (22)	Experimental result using standard ASTM specimen	1.0

Table (1)

Chapter (5)

J DOMINANCE OF SHORT CRACKS THE RESULTS OF EPFM CALCULATIONS

5.1 Introduction

In engineering components, crack initiation usually begins with small surface defects which are produced at stress concentrations under load levels that cause local plasticity (2,3,4,5). During the early stages of crack growth the cracks show fatigue growth rates much in excess of that expected on the basis of the elastic stress intensity factor. However for larger cracks linear elastic fracture mechanics has long been a potent tool in the analysis of the engineering components containing defects.

Most of the work published during the last 10 years has been concerned with deep cracks under fatigue and monotonic loading, or with the fatigue behaviour of shallow cracks. Unfortunately many brittle fractures start at shallow cracks, when it is not possible to make direct measurements of the fracture toughness by using the existing BSI (6) and ASTM (7) or other fracture mechanics standard tests methods.

Wang Tzu Chang (1) pointed out that short cracks are fundamentally different from deep cracks, because the net section stresses are so high that the crack tip plastic zone is so large that LEFM parameters do not characterise the elastic-plastic stress field a head of the crack with sufficient accuracy. Alternatively the crack itself may be so small that LEFM parameters can not quantify the fracture process zone at the crack tip

Short cracks are of interest to alloy designers because they represent a key to improving material properties. They are interest to the scientist because they can not be analysed by valid linear elastic fracture mechanics. But perhaps most importantly, they are of concern to the engineer as LEFM prediction of the growth rate, the calculated inspection interval and possibly the critical crack size may be non conservative.

In the work presented in this thesis, elastic-plastic finite element analysis has been used to study the stress and strain distribution ahead of short cracks in single edge cracked bend and tensile specimens using both small and large geometry change solutions. With the object of determining the conditions under which single parameter characterisation of the elastic plastic deformation ahead of the short cracks can be achieved by the J contour integral and the crack opening displacement.

5.2.Numerical Analysis and Finite Element Models

Four edge cracked bars have been analysed, with (a/W) ratios of 0.1, 0.2, 0.3, and 0.5 ,where a is the crack length and W is the width of the specimen as shown in Fig.(5.1). The models were meshed with eight noded plane strain isoparametric elements provided by the finite element code ABAQUS (10) as illustrated in Fig.(5.2). The details of each model are given in Table (5.1). The models were force loaded on the remote boundary by either a pure couple, or by a uniform tensile stress. The crack tip was modelled in two distinct ways. For the small geometry change solutions a focused mesh with initially coincident,but independent crack tip nodes was used as shown in Fig (5.3a. In contrast the large geometry change

solutions utilised a tip with a small but finite radius as described by McMeeking (8), and illustrated in Fig (5.3b). Typically the tip elements had dimensions of the order of $\delta_0/4$, while the initial opening δ_0 was approximately (a/100)

The material response was represented by a Ramberg-Osgood power law of the form

$$\frac{\varepsilon}{\varepsilon_0} = \frac{\sigma}{\sigma_0} + \alpha \left(\frac{\sigma}{\sigma_0}\right)^n \qquad (1)$$

For the small geometry change solutions the material constants α and n were set at 3/7, and 13 respectively. In contrast the large geometry change calculations were performed with a uniaxial stress strain relation of the form

$$\left(\frac{\sigma}{\sigma_0}\right)^{1/m} - \left(\frac{\sigma}{\sigma_0}\right) = \frac{\varepsilon}{\varepsilon_0} \qquad (2)$$

with a strain hardening exponent m =0.1 which allows contact to be made with the deeply cracked solutions of McMeeking (8) and McMeeking and Parks (9). The two uniaxial stress strain relations of equations (1) and (2) are shown in Fig (5.4) and can be seen to be similar. These uniaxial stress strain relations are generalised into J_2 deformation theory to give an incremental relation of the form

$$\frac{d\varepsilon_{ij}}{\varepsilon_0} = \frac{(1-\upsilon)\, d\sigma_{ij}}{\sigma_0} - \frac{\upsilon\, d\sigma_{kk}\, \delta_{ij}}{\sigma_0} + \frac{3}{2}\alpha n \left(\frac{\sigma_e}{\sigma_0}\right)^{n-2} \frac{\upsilon\, d\sigma_{kk}\, \delta_{ij}}{\sigma_0^2} \qquad (3)$$

The J-integral was determined by the virtual crack extension method of Parks(11) as implemented in ABAQUS(10) using sufficient contours to ensure path independence.

5.3 Small Scale Yielding Solutions

The small scale yielding plane strain solution was obtained from a finite element calculation for an elastic-plastic material with the small geometry change formulation. The finite element model had 144 8-noded isoparametric elements and 471 nodes. Twelve rings of 12 elements comprised the upper half of the crack from ø=0 to ø=π. The displacement field corresponding to the singular elastic field was imposed as the boundary condition at a distance remote from the tip. The calculated stress field is compared with the HRR singularity field Fig (5.5), calculated using the tabulated constants given by Hutchinson (12), although a more complete tabulation of HRR constants has been given by Shih (13).

One interesting result for the small scale yielding field as compared to the HRR field is shown in Fig (5.5) in which the calculated stress field obtained from the small scale yielding solution falls below the HRR solution., although a similar result has been found by Parks et al (22)

5.4 Stress and Strain Fields

5.4.1 Small Geometry Change Solutions

In order to study the stress distribution ahead of short cracks, the stress fields ahead of crack with (a/W) ratios 0.1 , 0.2, 0.3, 0.5 are shown in Figs (5.6) through (5.12), where they are compared with the SSY field. The stresses are non dimensionalised by the yield stress σ_0, while the original distance x of a point ahead of the crack is non-dimensionalised by ($J/\sigma o$). For small values of ($x\ \sigma o/J$) corresponding to small scale yielding conditions and contained plasticity the results for all the geometries with (a/w) $\geq$ 0.3 tend to converge on the SSY curve. For cracks with (a/W) = 0.1 Fig (5.6 and 5.10) the smallest value of ($a\sigma o/J$) was 312 which corresponds to more plasticity than the LEFM limit, and a plastic zone size of order the crack length. The stress at this level of plasticity falls somewhat below the SSY solution. It was difficult to obtain solution for $a\sigma o/J$ greater than 300 because of the extreme mesh refinement needed in this geometry. It can however be noted from Fig (5.13 a) that under conditions where the plastic zone size is of the order of the crack length (contained plasticity), outside the plastic zone and straight ahead of the crack the finite element solution converges towards the K field as the elastic plastic boundary is approached. Inside the plastic zone the SSY and HRR fields becomes similar to the stress field at a value of ($a\sigma o/J$) equal to 312. After plasticity has broken back to the cracked face Fig (5.13b) the stress field ahead of the crack diverges from the K field, and the SSY and the HRR field fail to describe the stress ahead of the crack tip inside the plastic zone. In these conditions J

no longer characterises the crack tip deformation.

For the crack with (a/w) =0.2 under small scale yielding conditions when the plastic zone is small compared with all relevant dimensions and ($a\sigma o/J$) equals 1200 (which is the limit of valid LEFM) the stress were close to, but slightly less than the SSY solution. Increasing deformation shows that the stresses continue to fall below the SSY value and the HRR field until at large values of (x $\sigma o/J$) corresponding to extensive plasticity the stresses converge to a fully plastic field which is geometry dependent. The development of the plastic zone for these two geometries are shown in Figs (5.14,5.15,5.16), from which it can be seen that plasticity extends to the back face of the specimen before the ligament becomes fully plastic. Fig (5.17) shows the stress field along a plane inclined at 45^{o} ahead of the crack under both contained and large scale plasticity conditions. In both cases the stresses does not agree with the HRR field. In contrast the stresses ahead of the crack fall rapidly below the HRR field with increasing the plastic deformation.

The results for (a/W) = 0.5 are given in Fig (5.9), from which it can be seen that the stresses can be described by the SSY field at non-dimensionalised distances (x σ_o/J) of the order of 2, even for extensive plasticity. The development of plasticity is confined to the ligament as illustrated in Fig (5.18) corresponding to the deeply cracked slip line field of Green (14).

5.4.2 Large Geometry Change Solutions

Large geometry change solutions have been used to investigate the deformation within one or two crack tip openings of the

blunting tip in the spirit of the work by McMeeking (8). In this case the original distance of a point x_0 ahead of the tip are non-dimensionalised by the crack tip opening δ which is defined by the convention introduced by Shih (13). Results are presented for three geometries (a/W) = 0.1 , 0.2 and 0.3 and these are compared with the calculations of McMeeking (8) and McMeeking and Parks (9) in Figs (5.19) through (5.24) for both tension and bending with strain hardening exponents m = 0.1 and 0.2. For the critical geometry defined by (a/W) = 0.3 the stresses ahead of the crack approach the small scale yielding solution over distances close to 2δ. However for the sub-critical geometries of (a/W) = 0.1 and 0.2 the stresses do not achieve the full values of the J dominated field but reach a maximum stress at distances of less than δ, although within this distance the fields are closely similar. The equivalent plastic strains ahead of the cracks are shown in Figs.(5 25a,5.25b) and are not dissimilar.

5.5 DISCUSSION

The reason for loss of J dominance for weakly hardening materials is most clearly seen by referring to the appropriate slip line field. The slip line field for a deeply cracked bar under bending given by Green (14) is shown in Fig (5.26). Here the deformation is confined to the uncracked ligament, and the field is thus independent of notch depth, and can be easily modified blunting by the inclusion of a log-spiral slip line field detail which extends to almost 2δ, giving a local stress field similar to that calculated in small scale yielding by Rice et al (15). J dominance thus applies for extensive plasticity. However for shallow cracked

bars, plasticity spreads to the surface of the bar on either side of the crack , in away that was proposed qualitatively by Green (14) and has been examined quantitatively by Ewing (16) using the extension to the deeply cracked slip line field indicated by the broken lines in Fig (5.26). Although Ewing did not explicitly consider cracked geometries the critical depth for plasticity to be confined to the ligament for a notch with an included angle of 3.21° is (a/W) = 0.3. The present finite element calculations for a weakly hardening material are consistent with these observations in that plasticity is confined to the uncracked ligament for (a/W = 0.5), while for the critical geometry (a/W = 0.3) plasticity is confined to the ligament until the highest load levels studied when a small amount of yielding appears on the cracked face , remote from the crack. Both of these geometries thus essentially behave as deeply cracked bars, and the stress straight ahead of the crack in the small geometry change solutions is closely similar to the HRR field, as shown in Figures (5.8) and (5.9), and this similarity is maintained as plasticity extends from small scale yielding into full plasticity of the uncracked ligament. For these geometries the size of the ligament is clearly the controlling dimension and the present results are consistent with the J dominance criteria of McMeeking and Parks(9) and Shih and German (17)

In contrast the sub-critical crack geometries of (a/W) = 0.1 and 0.2 shown in Figures (5.6,5.7,5.11,5.12) show that even under contained yielding conditions the stresses ahead of the crack fall below the small scale yielding values determined from the boundary layer solution until they approach another limiting

distribution which is geometry dependent in both tension and bending. Even for the valid LEFM result obtained for a/W=0.2 and $a\sigma o/J$ =1200 the stress falls slightly below the SSY value and may be necessary to conclude that the solution for the state of stress at the crack tip can not be characterised by the stress intensity factor K_I alone, even at the load levels close to the ASTM-limit (20).

In order to obtain a good agreement between the boundary layer formulation and a full geometry solution Larsson et al (20) found it necessary to modify the boundary layer solution. This modification consists of an addition to the boundary traction of the boundary layer problem of traction corresponding to the non-singular terms of the X direction stress of the actual geometry. The magnitude of this stress can be found from the elastic finite element solution for the geometry and called the T stress. (Rice (23))

The limiting fields for bending are shown in Figure (5.27) from which it is clear that the four geometries exhibit a consistent trend. This trend is also clearly seen in the large geometry change results illustrated in Figure (5.28). Deeply cracked geometries are represented by McMeeking's small scale yielding solution (8) and the loss of J dominance with crack length is clear.

Criteria for loss of J dominance are somewhat subjective, nevertheless it is clear that there is a marked loss of J dominance with crack length which is consistent with the criterion that the crack length should be greater than $200J/\sigma_0$ for ($a/W < 0.3$) in both bending and tension while for more deeply cracked geometries the criteria proposed by McMeeking and Parks(9) and Shih and German (17) applies. The loss of single parameter characterisation is

shown in both tension and bending, being most marked for the shortest crack (a/W) = 0.1

Experimental data on cracks with ratios a/W=0.1 and 0.3 have been given by Sumpter (18) who has given the value of {2 σo δ E/1-υ^2} which he defined as K_δ in both valid and non valid LEFM condition. K_δ was found to be geometry dependent at 0 ^{o}c, but experimental the results converged with decreasing temperature, until at (-100 ^{o}c) the K_δ became geometry independent and equal to 100 MN/m$^{3/2}$. This data has been re-analysed in terms of J in Fig (5.29). The J integral is calculated using the form

$$\delta = d(\alpha\ \varepsilon o,n)\ J/\sigma o \qquad (67)$$

Where d(α εo,n) is geometry independent function and equal to 0.7 for N=13 and εo =0.002. The CTOD was calculated from relation used by Sumpter with E=207 MN/m^2 and a temperature dependent value of yield stress σo, which was taken as 216 MN/m^2 at room temperature

$$\delta = K^2\ (1-\upsilon^2)/\ 2\sigma o\ E \qquad (68)$$

At low temperatures J for both a/W=01 and a/W=0.3 coincide at temperature of approximately (-100 ^{o}c) when (a σo/J=200) which is in a good agreement with finite element results obtained in the present work.

5.6 Conclusion

In the present calculations in which the stresses ahead of the crack with aspect ratios (a/W)=0.1,0.2,0.3 and 0.5 have been compared with the HRR field and the SSY solutions. The critical crack depth for plasticity to be confined to the ligament is close to 0.3 for both tension and bending. Both small geometry change solutions with sharp cracks and large geometry change solution with blunting cracks have been examined. The results of the small geometry change solution were compared with HRR field and the SSY solution. Edge cracked bars with the (a/W) ratios less than 0.3 are shown to lose J dominance for crack length less than 200 $J/\sigma o$ in both tension and bending. However for the geometries with ratios (a/W) ≥ 0.3 in which plasticity developed through the ligament without spreading to the back face maintain J dominance up to criteria given by McMeeking and McMeeking and Parks (8,9).

The results of the large geometry change solution were compared with the small scale yielding solution given by McMeeking (8). For the critical geometry defined by (a/W) = 0.3 the stresses ahead of the crack approach the small scale yielding solution over distances close to 2δ. However for the sub-critical geometries of (a/W) = 0.1 and 0.2 the stresses do not achieve the full values of the J dominated field but reach a maximum stress at distances of less than δ, although within this distance the fields are closely similar. For the critical geometry (a/W=0.3) plasticity confined to the ligament and the stress field ahead of the crack approaches that given by McMeeking (8). Both the small and large geometry change solution are thus consistent with proposal that J

dominance is lost for crack length less than ($200J/\sigma o$) in tension and bending for ($a/W \leq 0.3$). For the ($a/W \geq 0.3$) the edge crack bars behave as deeply cracked geometries and follow the criteria described by McMeeking and McMeeking and Parks (8,9) and Shih and German (17)

In the present small scale yielding solution the non singular terms have been neglected, and only the dominant singular term was retained. However as suggested by previous numerical investigation on the effect of the non singular terms on the elastic - plastic fields in the vicinity of a crack tip (19,20,21), the elastic-plastic field in the vicinity of a crack may be better characterised using singular and non singular terms.

Further work will investigate the effect of the non singular terms on a one parameter characterisation of the elastically contained plastic field ahead of short cracks in tension and bending.

5.7 REFERENCES

1. Wang Tzu Chiang and Miller K.J., Fatigue of Eng Mat and Structure Vol 5, pp 249-263, (1982)

2. Dowling N. E. and Begley, J. A., ASTM STP 590, pp82-130, (1976)

3. Haddad, M. H. , Dowling, N. E. Topper, T. H. and Smith, K. N., Int J of Fracture, Vol 16, pp 15-30, (1980)

4. Miller K.J.,Fatigue of Eng Mat and Structure Vol 4, pp 223-232, (1982)

5. Miller K. J and Ibrahim M. F. E., Fatigue of Eng Mat and Structure Vol 4, pp 263-277, (1981)

6. ASTM, Standard, E 394-78. A Standard Test Method of Plane Strain Fracture Toughness of Metallic Materials., ASTM, Standards, Part 10, pp 540-561, (1979).

7. British Standard 5447 'A Method for Test for Plane Strain Fracture Toughness Testing of Metallic Materials' . The British Standards Instution.

8. McMeeking, R. M. and Parks, D. M. " Elastic-Plastic Fracture Mechanics" ASTM STP 668, pp 175-191, (1979).

9. McMeeking, R. M., J. Mech. Phys. Solids. Vol 25, ppP 375-381, (1977).

10. Hibbitt, Karlsson and So rensen , ABAQUS Users Manual, (1984).

11. Parks, D. M., J of Fracture , Vol 10, pp 487-496, (1974)

12. Hutchinson, J. W., J. Mech. Phys. Solids. Vol 16, pp 13-31, (1968).

13. Shih, C. F. "Tables of Hutchinson-Rice-Ronengren Singular Field Quantities " Brown University Report, MRL E-147

14. Green, A. P. Q. J Mech Appl Maths. Vol 6 pp 223, (1953).

15. Rice, J. R. and Johnson., M. A., Inelastic Behaviour of Soild., ed

Kanninen et al, McGraw Hill New York, pp 641, (1970).

16. Ewing, D. J., J Mech Phys Solids. Vol 16, pp 305-213, (1968).

17. Shih, C. F. and German, M. D., Int J of Fracture, Vol 17, pp 27-43, 1981

18. Sumpter J. D. G , Int J Press Ves and Piping Vol 10, pp169-180 (1982)

19. Kfouri, A.P., Int J of Fracture, Vol 30, pp 301-315, (1986)

20. Larsson, S.G. and Carlsson, A.J., J Mech Phys solids, Vol 21, pp 263-277, (1973)

21. Leevers, P.S. and Radon, J.C., Int J of Fracture, Vol 19, pp 311-325, (1982)

22. Parks, D. M. and Wang Y.Y. "Elastic-Plastic Analysis of Part Through Surface Crack " To appear in ASME Symp July (1988)

23. Rice J. R. J Mech Phys Solids. Vol 16, pp 305-213, (1968).

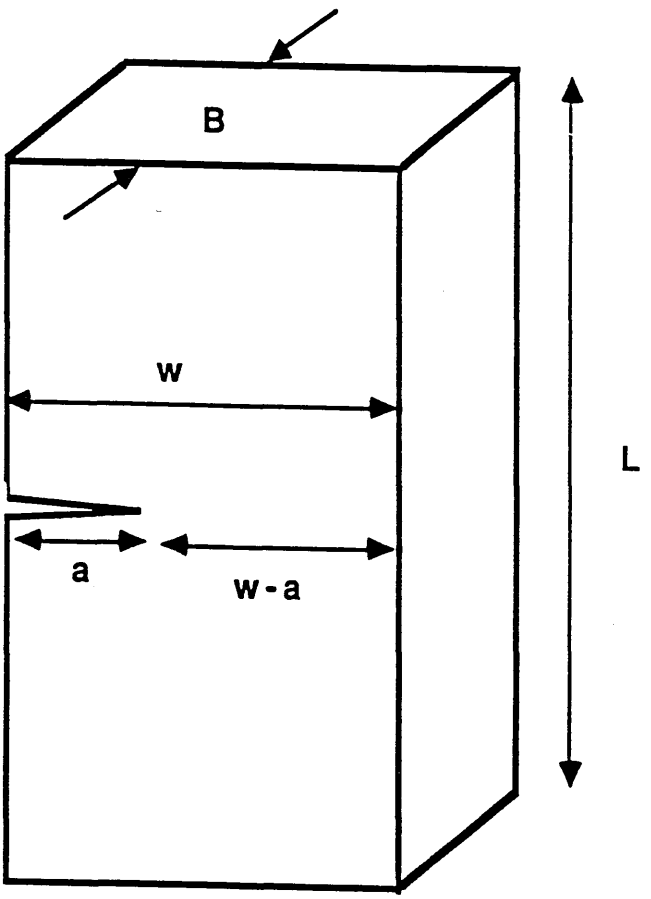

L=3 w

Fig (5.1)

The notation of the edge cracked bar

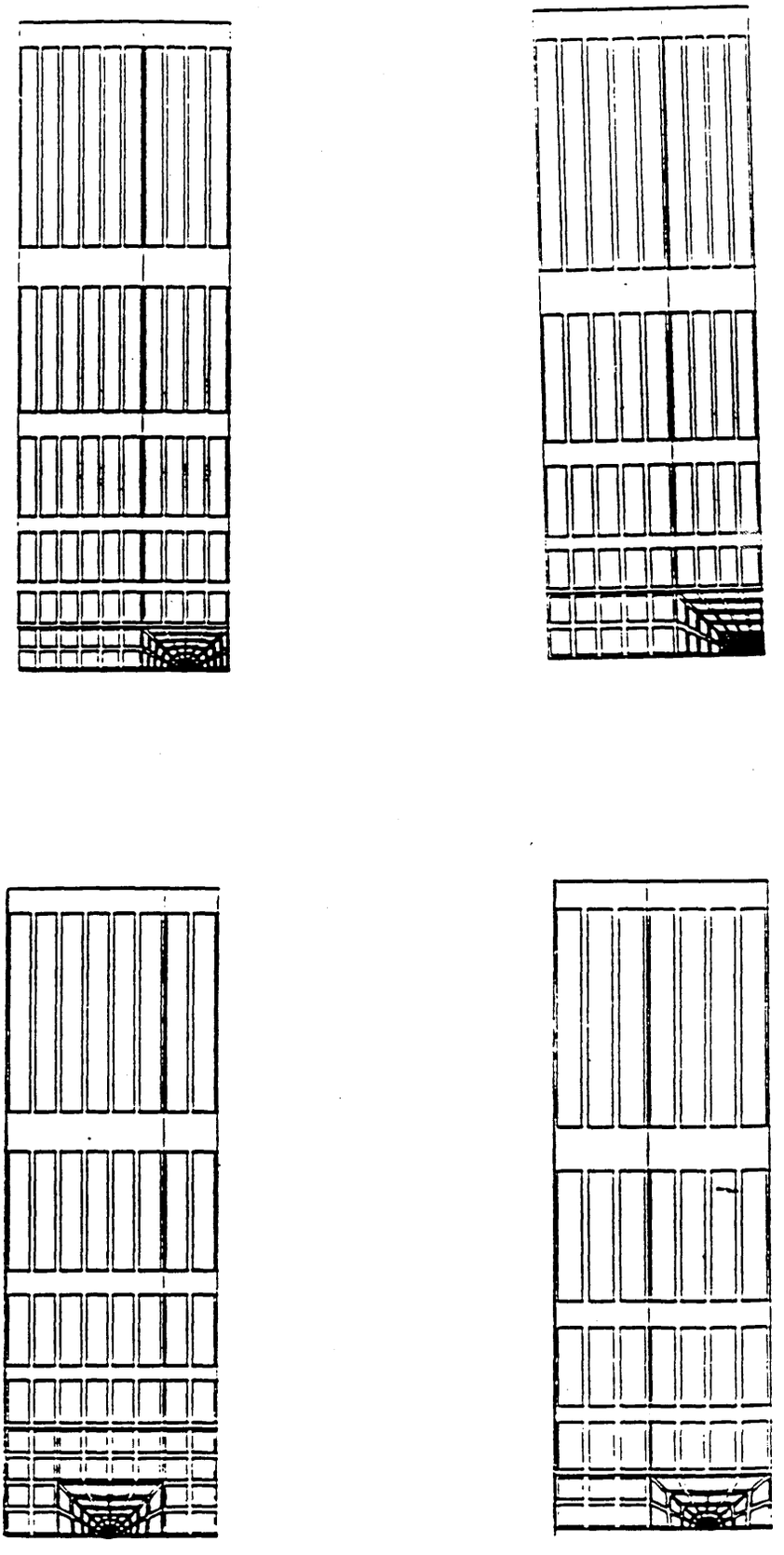

Fig (5.2)

The overall mesh geometry for (a/W = 0.1 0.2, 0.3, 0.5)

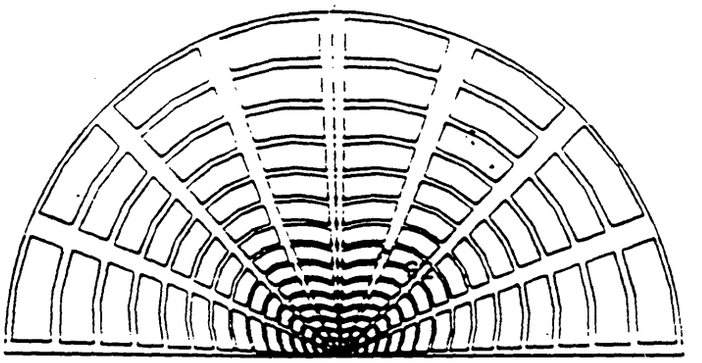

Fig (5.3a)

A focussed mesh at a sharp crack tip.

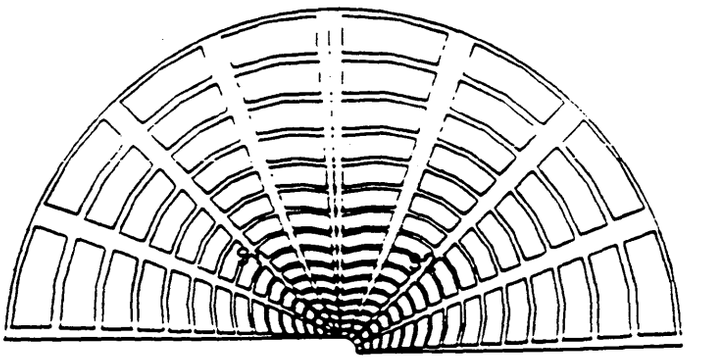

Fig (5.3b)

A blunt crack with a small initial radius

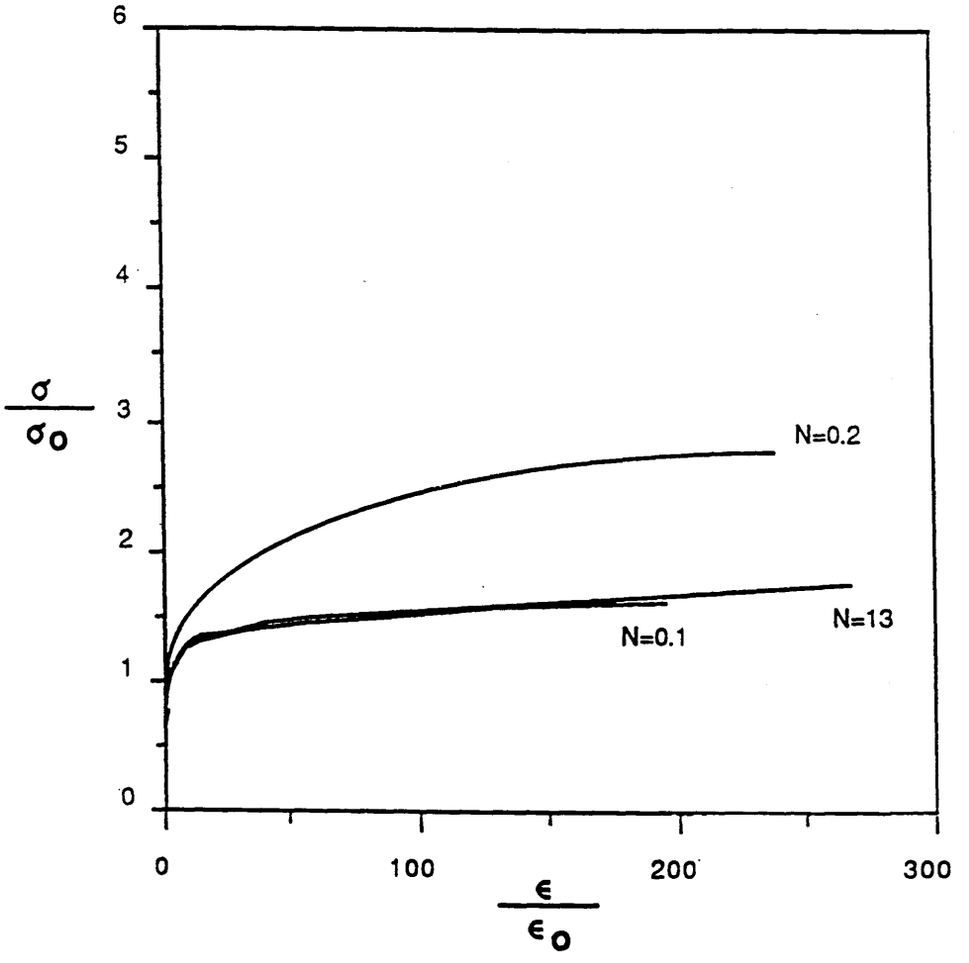

Fig (5.4)

Uniaxial stress- strain relations

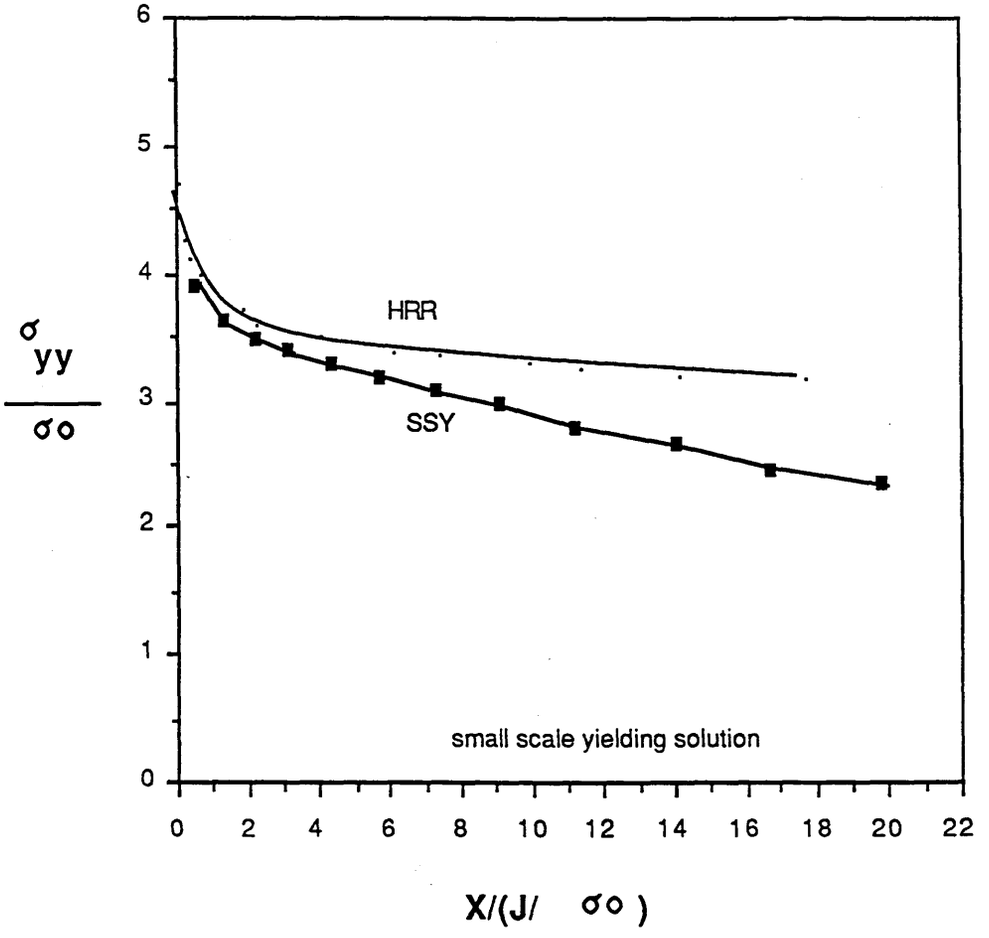

Fig (5.5)

The comprasion between the SSY solution and the HRR fields.

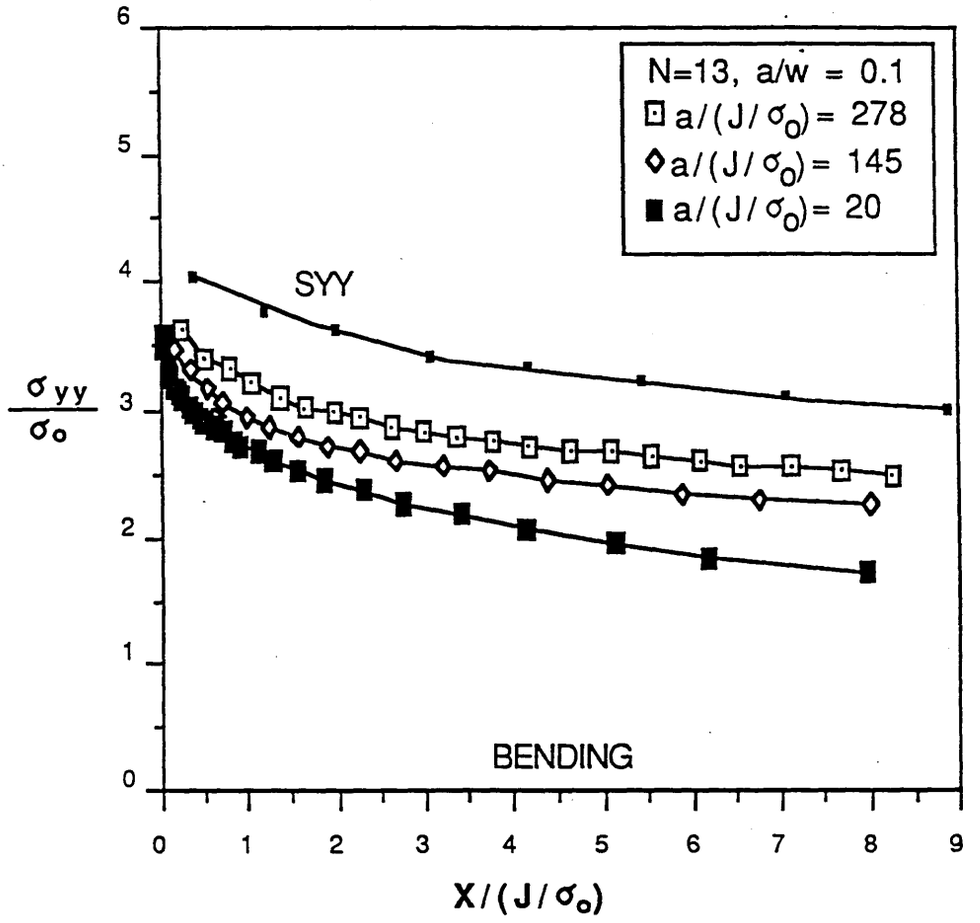

Fig (5.6)

The stress field ahead of a sub-critical crack in bending (a/W=0.1, n = 13)

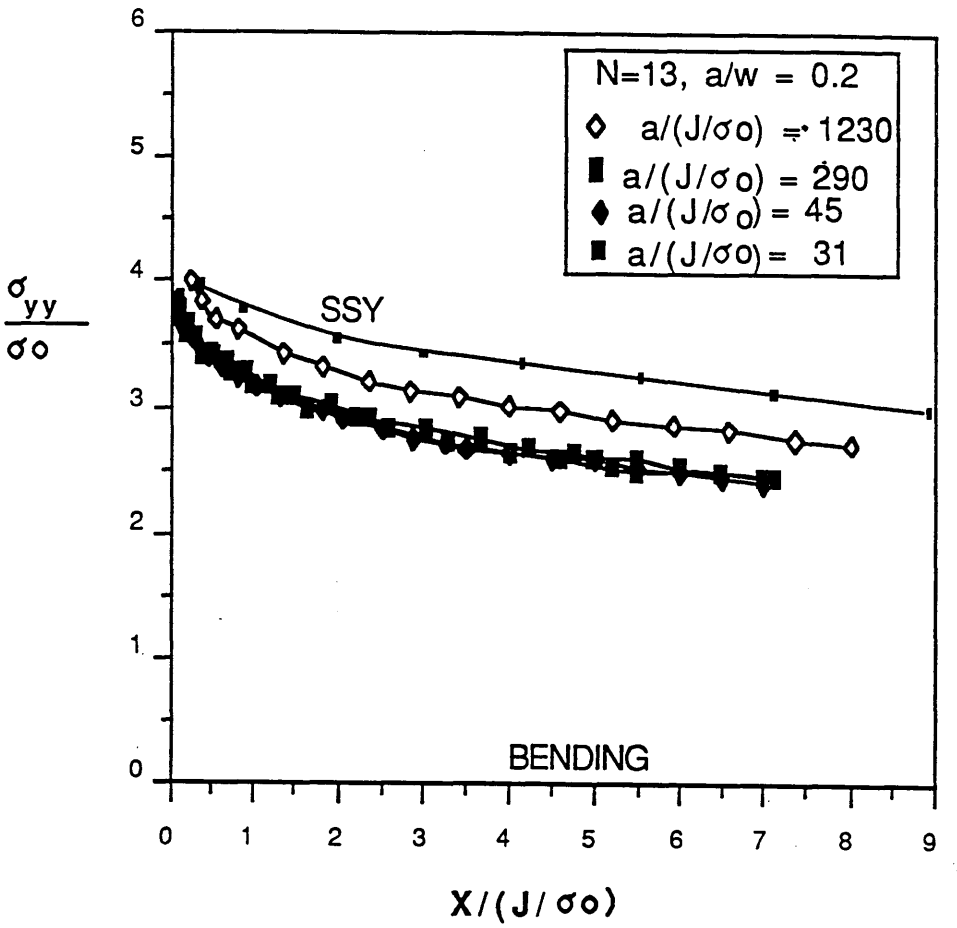

Fig (5.7)

The stress field ahead of a sub-critical crack in bending (a/W=0.2, n = 13)

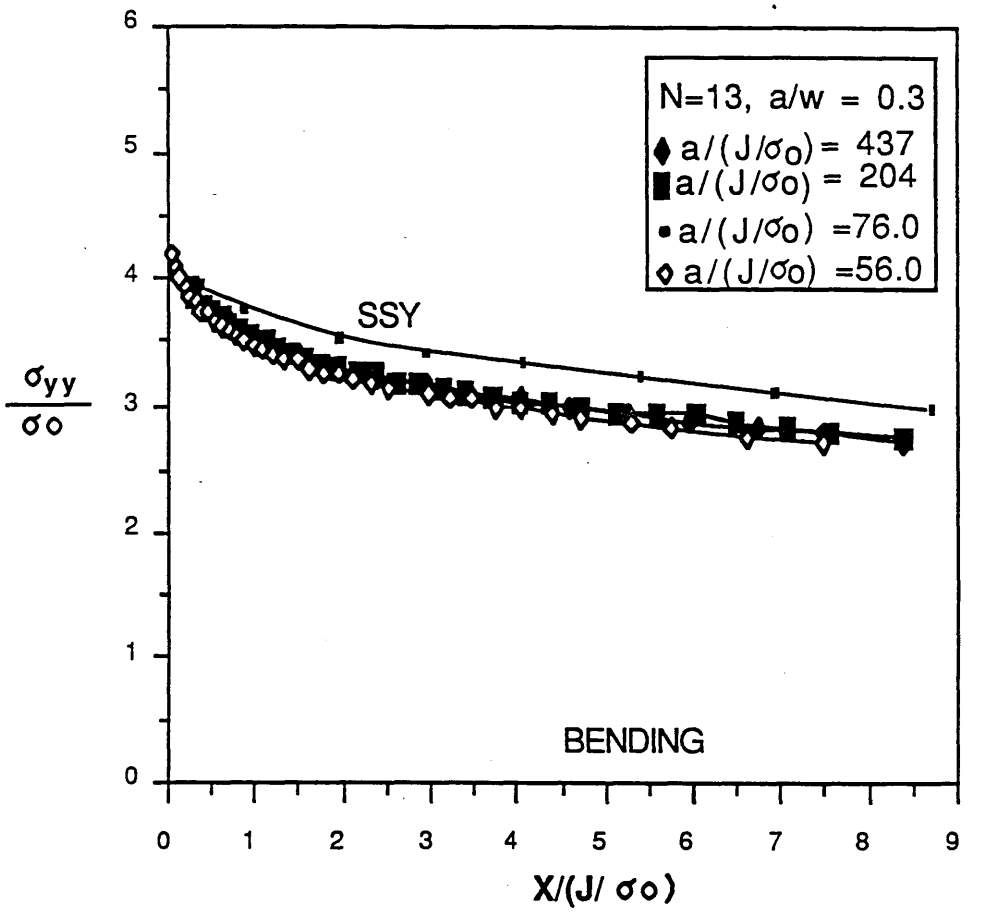

Fig (5.8)

The stress field ahead of a sub-critical crack in bending (a/W=0.3, n = 13)

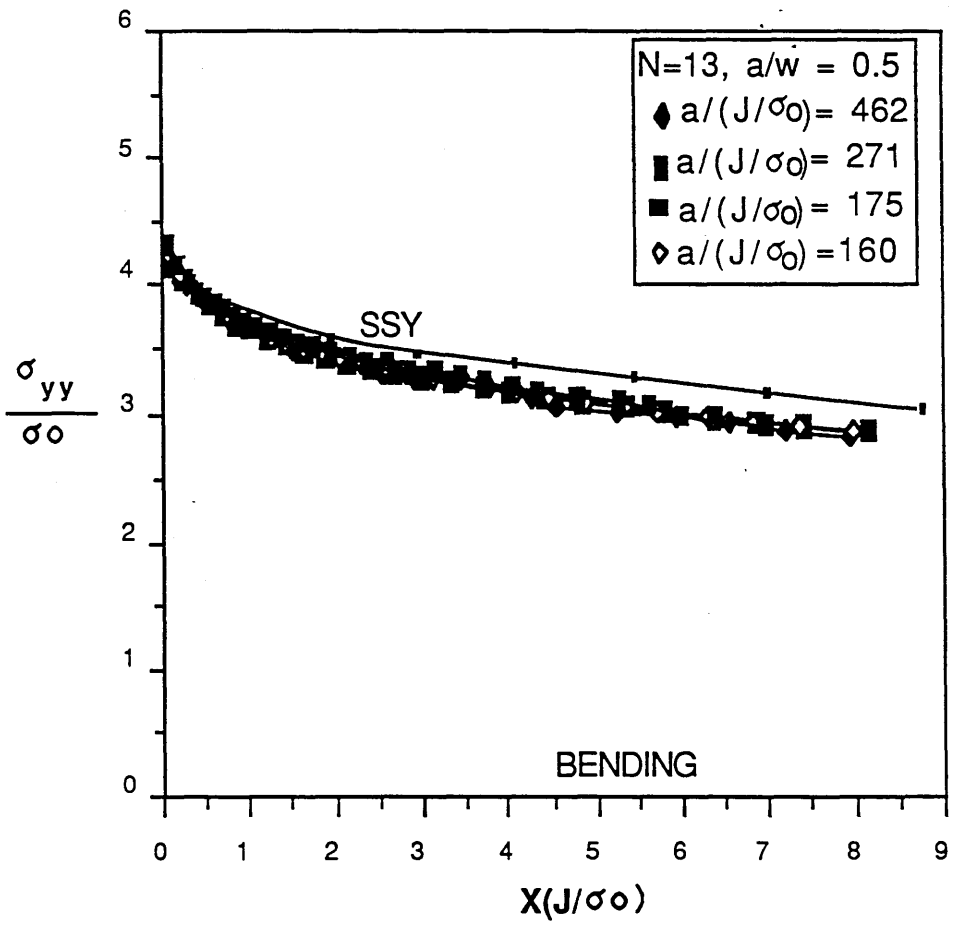

Fig (5.9)

The stress field ahead of a sub-critical crack in bending (a/W=0.5, n = 13)

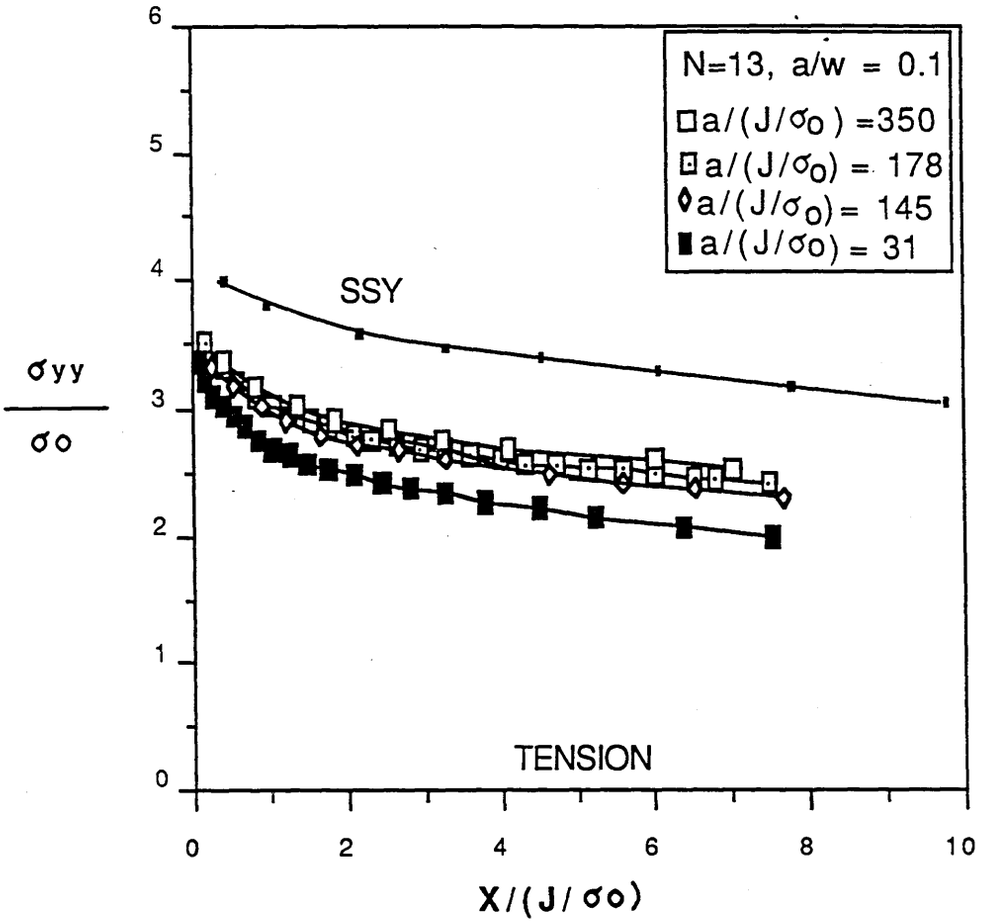

Fig (5.10)

The stress field ahead of a sub-critical crack in tension (a/W=0.1, n = 13)

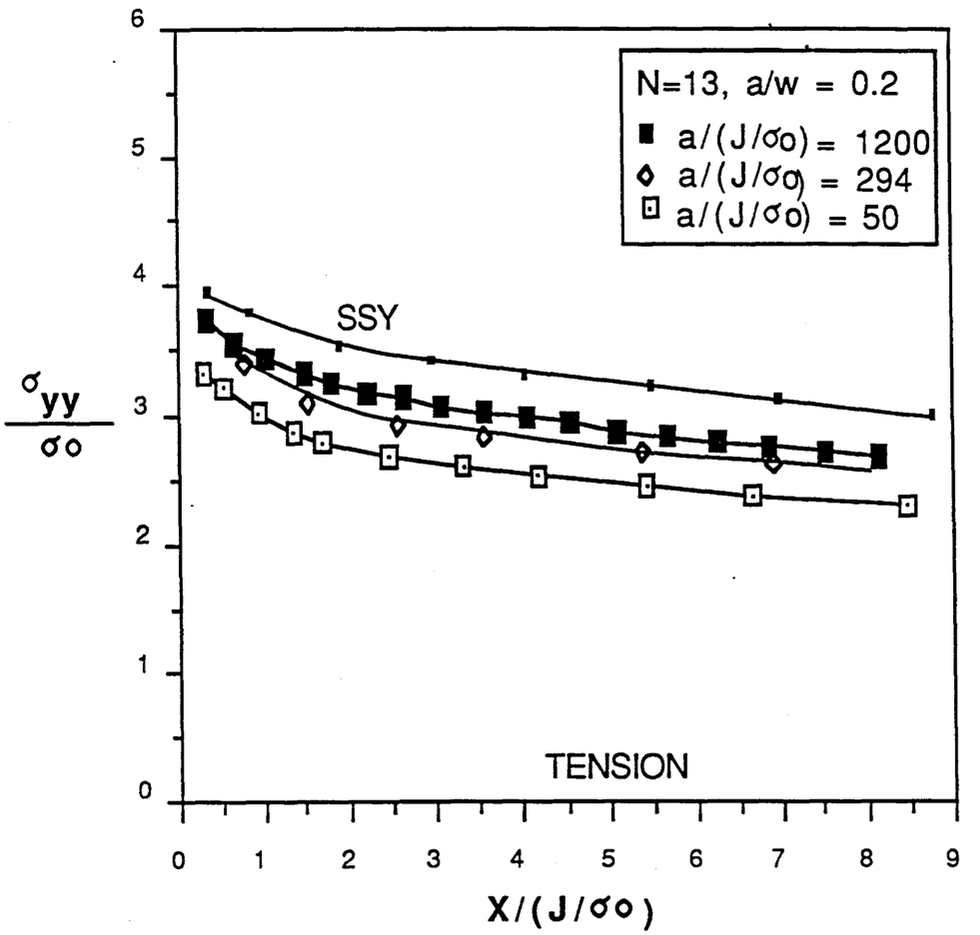

Fig (5.11)

The stress field ahead of a sub-critical crack in tension (a/W=0.2, n = 13)

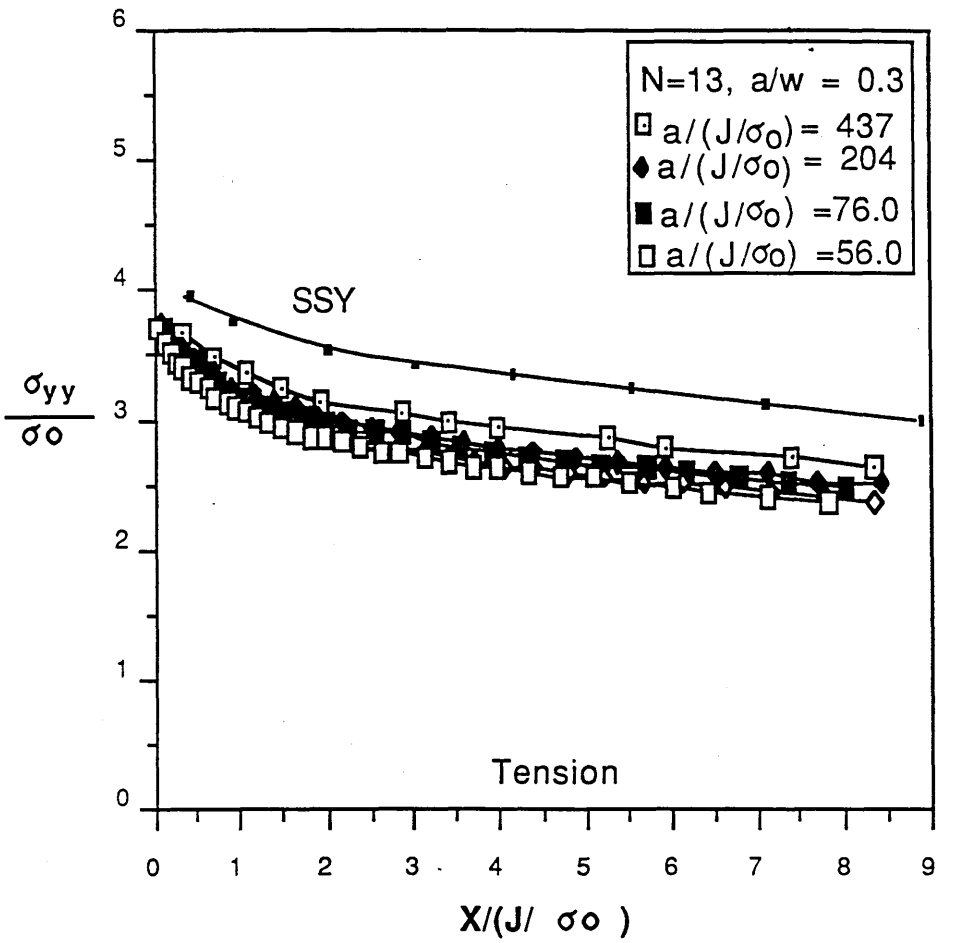

Fig (5.12)

The stress field ahead of a sub-critical crack in tension (a/W=0.3, n = 13)

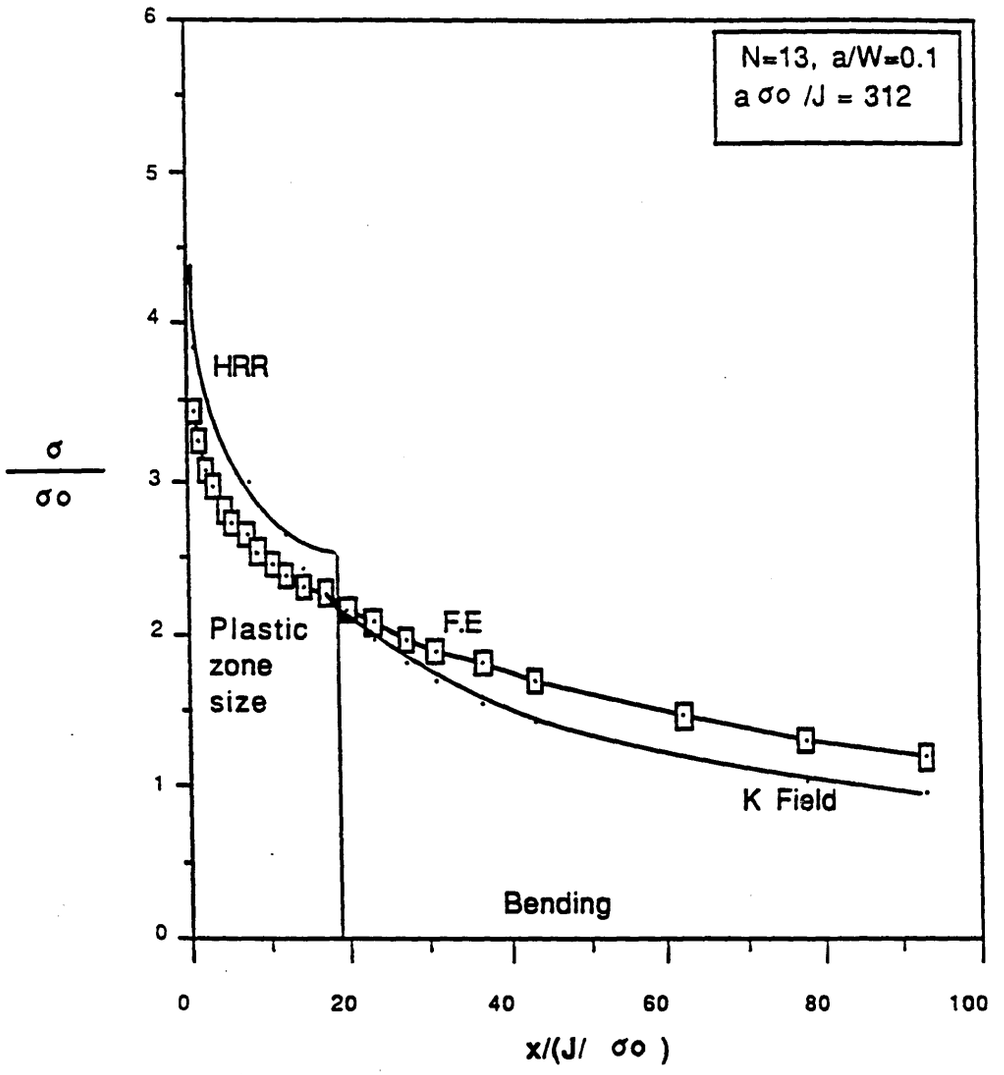

Fig (5.13a)

The stress ahead of the crack tip in side and out side the plastic compared with HRR solution and K field respectively at the small scale yielding condition

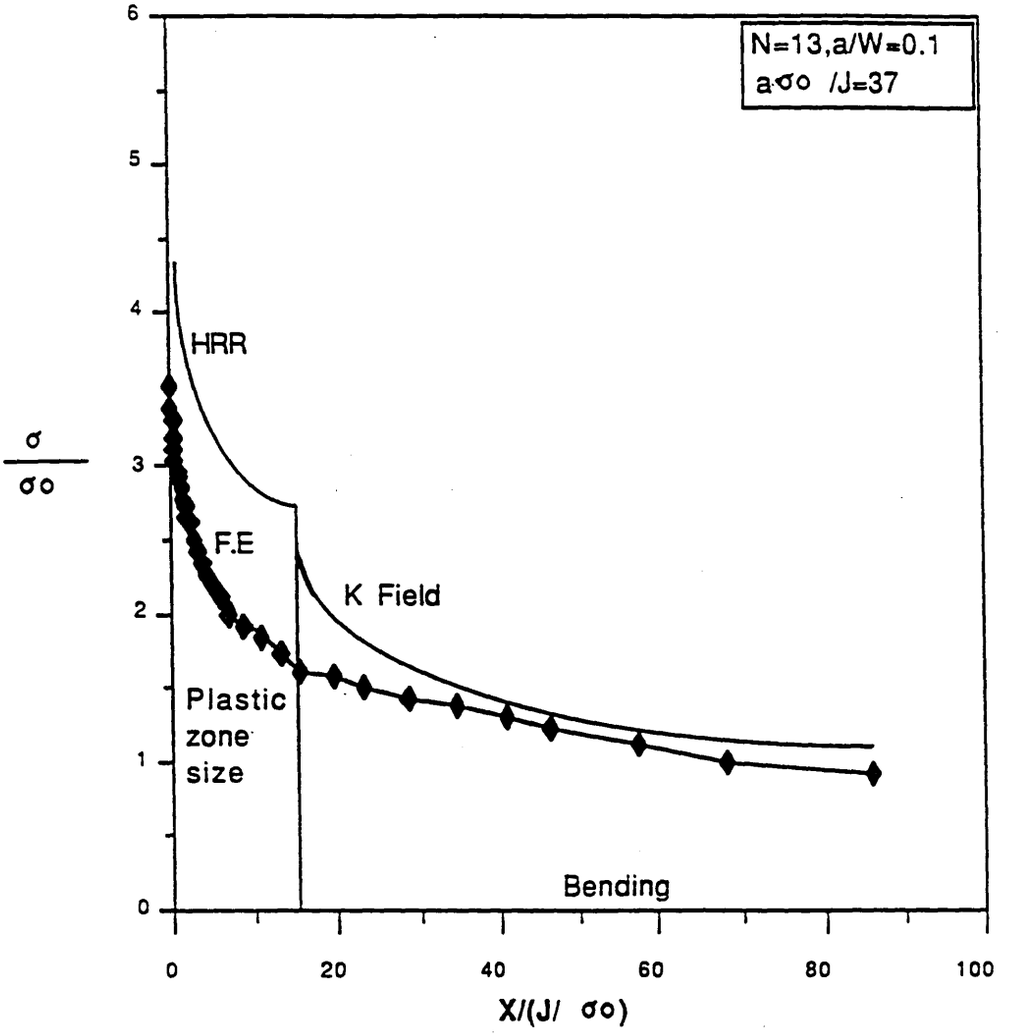

Fig (5.13b)

The stress ahead of the crack tip in side and out side the plastic compared with HRR solution and K field respectively at the large scale yieldin conditon

PLASTIC ZONE IN BENDING.

$\frac{a}{w} = 0.1$ N = 13

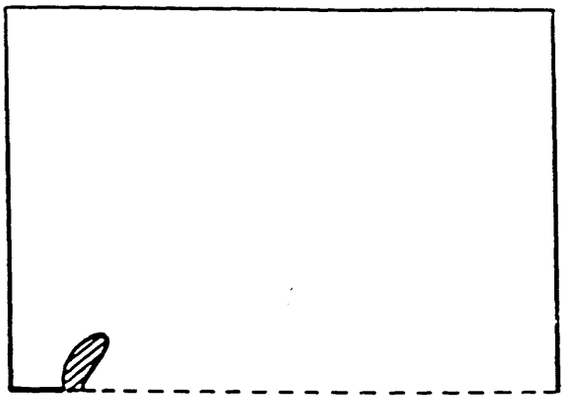

$\left(\frac{a\sigma_0}{J}\right) = 178$

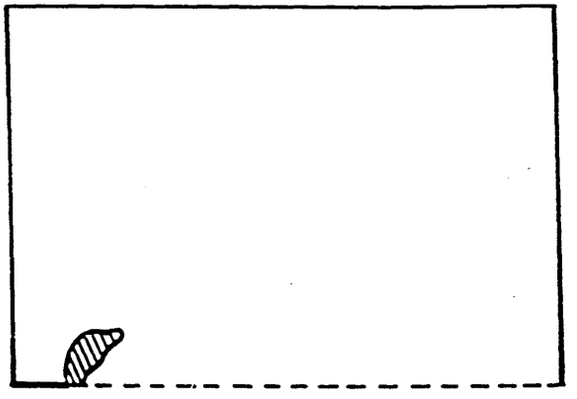

$\left(\frac{a\sigma_0}{J}\right) = 112$

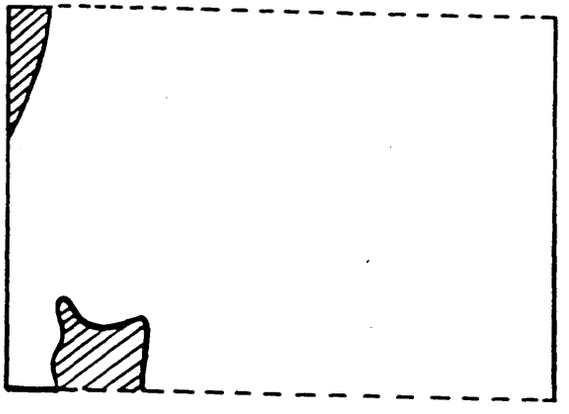

$\left(\frac{a\sigma_0}{J}\right) = 37$

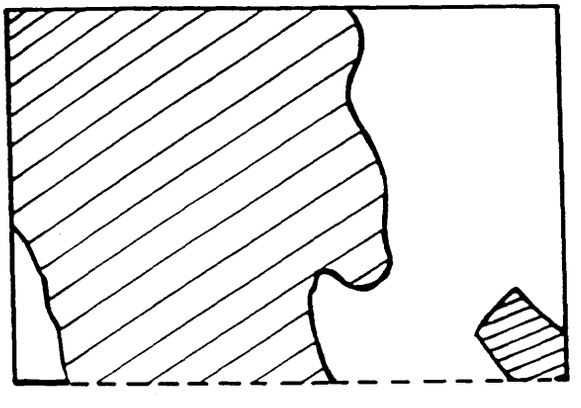

$\left(\frac{a\sigma_0}{J}\right) = 20$

Fig (5.14)

PLASTIC ZONE IN BENDING.

$\frac{a}{W}$ = 0.2, N = 13

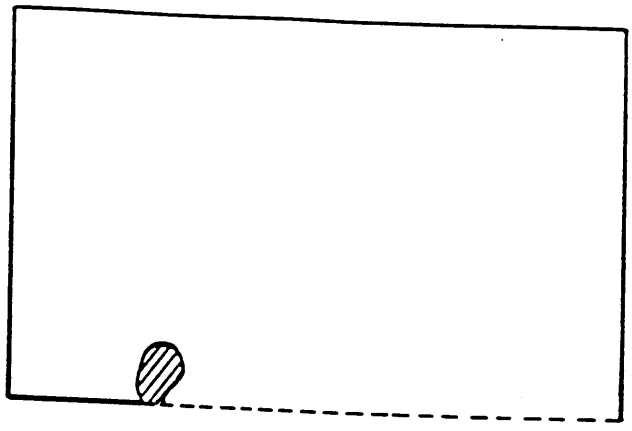

$\frac{a\sigma_o}{J}$ = 325

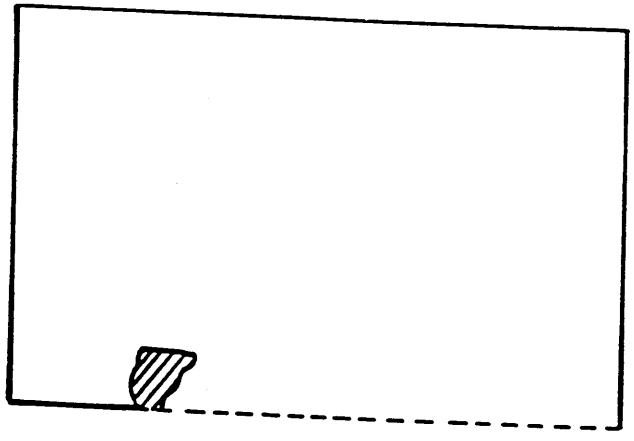

$\frac{a\sigma_o}{J}$ = 180

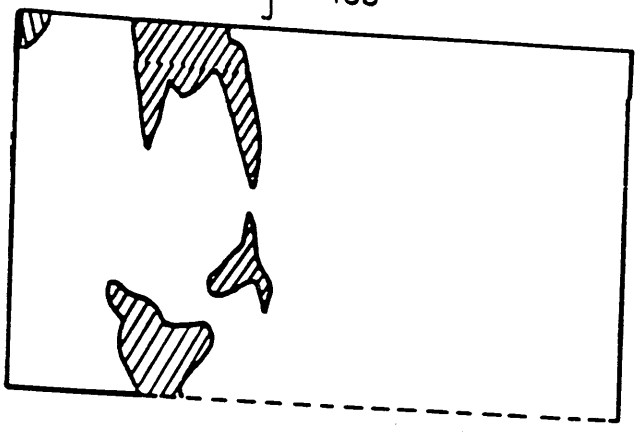

$\frac{a\sigma_o}{J}$ = 115

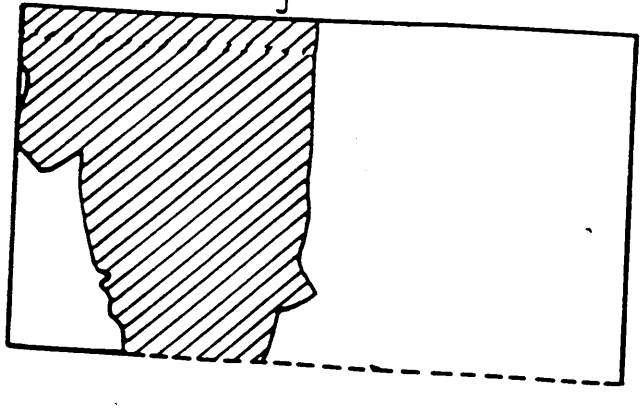

$\frac{a\sigma_o}{J}$ = 31·00

Fig (5.15)

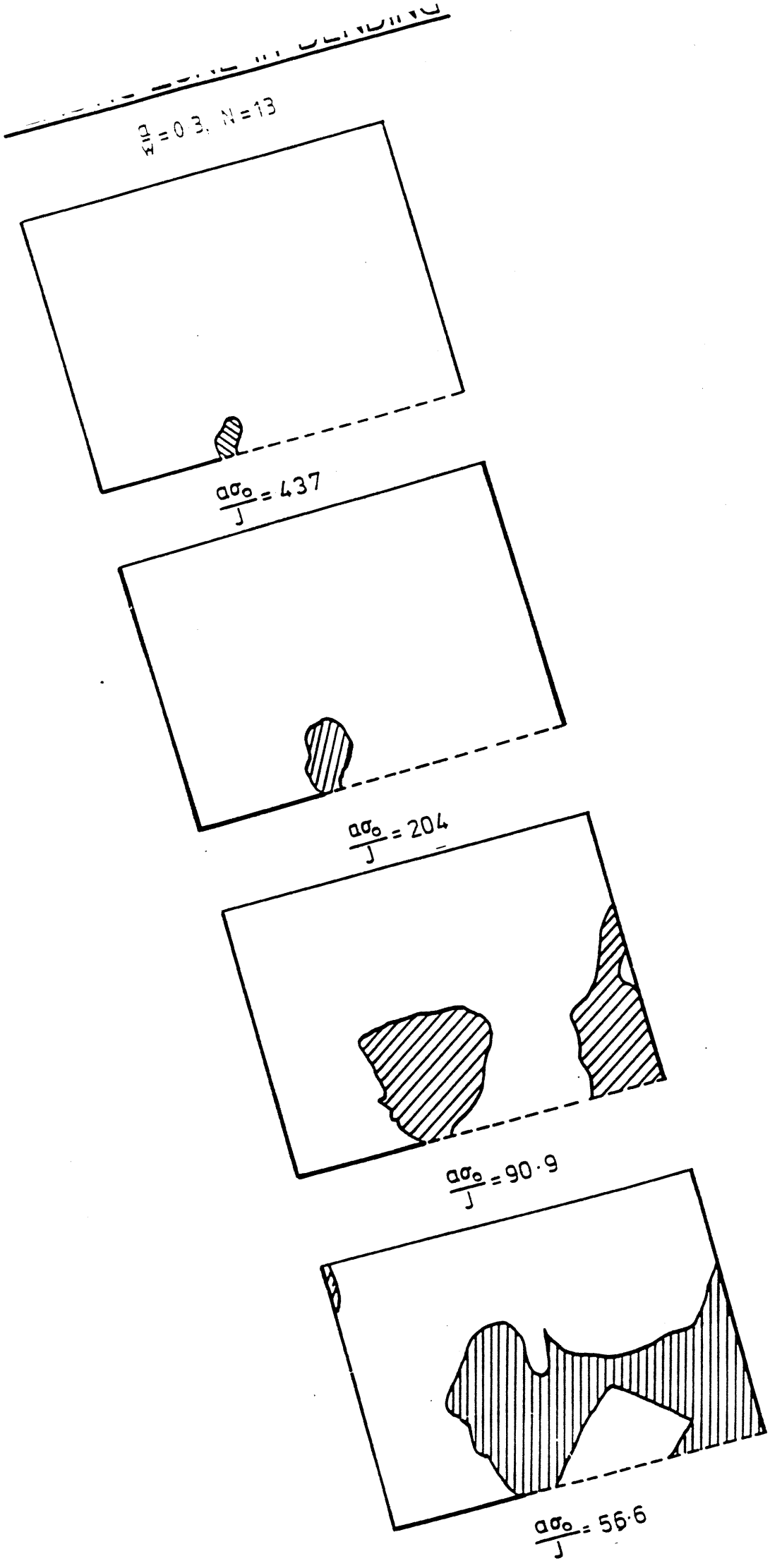
$\frac{a}{W}$ = 0.3, N = 13
$\frac{a\sigma_o}{J}$ = 437
$\frac{a\sigma_o}{J}$ = 204
$\frac{a\sigma_o}{J}$ = 90.9
$\frac{a\sigma_o}{J}$ = 56.6

Fig (5.16)

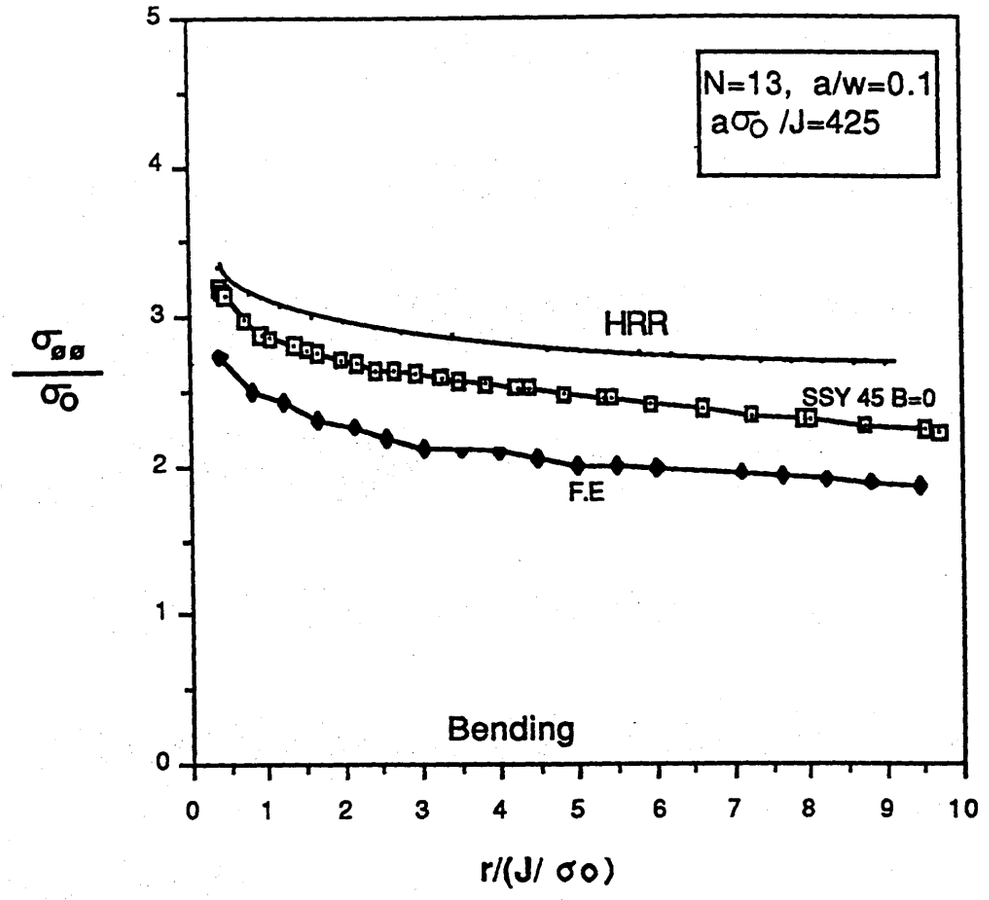

Fig (5.17)

The stress field at 45° of sub-critical crack in bending (a/W=0.1, n=13)

PLASTIC ZONE IN BENDING.

$\frac{a}{w} = 0.5$, N = 13

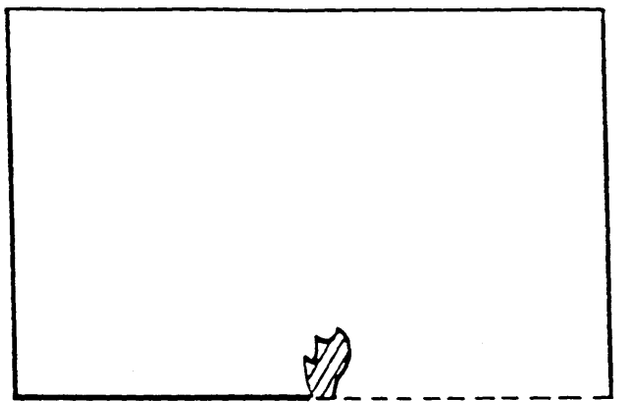

$\frac{a\sigma_o}{J} = 462$

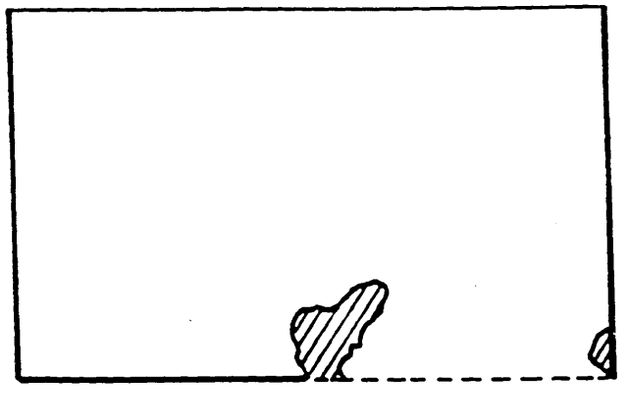

$\frac{a\sigma_o}{J} = 219{\cdot}9$

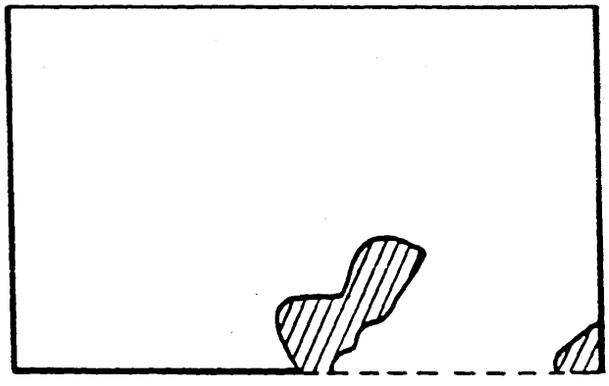

$\frac{a\sigma_o}{J} = 175$

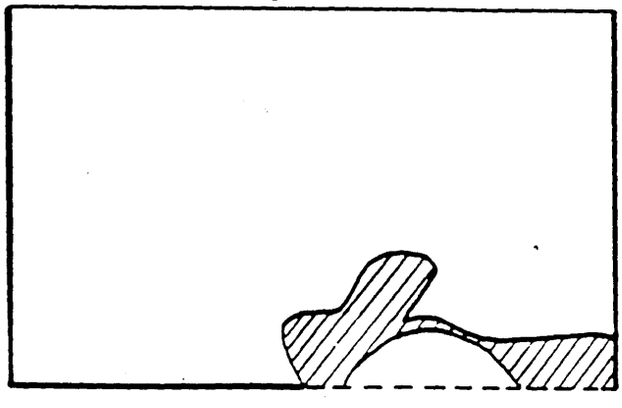

$\frac{a\sigma_o}{J} = 160$

Fig (5.18)

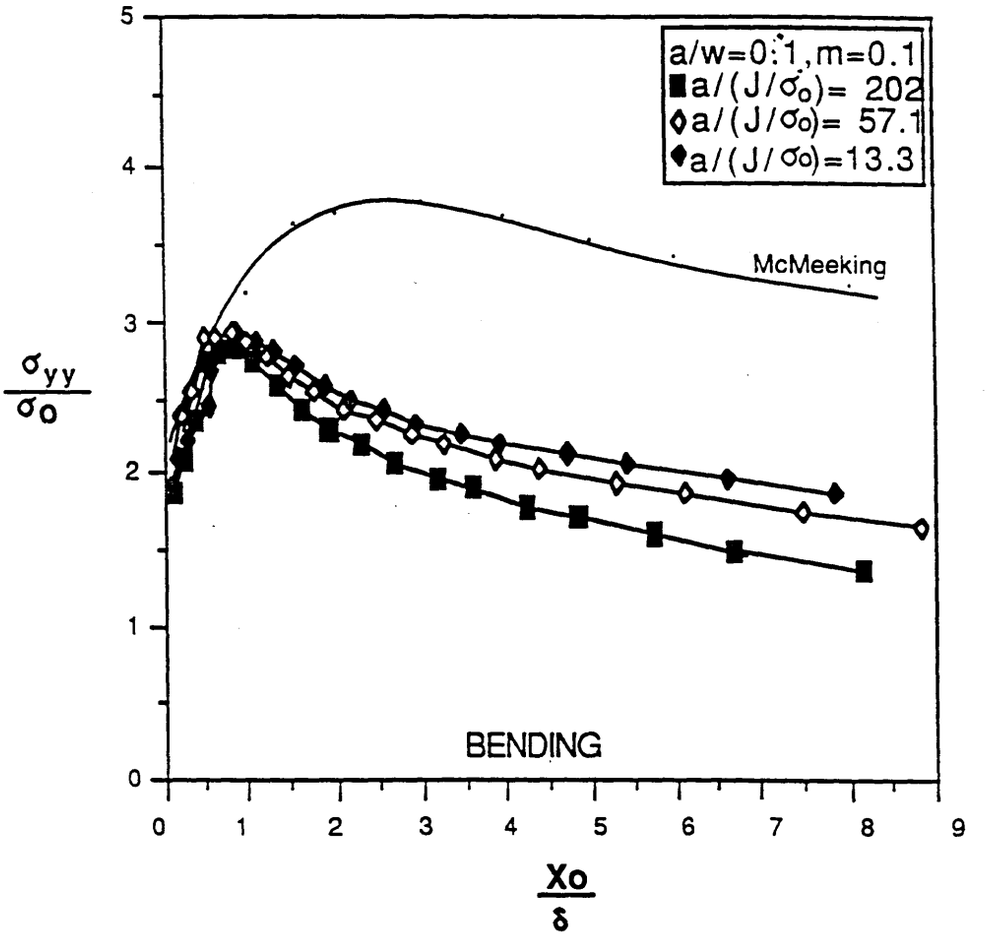

Fig. (5.19)

The stresses ahead of a blunting crack in bending (a/W = 0.1, m=0.1)

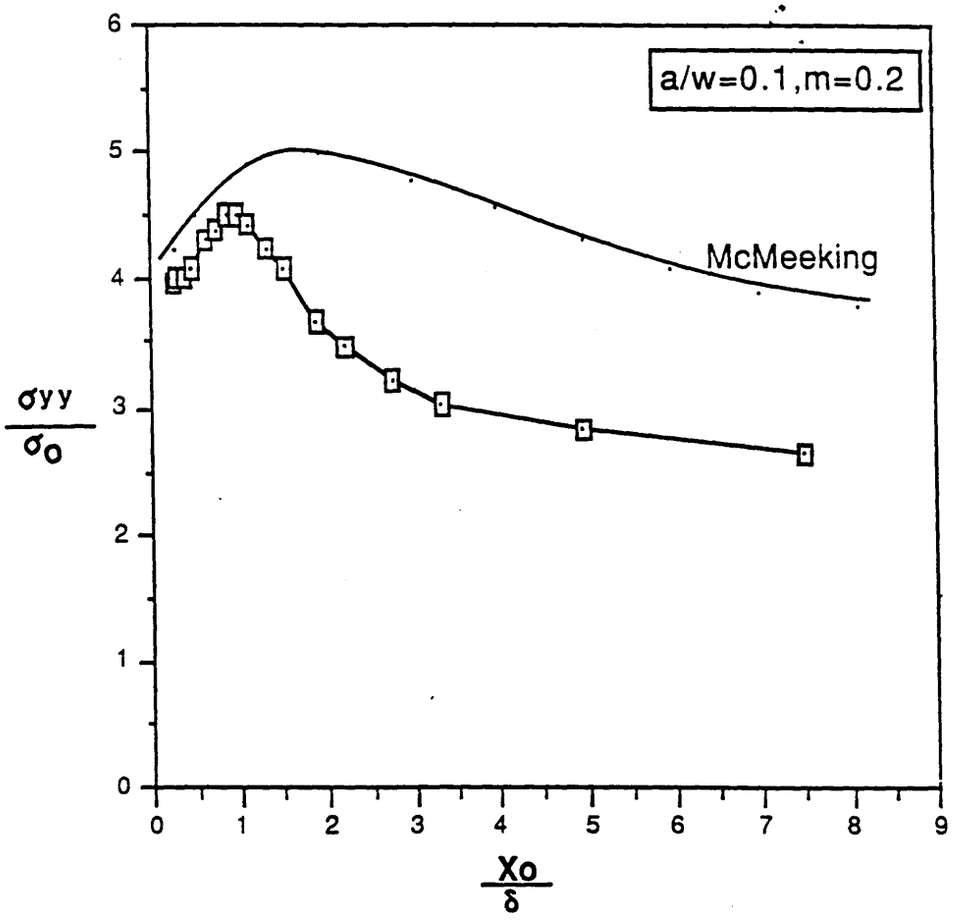

Fig (5.20)

The stresses ahead of a blunting crack in bending (a/W = 0.1, m=0.2)

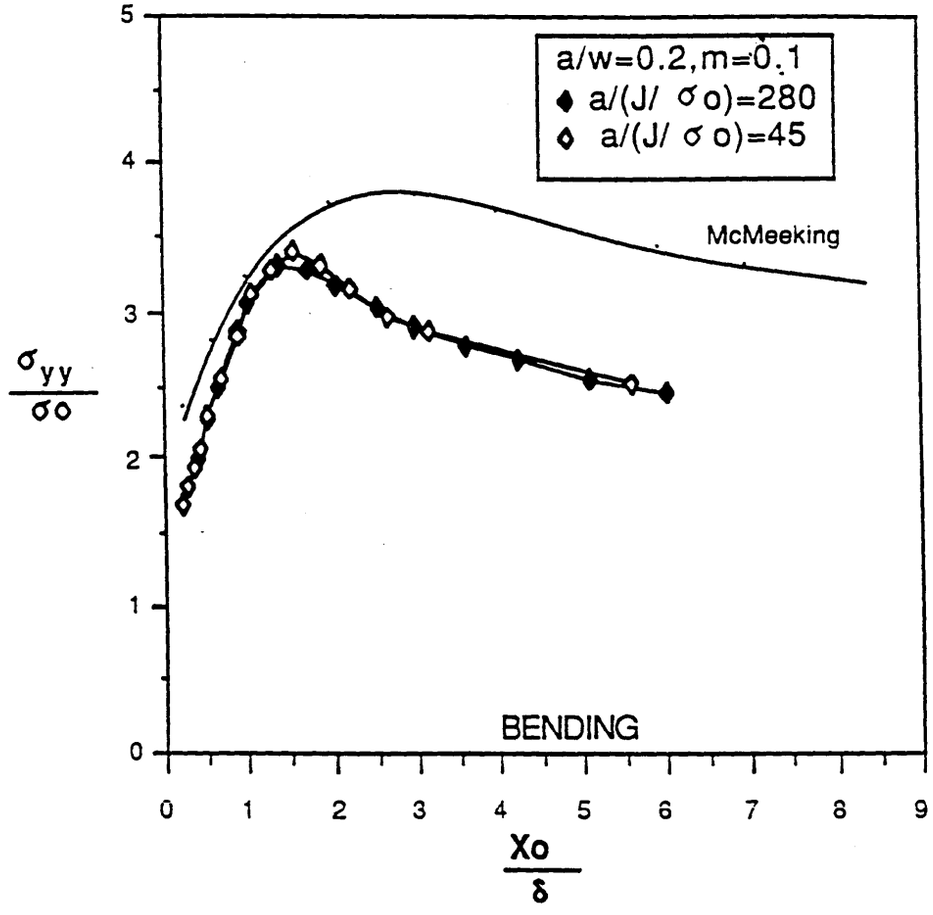

Fig (5.21)

The stresses ahead of a blunting crack in bending (a/W = 0.2, m=0.1)

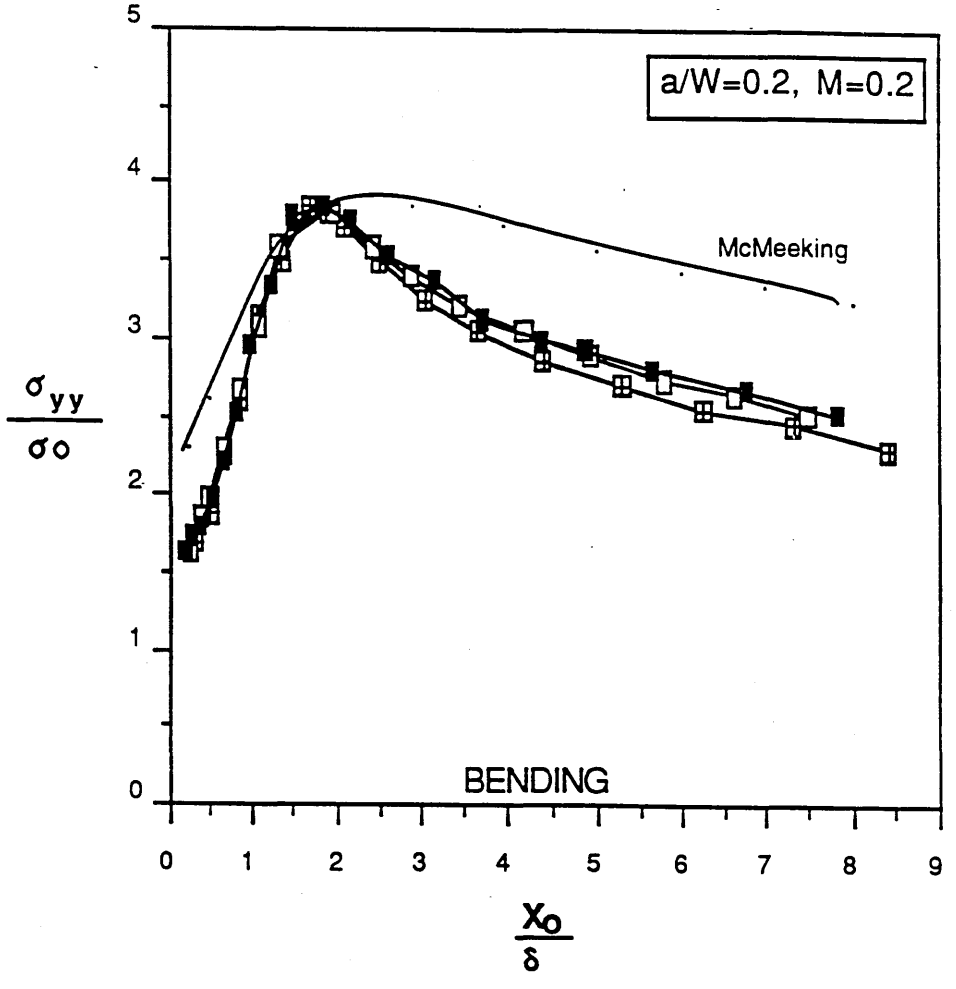

Fig (5.22)

The stresses ahead of a blunting crack in bending (a/W = 0.2, m=0.2)

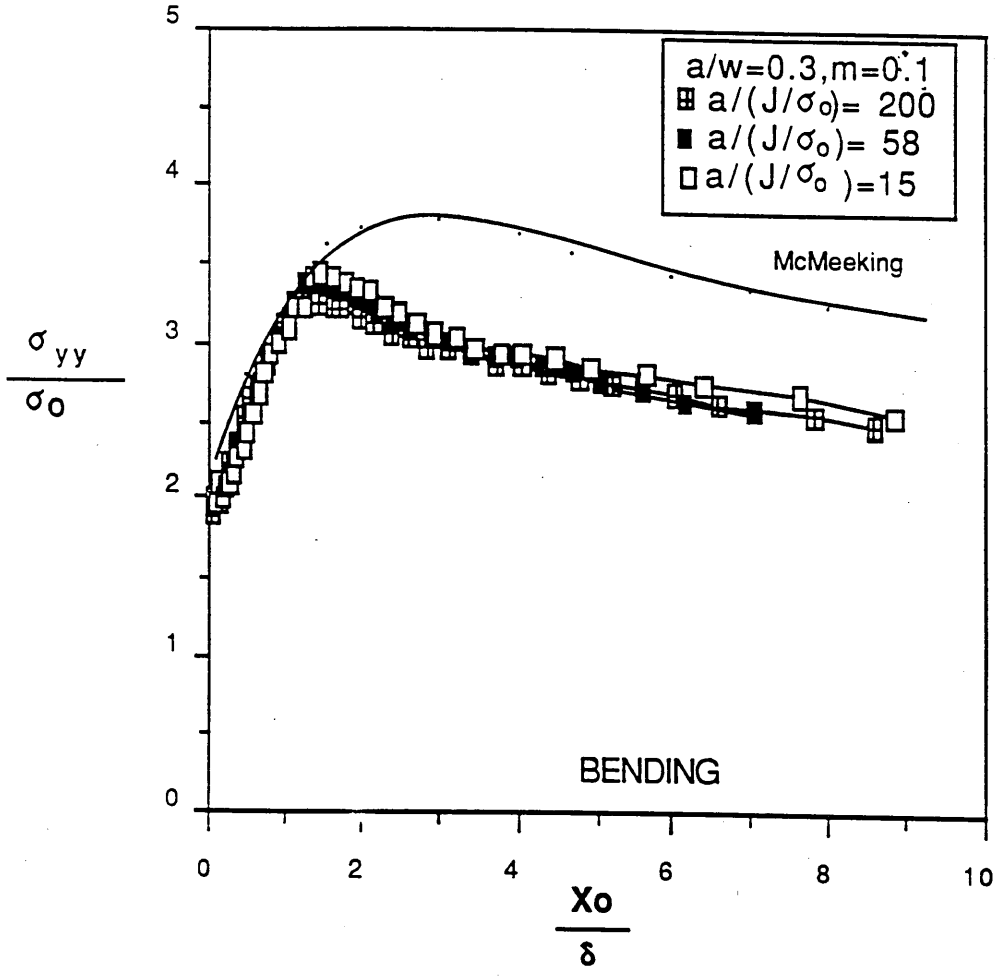

Fig (5.23)

The stresses ahead of a blunting crack in bending (a/W = 0.3, m=0.1)

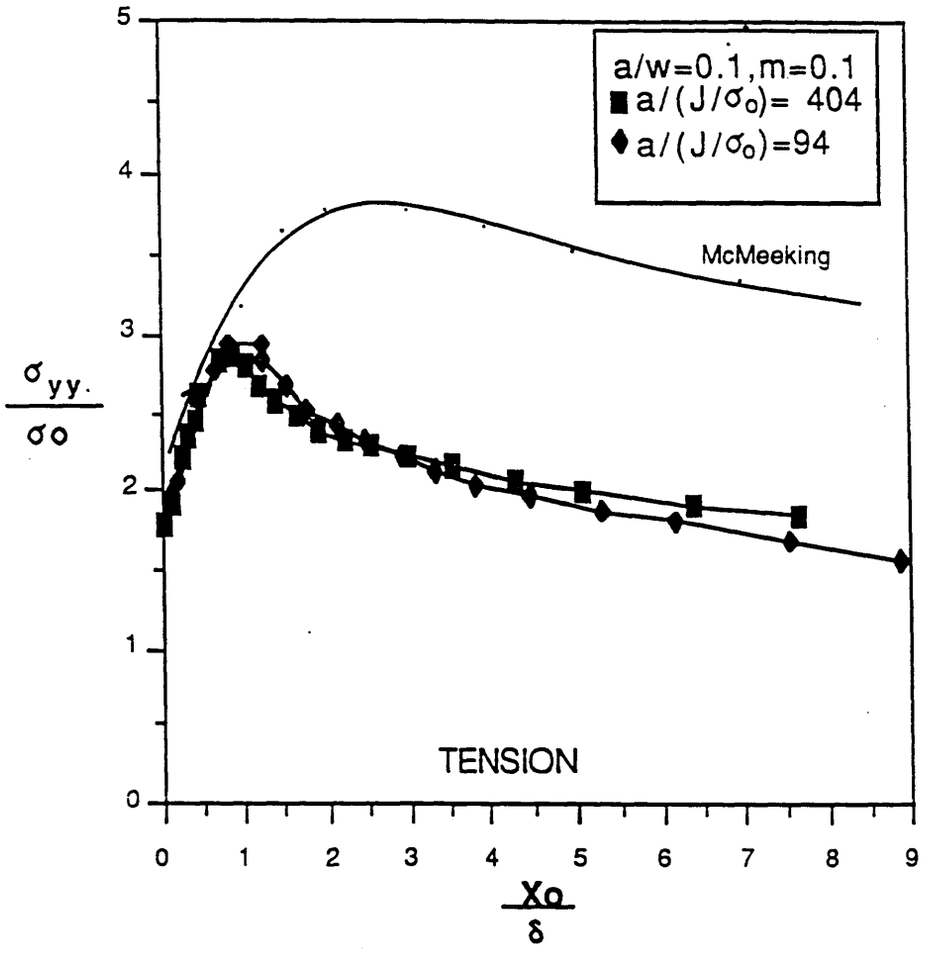

Fig (5.24)

The stresses ahead of a blunting crack in tension (a/W = 0.1, m=0.1)

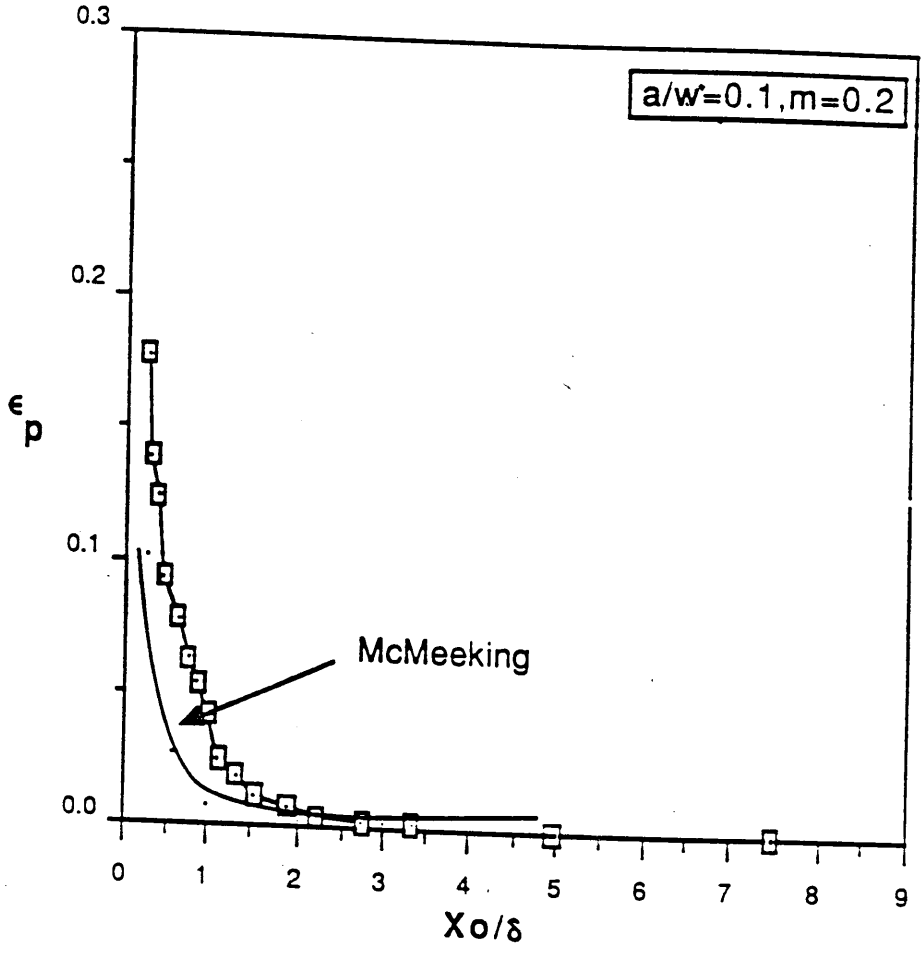

Fig (5.25a)

The equivalent plastic strain ahead of blunting cracks in bending (a/W = 0.1, m=0.1)

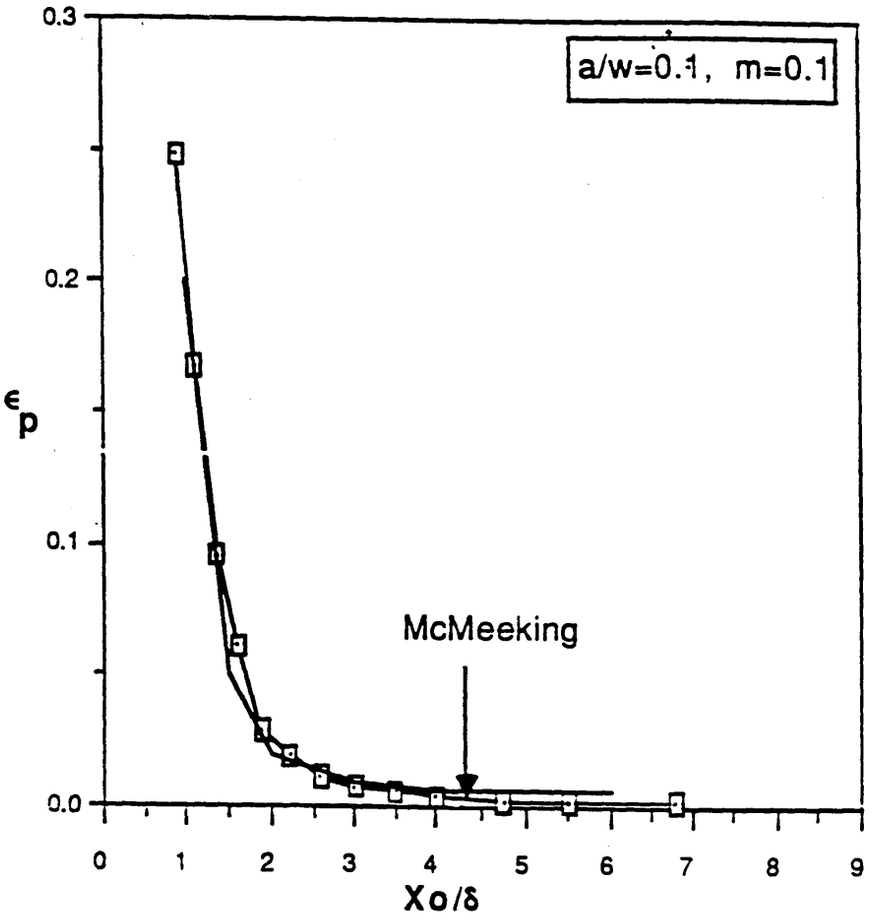

Fig. (5.25b)

The equivalent plastic strain ahead of blunting cracks in bending (a/W = 0.1, m=0.2)

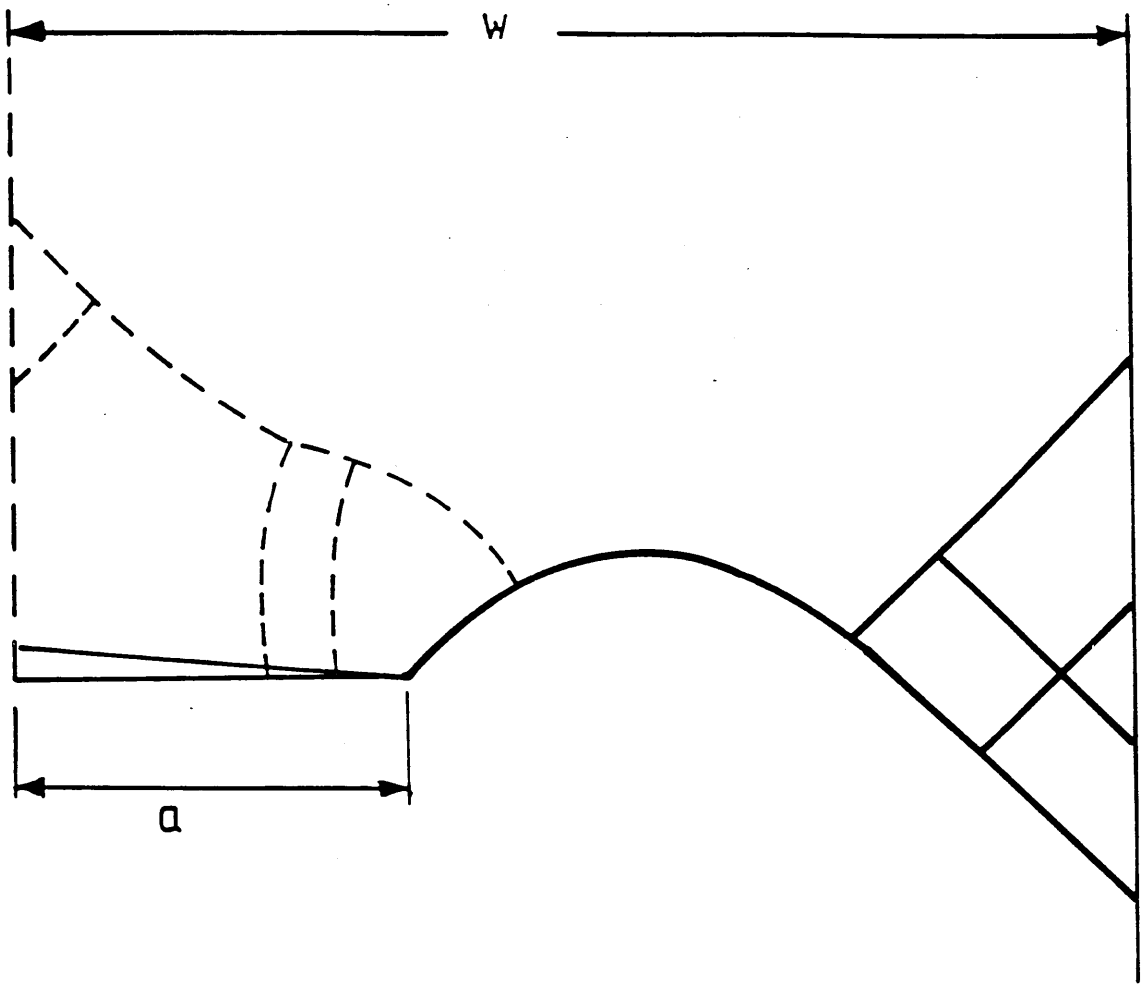

Fig (5.26)

The slip line field for the deep and shallow cracks following Green (14).

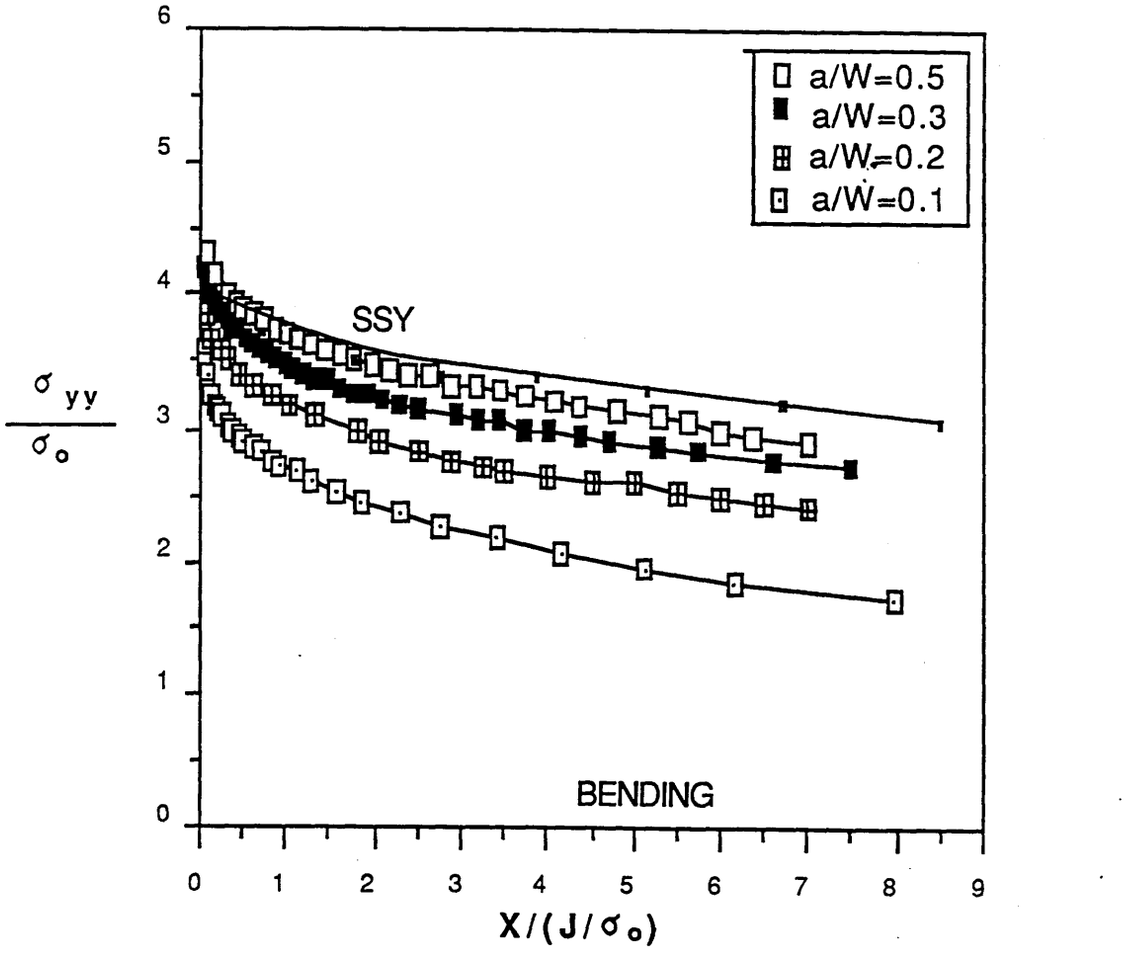

Fig (5.27)

The limiting Field for the Small Geometry Change solution in Bending for (a/W= 0.1,0.2,0.3 and 0.5)

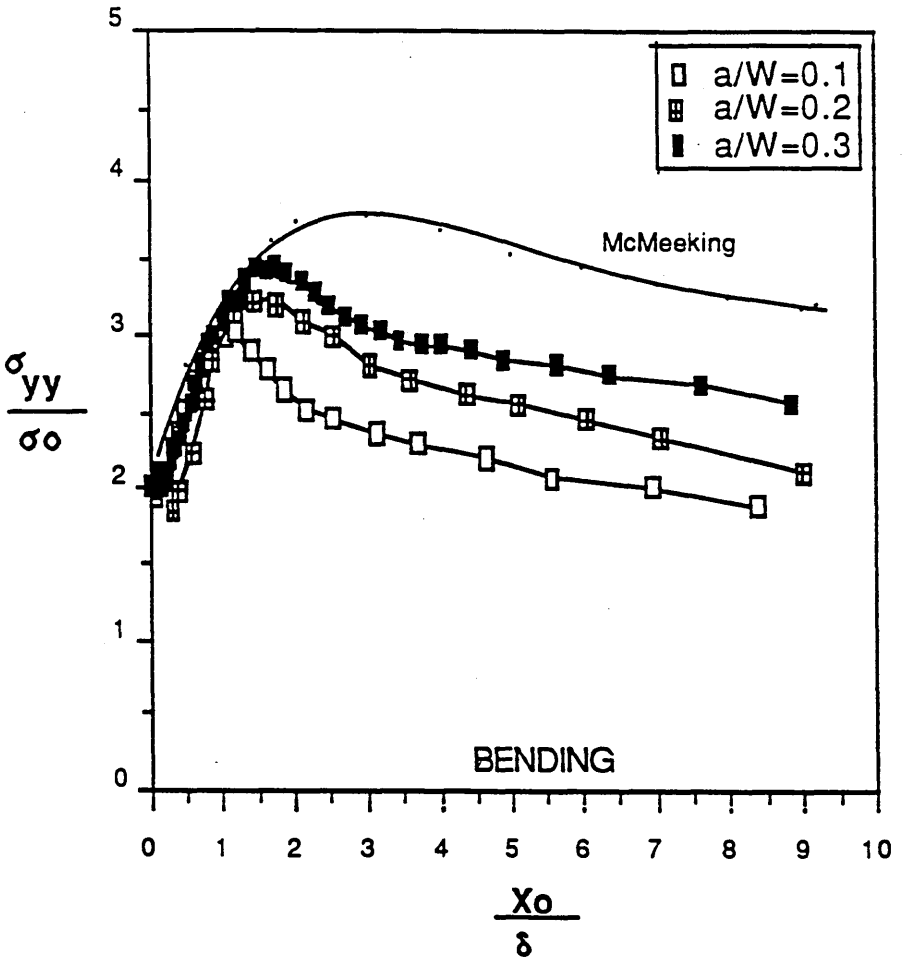

Fig (5.28)

The limiting Field for the large Geometry Change solution in Bending for (a/W= 0.1,0.2 and 0.3)

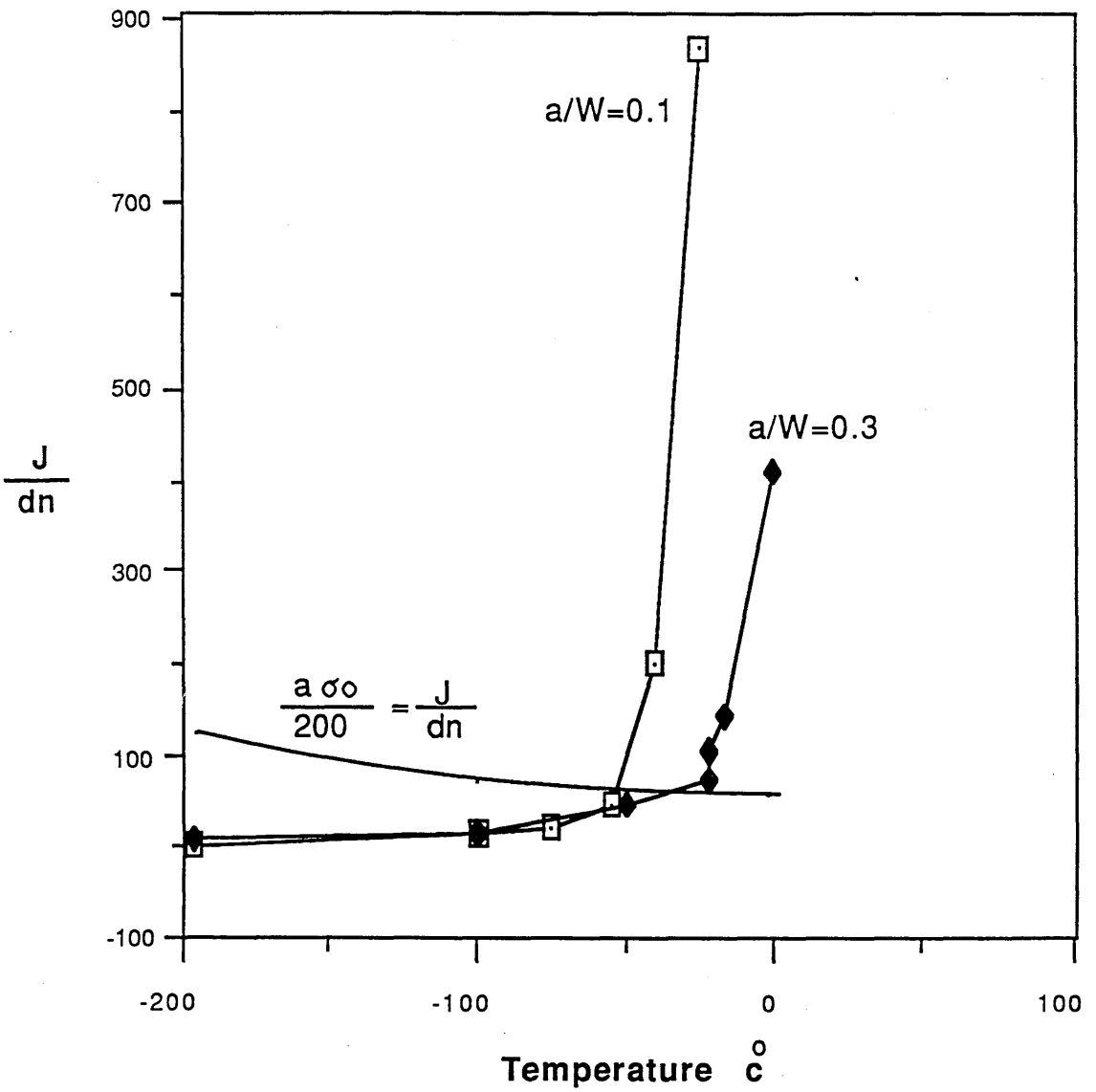

Fig (5.29)

The experimental result of the J-integral for deep and shallow cracks following Sumpter (18)